**SISSA**

**ISAS**

SCUOLA INTERNAZIONALE SUPERIORE DI STUDI AVANZATI
INTERNATIONAL SCHOOL FOR ADVANCED STUDIES

# BCS superfluid Fermi systems with large scattering length

Thesis submitted for the degree of
Doctor Philosophiæ

CANDIDATE
Sandra Patricia González Camelo

SUPERVISOR
Prof. Stefano Fantoni

October 2007

# Acknowledgment

Let me compare the stage I am finishing at SISSA, with a walk along a road which I look backwards now . I have learned that the path one describes in doing research is not a straight line. And yet, the joy of understanding or at least appreciating nature, makes it worthy.

I am so grateful to professor Stefano Fantoni, whose guide was more than essential in completing my Ph.D. He introduced me into the world of quantum fluids and suggested me the FHNC as a tool to face them. I must say that he continuously encouraged me to keep on walking and he trusted in me when no even myself saw a happy ending. His natural talent to analyze and describe a problem in simply way, together with his extraordinary sense of humor will stay in my memory.

I was also lucky to count on the guidance of Kevin Schmidt, who visited Trieste during the summer. His help in solving numerical and conceptual problems was very important. I appreciate his patience in explaining them to me more than once and his cleverness in putting together the pieces. I thank him enormously.

Special thanks to Andrea Trombettoni for his interest in this work as well as for many useful suggestions and corrections to the manuscript. I thank Alexei Illarionov for providing me some calculations and for reading and correcting also part of this work. My acknowledge goes also for the professors of the condensed matter sector for their interesting and useful lectures at the first stage of the PhD, particularly to Prof. De Gironcoli and Prof. Baroni. I thank also the people working at SISSA, the computer staff for their promptly help. To professor Fantoni's secretaries Alice and Silvia, as well as, Alex, Maria Sole and Tatiana for their patience and kindness.

During my stay in Trieste I had the opportunity of sharing my way with people from the almost all over the world. Actually this is not a common place; Trieste is itself a small world in which a variety of races, languages

and religions coexist in a peaceful environment characterized by the love for knowledge. Such a variety was for me a real treasure. I am very much in debt to many persons who supported me and gave me the best of them. My classmates Dario di Pavia, Liang, Osvaldo Zagordi and Tony Suriano, each of them in their own particular and unforgettable way made these years more than a nice memory. I was lucky to have also between my friends Lucia Scardia and Filippo Cagnetti, they were perfect hostess offering everybody their charm and happiness. To Yassir Dinar and Diana Bedolla for their friendship and her encouragement; in some dark days they made the sun to appear with their smile. In particular I thank Diana for her help during the last step of this work without her, life had been harder. To all my friends far from me, but always present with their thoughts and mails: Natalia, Solomon, Tuvshin and Fernando, to mention just a few, many thanks.

To my lovely Ricardo, for his endless affection, tenderness and constant support. Thanks for drawing blue skies above me and perfumed flowers under my feet. His love is the sweetest of the dreams. Finally I thank my mother, my father, my sister for their love and care in the distance. They are the reason why I have kept a smile in my face and strength in my soul. An ocean between us, made me realize how lucky I am of having them.

# Overview

The main purpose of this work is to describe the ground state properties of dilute Fermi fluids in the strongly interacting regime characterized by a large and negative scattering length. The study of such systems has generated great interest in various fields. A few years back, the experimental efforts in the physics of ultracold gases have allowed to create such systems, opening the possibility to test our knowledge of the pairing phenomena under a big variety of conditions. Strongly correlated particles were already very well known in condensed matter and nuclear physics, as well as in astrophysics where the description of neutron stars falls into this category.

In the asymptotic limit of the scattering length $a_s$ going to $-\infty$ (*unitary limit*), all the length scales associated to the interactions disappear, and the only characteristic length is the interparticle distance $r_0 = \frac{1}{k_F}\sqrt[3]{\frac{9\pi}{4}}$ (or equivalently the inverse of the Fermi momentum, $1/k_F$). In this limit the energy can be then expressed in terms of the Fermi gas energy, $E = \xi\frac{3\hbar^2 k_F^2}{10m}$. Analytical approaches and Monte Carlo simulations reveal that the proportionality constant $\xi$ is far from being unity, revealing the essential role of the correlations induced among the particles. Therefore any attempt to apply a mean field theory in this context fails.

Our approach to handle such systems is based on Quantum Monte Carlo and the Fermi-Hyper netted chain (FHNC), with particular attention to the last one. The main achievements presented in this thesis consist of:

- Formulation of the FHNC theory for a correlated BCS state (denoted hereafter by FHNC/BCS) for the case of longitudinal spin dependent Jastrow correlations, namely correlations which distinguish spin-parallel from spin anti-parallel pairs.

- Derivation of all the needed FHNC/BCS integral equations to compute the energy per particle, one- and two-body density matrix and the

excitation energies.

Calculations have been made for neutron matter with semirealistic spin-dependent NN potentials and for dilute Fermi systems interacting through Lennard-Jones potentials with large and negative scattering length/ The main results are the following:

- Large effects have been found in the energy per particle and consequently on the equation of state for the longitudinal spin dependency of the Jastrow correlations in the description of the BCS superfluid phase.

- The excitation energy of the superfluid system, and in particular the gap energy has been calculated for the first time in full FHNC theory. Good agreement has been found with QMC evaluations.

The structure of the thesis is as follows. The first chapter contains an introduction to the problem, followed by some insights into the Feshbach resonances mechanism which allows to produce the strongly interacting regime in laboratory for dilute Fermi gases. The mentioned resonances, offer the possibility of changing the effective scattering length between $a \to -\infty$ to $a \to +\infty$, giving access to the known BCS-BEC crossover, which will be briefly described later. The chapter finishes by introducing the reader to the superfluidity of neutron matter, which is also a system with large and negative scattering length. Chapter 2 concerns directly with the methods of calculations, starting by the Auxiliary Field Diffusion Monte Carlo (AFDMC) which was developed as an extension of the Diffusion Monte Carlo to address problems in which the Hamiltonian depends on spin variables, as the NN interaction requires. The main emphasis in this chapter as well as in the in whole thesis is given to the formalism of the FHNC. The extension of the FHNC/BCS to the case of longitudinal spin ($\sigma_z$) dependent correlations is described in detail including the expression of the energy for a spin dependent potential. The FHNC in the normal phase with and without $\sigma_z$ dependence are reviewed in the Appendices. In Chapter 3, the equation of state (EOS) for neutron matter and of dilute Fermi gases in the strongly correlated regime, are presented by direct application of the FHNC methods. Chapter 4 is devoted to presentation of the FHNC theory to calculate the momentum distributions in the superfluid phase. We present in Chapter 5 the implementation of the FHNC methods to calculate the gap energy of such superfluid systems, as well as calculation of the excitation energy.

# Contents

# Chapter 1

# Introduction

Superfluidity of strongly correlated Fermions is a subject of current interest. Dilute Fermi gas, high $T_c$ superconductivity, liquid ${}^3$He and neutron matter are only few examples of interesting systems, for which a better understanding of the interplay between long range order phenomena and strong correlations is needed. The question of whether many-body effects are important also in the low density regime, where the superfluid phase transition may occur, for quantities such as ground state and gap energies, momentum distribution or pairing function is still an open and challenging problem. Most of the ground state and gap energy calculations are limited to either uncorrelated BCS theory or at most to two-body correlated approximation, based upon Brueckner Hartree-Fock (BHF) or Correlated Basis Function (CBF) theories. The argument of the superfluid phase transition occurring at low density which has been used to justify the above approximations is however not valid for those systems in which particles interact strongly.

The important parameter in the system is $\zeta = k_F a$, where $k_F = (6\pi^2 \rho/\nu)^{1/3}$, with $\rho$ being the fluid density and $\nu$ its spin degeneracy, $k_F$ is the Fermi momentum and $a$ is the ${}^1S_0$ scattering length. Large and negative values of $\zeta$ favor weak coupling BCS superfluid [1] and, at the same time, induce strong correlations amongst the particles. In the asymptotic limit (unitary regime) $\zeta \to -\infty$, the limit that Bertsch proposed to study in 1998 [2], the only remaining length is $k_F$, and therefore the ground state energy is proportional to the Fermi kinetic energy $E_F = \frac{3}{5}\frac{(\hbar k_F)^2}{2m}$. It turns out that the proportionality constant is 0.44 instead of being 1 [3], implying that mean field approximations fail even in the low density regime.

Ultracold dilute gas of Fermi atoms have been produced in atom traps in

the regime of interaction having large negative scattering length by using the Feshbach resonance mechanism. In the experiment by K.M. Ohara et al. [4] with $^6$Li $\zeta = -7.4$. As the atomic interaction strength is increased towards the Bertsch limit, namely that corresponding to $a \to -\infty$, one gets bosonic two-Fermions bound state. Therefore one may consider dilute Fermi gases with large scattering length as being intermediate systems between weak coupling BCS superfluids and dilute Bose gas undergoing Bose-Einstein condensation (BEC) [5], [6]. Dilute Bose gas in the strongly interacting regime of large $a/r_0$, where $r_0 = (\frac{3}{4\pi\rho})^{1/3}$ is the average interparticle spacing, have been experimentally produced [7], [8] and theoretically studied [9], [10], [11]. A second important example is provided by neutron matter which can be found in the interior of neutron stars and which shows up superfluid properties [12]. The scattering length of NN interaction has been found to be $\sim -18.5$ fm in $^2$H$(\pi^-, \gamma$ nn) reactions [13] and $\sim -16.3$ fm in deuteron break up experiments [14]. At densities as small as $10^{-3}$ fm$^{-3}$ the parameter $\zeta$ ranges from 5 to 5.7, namely is much larger than one. Quantum Monte Carlo methods have been recently applied to perform numerical simulations of Fermi fluids in the superfluid phase. The Diffusion Monte Carlo (DMC) [15] and the Auxiliary Field Diffusion Monte Carlo (AFDMC) [16] for the case of spin dependent interactions, have recently been implemented to use correlated pfaffians as guiding functions ([3], [17]).

We develop here a technique based upon Fermi Hyper Netted Chain (FHNC) theory [18], and denoted as FHNC/BCS to perform variational calculations with correlated BCS wave functions. The type of correlation we consider is of the Jastrow-type, namely $\prod F_{ij}$, with $F_{ij}$ depending on $\sigma_z(i)$ and $\sigma_z(j)$, the $z$-components of the spins of particles $i$ and $j$, in order to distinguish parallel from antiparallel spin pairs. FHNC integral equation methods have been thoroughly used in CBF theory to perform ab initio calculations of the static and dynamical properties of several strongly interacting Fermi fluids at low temperature ranging from liquid helium to nuclear matter in both bulk and confined geometries [19]. In the eighties, FHNC theory has been generalized to deal with pure Jastrow correlated BCS wave functions (but with no $\sigma_z$-dependence). In that paper ([20] denoted here as I) the FHNC/BCS integral equations have been derived to compute the two-body distribution function $g(r_{12})$, the momentum distribution $n(k)$ and the pairing function $\chi(k)$, but they have never been applied to perform calculations of the ground and excited states energies of strongly interacting Fermi systems

in the continuum. The FHNC/BCS theory has only been applied in Hubbard model calculations of strongly correlated electron in a lattice [21], [22], [23], where the knowledge of $g(r_{12})$ and $n(k)$ were the only required quantities.

## 1.1 Dilute Fermionic gases

Bose-Einstein condensation in dilute gases was achieved experimentally in 1995 for the alkali gases: rubidium [24], sodium [25] and lithium [26]. In this striking phenomenon, the quantum nature of particles shows up at temperatures of the order of $10^{-5}$ K and low densities around $10^{13} - 10^{15}$ cm$^{-3}$, more than four orders of magnitude lighter than air. Since that time a vast number of work have been published in the experimental as well as in the theoretical field. The most important achievements concern the manifestation of superfluidity through the observation of Josephson-like effects [27], [28], the realization of quantized vortices [29], the interference of matter waves [30] and the study of coherence in atomic laser configurations [31], to mention just of a few. Later on the with the achievement of degeneracy in a Fermi gas [32], the research has focused on the realization of a superfluid and the understanding of the pairing phenomena in this type of systems.

The quantum essence of particles becomes important when the de Broglie wavelength, defined as:

$$\lambda = \sqrt{\frac{\hbar}{2mk_BT}}$$

is comparable with the average interparticle spacing. The need of low temperatures to reveal the quantum world, can lead the particles to form molecular states and reach a solid or liquid transition. Therefore a delicate balance between temperature and density must hold in order to keep the atomic system in gaseous phase. Two types of scattering processes play important roles: the binary collisions which allow the system to thermalize at a rate proportional to the density $\sim \rho$ (process which leads to cooling the system), and the 3-body collisions whose rate is proportional to $\sim \rho^2$, which lead to the formation of molecules. Thus extremely low densities allow to achieve degeneracy in a gas.

Although the range of temperatures at which quantum degeneracy appears in Fermions and bosons is the same, its effects are manifested in a different way. In the Bose case, quantum statistical effects are translated into the onset of a phase transition to the Bose-Einstein condensate. On the contrary, the

appearance of quantum behavior in Fermi systems, does not coincide with the occurrence of a superfluid phase, which actually does not take place if there are no interactions between Fermions. From the theoretical point of view the many body physics of Fermions at low temperature is particularly rich and challenging.

The experimental process to reach such low temperatures and densities starts usually with laser cooling and magnetic trapping, followed by evaporative cooling . These techniques apply to both bosonic and fermionic species, but for the latter when only a single component is present, the Pauli exclusion principle inhibits the thermalization process, challenging any further reduction of the temperature. To overcome this difficulty the technique of sympathetic cooling with mixtures of different fermionic or bosonic-fermionic species is used. Quantum degeneracy has been reported for instance by Truscott *et al.* [33] in Lithium by applying sympathetic cooling between the Fermion $^6$Li and its bosonic isotope $^7$Li, and by DeMarco and Jin [32] mixing the hyperfine states $|9/2, 9/2\rangle$ and $|9/2, 7/2\rangle$ of $^{40}$K.

At such low temperatures the most important physical processes is lead by two body scattering, characterized by the scattering length $a$, while the relevant internal states of the atom are the hyperfine states. The coupling between such internal states in the presence of the external magnetic field gives rise to the so called Feshbach resonances, which then provide a control mechanism of the strength of the interactions.

The feasibility of this mechanism opened a new tool to achieve superfluidity in fermionic systems. As a result, novel conditions were reached by varying the external magnetic field. In 2002, O'Hara *et al.* [4] succeeded in creating a *dilute gas* in a *strongly interacting regime*. This particular situation is produced by working close to the Feshbach resonance, where the scattering length blows up to infinity. In the *unitary regime*, which is characterized by the disappearance of all the lengths associated with the interactions, the remaining length scale is $1/k_F$. As a consequence, the description of these Fermi dilute gas is expected to exhibit a universal character. Another interesting feature is the critical temperature, which is much higher than the one predicted in the BCS regime; its estimations are of the order of the Fermi temperature, therefore the superfluid phase is more easily reachable. In Table 1.1. is shown the order of magnitude of the critical temperature in terms of the Fermi temperature, for various Fermi systems.

| System | $T_c/T_F$ |
|---|---|
| Classical superconductors | $10^{-4} - 10^{-4}$ |
| Superfluid $^3$Helium | $10^{-3}$ |
| High $T_c$ superconductors | $10^{-2}$ |
| Dilute Fermi gases in the vicinity of a Feshbach resonance | $\sim 0.2$ |

Table 1.1: Ratio between Critical and Fermi temperature for different fermionic systems. Taken from [34]

The presence of an external magnetic field turns out to be important not only as a tool for trapping and cooling the alkali gases, but also to modify the effective interactions between atoms. The tunability of the interactions makes it possible to change from attractive ($a < 0$) to repulsive ($a > 0$) effective interactions; this is known as the BCS-BEC crossover. In the next subsections a brief overview of the Feshbach mechanism and the crossover is given.

## 1.1.1   Feshbach resonances

One of the most appealing aspects in the physics of dilute systems is the ability to tune the type of effective interactions. The central mechanism responsible for the tuning is the magnetic field, which reveals and modifies the hyperfine structure of the probe, which is particularly rich for alkali atoms. The phenomenon first investigated in the context of nuclear matter [35], was primarily observed in dilute atomic gases for sodium, undergoing BEC in 1998 [36], [37]. Soon after, Feshbach resonances made possible the achievement of condensation in Rb$^{85}$ [38]. It has also been verified in fermionic vapors such as K$^{40}$ [39] and Li$^6$ [40].

The interactions between alkali atoms are basically determined by the state of the valence electrons. Two colliding atoms can form a singlet state therefore sharing the same orbital with different spin states. The Coulomb repulsion between them is reflected in a strongly repulsive potential. In contrast a triplet state does not support such reduction in energy and the electrons are far from each other in order to maintain the antisymmetry of the wave function.

Due to magnetic interaction with the nuclear spin, a coupling between

both configurations can arise. As a consequence if two atoms are colliding in a triplet state for instance, the electronic and nuclear spin of one of the atoms may be flipped, thus resulting in a singlet state. This state is usually formed for a short life time up to another collision process bringing back the triplet initial potential.

The electronic Zeeman coupling to the triplet state in the presence of an external magnetic field, can shift its relative energetic position with respect to the singlet configuration. Let $\delta$ be the shift introduced in the scattering threshold of the singlet and triplet states. Usually the singlet threshold is above the triplet one, therefore is energetically unfavorable for atoms in the singlet to escape out. It is very common in this problem to refer to a state (set of quantum numbers) as *channel*. With this convention, the singlet configuration is denoted as *closed channel* while the triplet, as *open channel*. This terminology is more appropriate, because in general the interactions are made of a superposition of both singlet and triplet states.

The example shown in Fig. 1.1 shows the potential felt by the scattering atoms in the singlet $S = 0$ or in the triplet $S = 1$ two-body states. For a Feshbach resonance to occur a bound state belonging to the closed channel must lie close to the scattering threshold of the open channel. The energy difference $\nu$ between the bound state energy and the zero energy corresponding to the continuum of scattering states of the triplet or open channel is referred to as *detuning parameter*.

The scattering process is then tremendously affected by the existence of bound states in closed channels. Adjusting the magnetic field it is possible to change the detuning parameter from positive (bound state of the closed channel above the threshold of the open channel) to negative (bound state bellow the zero energy). The intermediate situation when $\nu = 0$, occurs for a particular value of the magnetic field $B_0$. As a consequence of the coupling between both channels, the scattering length is modified with respect to the background scattering length $a_{bg}$, if there is no coupling between channels. The dependence of the scattering length with the magnetic field is ruled by,

$$a = a_{bg}\left(1 - \frac{\Delta B}{B - B_0}\right),$$

where $\Delta B$ is a measure of the width of the resonance, and the detuning parameter $\nu \sim B - B_0$. When the energy of the scattering particles is below that of the bound state, an attractive ($a < 0$) effective interaction arises between them and when the opposite situation occurs a repulsive ($a > 0$)
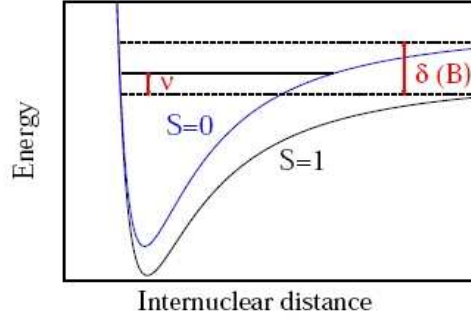
Figure 1.1: Pictorial description of a Feshbach resonance. The lower line corresponds to the potential between two scattering atoms in triplet spin state (open channel) and the upper to the interaction potential in the singlet state (closed channel). The shift between the continuum states (represented with dashed lines) between open and closed channels due to the magnetic field, corresponds to $\delta(B)$. The detuning parameter $\nu$ measures the difference between the bound state in the closed channel and the zero energy of the open channel. Taken from [41].

interaction is established (See for instance Fig. 1.2). Thus it follows that in the former case there is no bound state; for that side of the resonance when $a \to -\infty$ the system is at the onset of a molecular bound state. From the other side when the $a \to +\infty$, the bound state reaches the stability. Therefore the picture of the system evolves from Cooper pairs (weakly interacting particles) to the BEC of bosonic molecules made of two Fermions.

The magnetic field acts like a knob for the interactions opening a wide range of possibilities to test our knowledge in the many body process giving rise to the condensation of particles. Although the scattering length passes through $|a| \to \infty$, the N body problem of superfluidity evolves in a smooth way, showing that weak coupling and strong coupling pairing corresponds to two faces of the same coin; the crossover between BCS and BEC is based precisely on this fact.
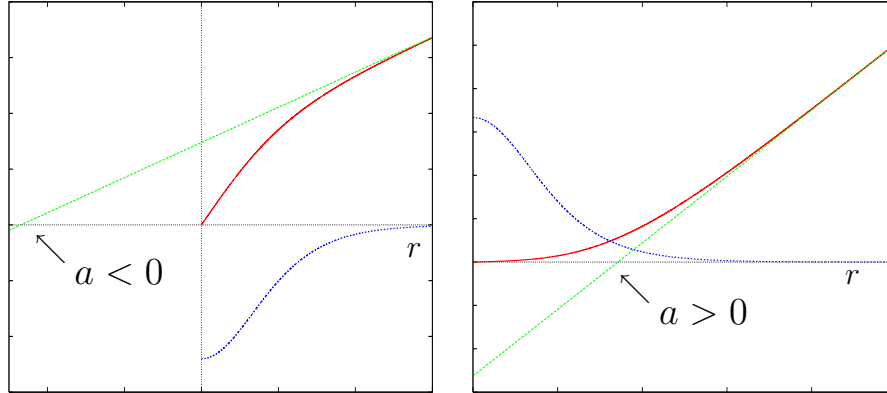
Figure 1.2: *Left*: Example of an attractive potential (blue line) together with the solution of the reduced radial equation (red line). *Right*: Idem situation for a repulsive potentail. The scattering length $a$ is given by the intercept of the asymptotic reduced radial wave function on the $r$ axis (green lines).

### 1.1.2   BCS/BEC crossover

In the context of pairing in Fermi systems there are two different pictures involved. On one side the weak pairing case ($a$ small and negative), successfully explained by standard BCS theory and on the other the model of composite bosons (dimer molecule of Fermions) undergoing BEC. Through the Feshbach resonances for instance, the pairing phenomena evolves from dealing with Cooper pairs whose size is huge compared to the interparticle Fermion distance, to real tightly bound bosonic molecules, experiencing the crossover which is characterized by $|a|$ large corresponding to a strong coupling regime. This is the region of interest for us. In Fig.1.3 a pictorial representation of the pair formation is shown in both cases.

Beside the differences in the pair size, also the transition temperatures differ considerably. In the BCS theory the Fermi liquid undergoes a pairing instability at  a temperature much smaller than the characteristic Fermi temperature $T_c \ll T_F$. The formation of Cooper pairs coincides with the transition to the superfluid (or superconductivity) state. In contrast Bosons condense at a temperature of the order of their degeneracy temperature. Bosons are composite objects made up of an even number of Fermions and the temperature required to dissociate them is tremendously larger than the condensation temperature, $T_c \ll T_{dissoc}$.
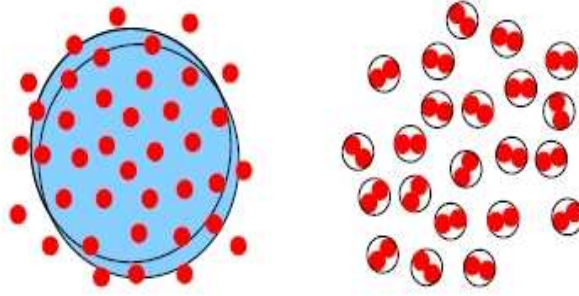
Figure 1.3: Representation of the pairs in the BCS (left) and BEC (right) case. The BCS pairing is characterized by the strong overlapping of the Cooper pairs while in the BEC superfluid, real bound molecules condense in a macroscopic wave function. the difference between the

Certainly there are many common features concerning their macroscopic behavior. Bosonic and fermionic superfluids are described by a coherent wave function and in three dimensions, their density matrices exhibit Off-diagonal long range order (ODLRO).

The quantity of works done in this field is large and the motivations behind them come from very diverse interests. A variety of techniques ranging from renormalized mean field theories, variational approaches, random phase approximation (RPA) and numerical simulation have constructed the rich map of the field, but still open questions are left, especially concerned with the intermediate regime.

In this brief introduction we will show the behavior of important quantities in the crossover, emphasizing in the limiting regimes of weak and strong coupling. This follows the work done by Randeria *et. al* [5].

Commonly one starts with a system of Fermions with attractive two body interactions. The fermionic nature of the particles is an important condition in the experiments, since the bosonic counterpart would require a large amount of energies to be broken into their constituent Fermions. Following Randeria [5] notation, the Hamiltonian density for a continuum model[1] is

---

[1]Lattices models are also very used, the most important being the Hubbard model. Here there are two parameters which rule the crossover, the filling factor and the coupling $U/t$. Where $U$ is the on-site attraction and $t$ the hoping constant.

written like

$$H = \overline{\Psi}_\sigma(x) \left[ -\frac{\nabla^2}{2m} - \mu \right] \Psi_\sigma(x) - g \overline{\Psi}_\uparrow(x) \overline{\Psi}_\downarrow(x) \Psi_\downarrow(x) \Psi_\uparrow(x)$$

where $\overline{\Psi}_\sigma(x)$, $\Psi_\sigma(x)$ are the creation and destruction field operators at position $x$, spin $\sigma$. The chemical potential is introduced to fix the average density and $g$ is the strength of the bare attractive interaction (this is the only parameter introduced so far in the model). Natural units are used. At the temperatures of interest, only the $s$ wave scattering length $a_s$, characterizes the two body interaction.

In order to find the temperature at which the system is unstable against pair formation, basically the same path as in pure BCS is followed. However this time the chemical potential is no longer fixed to the Fermi energy and the constrain that only the Fermions around the Fermi surface feel the attraction is no longer assumed. Instead the ultraviolet divergence is solved by replacing the bare $g$ interaction by a renormalization of the scattering length, which is valid in the low energy limit. This condition is stated in

$$\frac{m}{4\pi a_s} = -\frac{1}{g} + \sum_{|k| < \Lambda} \frac{1}{2\varepsilon_{\mathbf{k}}}$$

where $\Lambda$ is a cut off for low energy states. In the BCS weak coupling region $g \to 0$ while for strong attractive interactions $g \to \infty$, therefore the scattering length goes from $a_s \to -\infty$ in the weak limit to $a_s \to \infty$ in the strong one. The temperature $T_0$ we look for satisfies

$$-\frac{m}{4\pi a_s} = \sum_{\mathbf{k}} \left[ \frac{\tanh(\frac{\xi_{\mathbf{k}}}{2T_0})}{2\xi_{\mathbf{k}}} - \frac{1}{2\varepsilon_{\mathbf{k}}} \right],$$

where $\xi_{\mathbf{k}} = \varepsilon_{\mathbf{k}} - \mu$, is the single particle energy measured with respect to the chemical potential. Finally the equation for the density allows to find $\mu$, this quantity will have an important role in the whole crossover.

$$n_0(\mu, T) = \sum_{\mathbf{k}} \left[ 1 - \tanh\left( \frac{\xi_{\mathbf{k}}}{2T} \right) \right]$$

It can be found that in the weak coupling limit, the BCS results are recovered, namely $\mu = \epsilon_F$ and $T_0 = 8e^{-2}\gamma\pi^{-1}\epsilon_F \exp(-\pi/2k_F|a_s|)$, which coincides

with the transition temperature. On the contrary in the limit ($\frac{1}{k_F a_s} \to \infty$) the pairs are strongly bound with energy $E_b = \frac{1}{ma_s^2}$, the chemical potential is negative $\mu \simeq -E_b/2$ and $T_0 \simeq (E_b/2)\ln(E_b/\epsilon_F)^{3/2}$. Therefore when the scattering length reaches large and negative values, $a_s \to -\infty$ the system is on the onset of a two body bound state, the limit $1/a_s = 0$ corresponds to a threshold for the existence of a true molecule with binding energy $E_b$.

However this approach does not apply properly in the strong interaction regime, basically because the normal phase we have assumed corresponds to Fermi gas, which is not true in Bosonic limit. There is no possibility to recover the bosonic degrees of freedom without including a dependence of the frequency in the quantum fluctuations which leads to the formation of a tight bound pair (Gaussian approximation). We will limit ourselves to mention the result without giving details of the calculation [42]. The temperature at which the superfluid transition takes places $T_c$ differs from $T_0$ which is related to the dissociation temperature, while in the weak coupling turn out to be the same quantity (in general this treatment does not affect the outcome we underlined for the weak coupling limit). The known BEC critical temperature is obtained, $T_c = \frac{\pi}{m}\left[\frac{n}{2\zeta(3/2)}\right]^{2/3}$ where $2m$ is the mass of the composite boson and $n/2$ its density. The chemical potential at the critical temperature corresponds to the energy necessary to break a pair, $\mu(T_c) = -E_b/2$. Clearly it changes sign through the crossover and it evolves between the two extreme cases smoothly. In Fig. 1 and 2 we show the behavior of the critical temperature and the chemical potential respectively, as a function of the inverse of the scattering length.

In this work we will constrain to work with Fermi dilute gases in the the limit when $a \to -\infty$, therefore far from the weak coupling limit, where we presume correlations between particles are no longer negligible.

## 1.2  Neutron Matter

Neutron stars are the densest objects known so far in the universe. Improving our understanding of this exotic systems implies a cooperative effort between different branches of physics, since all the forces (strong, electroweak and gravitational) are involved. Through the accessible observational probes, such as pulse radio emission, thermal X-ray radiation emitted from the surface and gravity waves, valuable information on their composition and dy-
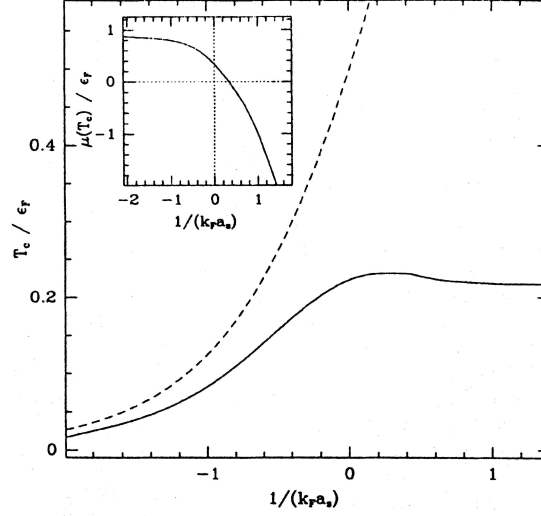
Figure 1.4: Chemical potential and Critical temperature in the crossover. Taken from [43]

namics is obtained, and reciprocally constituting a good test of our knowledge of nature at short distances and under strong interactions.

At such high densities (the Fermi temperature is around KeV, very small compared to the usual $T_F \sim$ MeV of Fermions in solids for instances), the nucleons undergo strong interactions which are responsible for the appearance of a superfluid phase. The existence of this state in neutron stars had already been predicted theoretically by Migdal [44] in 1959, two years later than the arrival of the BCS theory, but the observational proof did not arise until 1967 with the discovery of radio emissions of pulsars by Jocelyn Bell. These pulsed emissions turn out to have a perfect periodicity around seconds or less, which are closely related with the rotational period of the star. However some deviations in their periods have been registered, which can be divided in three kinds:

a) *Glitches or macrojumps*: They correspond to sudden increases in the rotational speed around $\Delta\Omega/\Omega \sim 10^{-6} - 10^{-8}$ and spin down rates of pulsars by $\Delta(d\Omega/dt)/\Omega \sim 10^{-3}$. The system returned to the initial values in a time that can vary from weeks to years, but in some cases the process is completely irreversible.

b) *Timing Noise or Microjumps.* Correspond to stochastic variations in

the spin and spin down rates which appear in superposition to the perfect periodicity of the star.

c) *Long Term Periodic Variabilities.* They are associated with the precession but this is a more rare event.

It is believed that the explanation for these anomalies is connected to the presence of a superfluid component which in the case of glitches is weakly coupled to the normal part of the star where the pulsed emission takes place. For microjumps, a stochastic coupling between the two components might be the reason, but it is unclear up to now. A schematic description of a neutron star is shown in Fig. 1.5

The hypothesis of superfluidity in the interior of neutron stars is supported by experimental evidence. The surface temperatures would be lower if no nucleon superfluidity was present. Many new information about dissipative processes is expected to confirm this picture, through the study of the gravitational waves emitted by such dense objects.
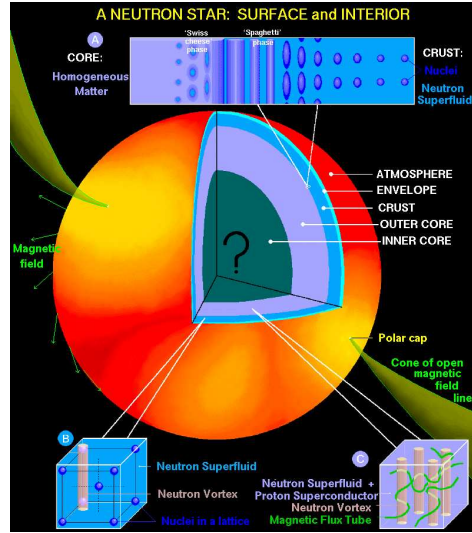


Figure 1.5: Schematic representation of the interior of a neutron star. Taken from [45]

The analysis of scattering process reveals the type of pairing channel preferred by the nucleonic system under study. The density and the isospin symmetry (balanced or unbalanced population of protons and neutrons), are

the parameters which tune the kind of dominant pairing channel, for instance at high densities (laboratory energies above 250 MeV) and for slightly broken isospin symmetry, the tensorial part of the Nucleon-Nucleon (NN) interaction is the most attractive, leading to a coupled $^3P_2 -^3 F_2$ favorable pairing channel. This is in general the case inside neutron stars. On the contrary when nucleonic matter is isospin symmetric, the $^3D_2$ is the most favorable.

At low density for symmetric nuclear matter, the tensorial part of the force, makes $^3S_1 -^3 D_1$ the most interacting pairing channel. This attractive interaction exhibits a bound state (the deuteron) in free space. For highly asymmetric isospin, the superfluidity phase is not supported due to the large difference in the Fermi momentum of proton and neutron components. In the inner crust of the neutron star, $^1S_0$ pairing in the neutron gas component, may occur at densities much lower than the saturation density $\rho_0 = 0.16$ fm$^{-3}$.

The study of the pairing phenomena cannot be treated without paying special attention to the strong coupling between Fermions which enriches but also complicates any approach. Many different techniques have been used to cope with it. Among them Green's function methods and the BCS mean field have described qualitatively the problem, and many of their insights became the starting point of *ab initio* calculations. From that knowledge, it is well known that the Gap in the weak coupling limit, behaves like

$$\Delta(p_F) = \mu^* e^{-\frac{1}{\nu(p_F)|V(p_F,p_F)|}}$$

where $\mu^*$ is an effective chemical potential, $\nu(p_F)$ is the density of states and $V(p_F, p_F)$ is the matricial element of the interaction at the Fermi momentum. Although the magnitude of the gap is correctly estimated, the approximation fails when having potentials whose matricial elements acquire a dependency on the momentum, for instance due to the presence of short range repulsive cores, as it is the case of realistic NN forces.

A first refinement of the theory consist of taking into account the influence of the medium in the interactions among the particles, which is addressed in the literature as the polarization effect. This has important consequences on the gap. On one hand, the density fluctuations tend to enhance the magnitude of the gap, since the effective attractive interactions are enlarged, but on the other hand the spin-density fluctuations tend to reduce the superfluid, and this is the leading effect in the inner crust of the neutron stars. Recently
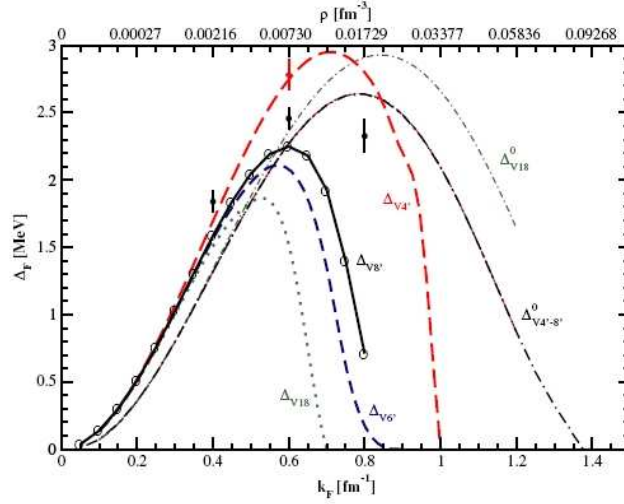
Figure 1.6: Single $S$-wave ($^1S_0$) pairing gap in neutron matter versus the Fermi momentum and the density. $\Delta^0_{v_n}$ stands for the Gap in the case of a pure BCS state. Instead $\Delta_{v_n}$ or $\Delta_{v'_n}$ corresponds to the Gap for correlated BCS state by using $v_n$ or $v'_n$ potentials respectively. The black points with error bars come from ADMC calculations. Taken from [17].

microscopic calculations based on the auxiliary field diffusion Monte Carlo (AFDMC) and lowest order Correlated Basis Function (CBF) and in pure neutron matter revealed that the effect of the polarization in $^1S_0$ pairing type has smaller influences than what found in previous studies [17].

In the same work, a calculation of gap was performed pointing a slight reduction with respect to the standard BCS theory. The maximum gap being 2.5 MeV at $k_F = 0.8$ fm$^{-1}$. In Fig. 1.6 we report their results for different nucleon-nucleon potentials ($v_n$), characterized by different number of spin-isospin operators: $v_4$, $v_6$, $v_8$, $v_{18}$ and $v_{4'}$, $v_{6'}$ and $v_{8'}$. For instance the first 6 operators $O^p(ij)$ for the pair of particles $ij$ are given by;

$$v_6(ij) = \sum_{p=1,6} v^p(r_{ij})O^p(ij)$$

where $O^1(ij) = 1$ (scalar term), $O^2(ij) = \overrightarrow{\sigma_i} \cdot \overrightarrow{\sigma_j}$ (spin spin interaction), $O^3(ij) = S(ij) = [3\widehat{r}_\alpha(i)\widehat{r}_\beta(j) - \delta_{\alpha\beta}]\,\sigma_\alpha(i)\sigma_\beta(j)$ (tensor operator) and $O^{p=p+3}(ij) = O^p(ij) \times \overrightarrow{\tau_i} \cdot \overrightarrow{\tau_j}$, with $\overrightarrow{\tau}$ the isospin and $p = 1, 2, 3$. The greek

indices stand for cartesian components.

The NN potential $v_{18}$ includes 18 operatorial components and it is obtained by fitting the NN data up to the threshold energy. The potentials $v_4$, $v_6$, $v_8$ are calculated from the $v_{18}$ potential by cutting out the extra 14, 12 and 10 operatorial components. The potentials $v_{4'}$, $v_{6'}$ and $v_{8'}$ are fitted to the lower energy NN scattering data, and they should consider as semirealistic potentials.

The short range correlations induced by the strong nuclear interactions can be incorporated within a variational description of the problem. The simplest level of the CBF theory (which this work concerns with) is to consider a pure Jastrow ansatz, namely,

$$\Psi_J(1, 2, ..., N) = \prod_{i<j=1,...,N} f_J(r_{ij})\Phi(1, 2, ..., N).$$

in which $\Phi(1, 2, ..., N)$ is a model function that describes the system at the noninteracting or weakly interacting level. In the case of superfluids, the model function is a BCS state,

$$|\text{BCS}\rangle = \prod_{\mathbf{k}}[u_{\mathbf{k}} + v_{\mathbf{k}}a_{\mathbf{k}\uparrow}^{\dagger}a_{-\mathbf{k}\downarrow}^{\dagger}]|0\rangle,$$

where $a_{\mathbf{k},\sigma}^{\dagger}$ $(a_{\mathbf{k},\sigma})$ is the creation (annihilation) operator of a Fermion in the single particle state with momentum $\mathbf{k}$ and $z$-spin component $\sigma$.

A useful improvement consist of constructing N body correlators having an operatorial dependence, for instance on the total spin-isospin, denoted as $\widehat{P}^{(ST)}(ij)$ (S stands for the singlet states and T for triplet).

$$\widehat{F}_4(1, 2, ..., N) = S\left[\prod_{i<j=1,...,N}\widehat{f}_4(ij)\right]$$

where

$$\widehat{f}_4(ij) = \sum_{S,T=0,1} f^{(ST)}(r_{ij})\widehat{P}^{(ST)}(ij)$$

However the feasibility of a full expansion by using FHNC methods is limited, because the different operators do not commuter among them. A Gap

equation has been derived by using such trial correlated state, performing a lowest order cluster expansion with the $\widehat{v}_4$ version of the Reid soft potential [46], [47]. In this formalism the correlation factors do not depend on the BCS amplitudes $u_{\mathbf{k}}$ and $v_{\mathbf{k}}$; this approach is denoted as Independent Cooper pairs (ICP). A larger gap of the BCS is obtained as a consequence of the repulsive behavior of the correlation.

The inclusion of tensor components also under the ICP for the Reid $\widehat{v}_6$ potential leads to a reduction of the Gap with respect to BCS. The calculations done by Chen [48] consider a simple choice for the Jastrow but the energy is calculated at higher order in the FHNC expansion. Polarization effects have also been taken in that work, which reduced the Gap by 80% compared to other studies and in contradiction with the X-ray observations. This underlying reason might be that second order is not enough in the problem of nuclei.

In this work we will consider the 4-term semirealistic Afnan-Tang potential, which for the case of neutron matter $\overrightarrow{\tau_i}=1$, becomes a 2-term potential. $^1S_0$ neutron pairing is considered therefore the BCS state is considered as the model state. Spin independent and dependent ($z$ component) correlations are assumed to correlated the particles. Under this simplified assumption the operators do commute among themselves and the FHNC expansion can be fully applied. The calculation of the energy as well as the one and two body momentum distributions is performed at full order. Although we do not expect to give a realistic description of the problem, our work constitute the first step towards a more careful approach to the pairing effects in neutron matter.

# Chapter 2

# Many-body methods

Many body systems have been widely studied under a great variety of techniques. Roughly we can divide them into two branches namely stochastic and non stochastic methods. The last approach implies an analytical procedure based either on perturbation theory or variational theories like for instance Fermi Hypernetted Chain (FHNC) [18]. In dealing with strongly correlated systems it is common to introduce a diagrammatic notation and devise resummation techniques to sum up infinite class of diagrams. On the other side stochastic methods are based on the use of random walks to sample the expectation values of physical quantities or the Schrödinger equation itself from a suitable distribution.

In the following, a general description of the auxiliary field diffusion Monte Carlo and of FHNC methods is given, referring them specifically to the treatment of superfluid systems.

## 2.1   Quantum Monte Carlo methods

The ability to introduce strong interactions in the problem relies on the previous knowledge obtained by a non stochastic previous study. Concerning the method itself, it is free from convergence problems (typical in the perturbative approach), but its main shortcoming is in the fact of considering a finite number of particles ("granular" simulations), which is particularly inconvenient when studying long range effects.

Among this methods the simplest version in the Variational Monte Carlo (VMC) in which a trial wave function is carefully chosen. The many body

integrals involved in the evaluation of the expectation values, are calculated by the Metropolis algorithm, and the generated statistical errors are controlled by variance reduction techniques. Comparing this method with its non stochastic counterpart, the FHNC, the former is more precise because the accurate evaluation of the integrals is translated into the inclusion of diagrams of higher order. In order to mimic the system a fixed number of particles is allocated in a cubic box of adjusted length to have the required density, then periodic boundary conditions are imposed.

A more refined stochastic method is the diffusion Monte Carlo (DMC),which solves the imaginary time Schrödinger equation for a $N$ body system, taking advantage of its similarity with a diffusion equation. It will be described briefly in what follows.

The Schrödinger equation in imaginary time, is given by:

$$-\frac{\partial \Psi}{\partial t} = (H - E)\Psi(\mathbf{R}, t), \tag{2.1}$$

where $\mathbf{R} = (\mathbf{r}_1, \mathbf{r}_2, ..., \mathbf{r}_N)$ is the $3N$ dimensional vector that allocates the position of the $N$ particles and $t$ is the imaginary time measured in units of $\hbar$.

The time dependent wave function $\Psi(\mathbf{R}, t)$ can be expanded in terms of a complete set of eigenfunctions $\phi_i(\mathbf{R})$ of the Hamiltonian:

$$\Psi(\mathbf{R}, t) = \sum_i c_i e^{[-(E_i - E)t]}\phi_i(\mathbf{R}), \tag{2.2}$$

where $E_i$ is the eigenvalue associated to the eigenvectors $\phi_i(\mathbf{R})$.

At large $t$ the ground state $\phi_o$ is projected out. DMC solves this diffusion equation stochastically by sampling the configurations $\mathbf{R}$ (called "walkers") according to Eq. (2.1). In order to efficiently solve the diffusion equation the importance sampling technique is used. It rewrites the Schrödinger equation in terms of the function

$$f(\mathbf{R}, t) \equiv \Xi(\mathbf{R})\Psi(\mathbf{R}, t) \tag{2.3}$$

where $\Xi(\mathbf{R})$ is a time-independent trial wave function that describes approximately the ground state of the system at the variational level.

When the Hamiltonian is of the form

$$H = \frac{\hbar^2}{2m}\nabla_{\mathbf{R}}{}^2 + V(\mathbf{R}), \tag{2.4}$$

Eq.. (2.1) turns out to be

$$-\frac{\partial f(\mathbf{R}, t)}{\partial t} = -D\nabla_{\mathbf{R}}^2 f(\mathbf{R}, t) + D\nabla_{\mathbf{R}}(F(\mathbf{R})f(\mathbf{R}, t)) + (E_L(\mathbf{R}) - E)f(\mathbf{R}, t),$$
(2.5)

where $D = \hbar^2/(2m)$ is called the diffusion coefficient and $E_L(\mathbf{R}) = \Phi(\mathbf{R})^{-1}H\Phi(\mathbf{R})$ is the local energy. The term

$$F(\mathbf{R}) = 2\Phi(\mathbf{R})_{-1}\nabla_{\mathbf{R}}\Phi(\mathbf{R}),$$
(2.6)

acts as an external force that guides the diffusion process to regions where $\Phi$ is large and it is called *drift* or *quantum force*.

In dealing with Fermions, which requires an antisymmetrized wave function, the problem of finding the right node surface appears. This is the main drawback of this method, which somehow it is cured by using the Fixed Node approximation. Such approximation is based on freezing the nodes of the trial wave function during the simulation. Therefore a bad nodal initial picture necessary in mapped in the final result. Details of DMC can be found in [49], [50].

Since this work is focuses in the study of fermionic pairing, a very good starting trial wave function is the BCS. This choice is constructed by anti-symmetrizing the product of the two-body (pair) functions having organized the particles of the system in pairs; perfect pair matching. Therefore any numerical simulation which made use of the BCS as a trial wave function requires a more sophisticated tool than a simple determinant (Slater type), called Pfaffian.

## 2.1.1 The Pfaffian

Let us start with the mathematical definition of the Pfaffian [51]. Let's consider a pair of elements $x$ and $y$, belonging to an index set $X$. Consider the quantity $h[xy]$, which satisfies the law of skew symmetry (antisymmetry):

$$h[xy] = -h[yx] \qquad \text{for} \qquad x, y \in X$$
(2.7)

This property can be extended to an arbitrary even number of elements, by defining the *Pfaffian*. For instance,

$$
\begin{aligned}
h[wxyz] &= h[wx]h[yz] - h[wy]h[xz] + h[wz]h[xy] \\
&= h[wx]h[yz] + h[wy]h[zx] + h[wz]h[xy].
\end{aligned}
\tag{2.8}
$$

Notice that $h[wxyz] = -h[xyzw]$. In general any odd permutation of the elements reverses the sign.

The Pfaffian can be written like the square of the determinant of a skew matrix $(c_{ij} = -c_{ji})$, *i.e*

$$
\det C = (\mathrm{Pf}\, C)^2
\tag{2.9}
$$

where $C$ correspond to the matrix of the perfect matchings between the elements, for instance

$$
C = \begin{pmatrix}
0 & c_{12} & c_{13} & c_{14} \\
-c_{12} & 0 & c_{23} & c_{24} \\
-c_{13} & -c_{23} & 0 & c_{34} \\
-c_{14} & -c_{24} & -c_{34} & 0
\end{pmatrix}.
$$

Determinants are special cases of Pffafians when the skew matrix is *bipartite*. Suppose that $h[xy] = 0$ when $x$ and $y$ belong to the same part. It is useful to imagine that the set of indices consists of two disjoint sets $X$ and $\overline{X}$ so that $x \in X$ and $\overline{x} \in \overline{X}$. Then the matrix is bipartite if $h[xy] = 0$ and $h[\overline{xy}] = 0$. For instance, let particles 1 and 2 belong to the set $X$ and 3 and 4 to $\overline{X}$, therefore $c_{12} = 0$ and $c_{34} = 0$. In that case we can write the matrix $C$ in the form:

$$
C = \begin{pmatrix} 0 & B \\ -B^T & 0 \end{pmatrix}
$$

where $B$ is the matrix of non zero elements of $C$, $B^T$ is its transpose and 0 is the zero matrix. In such a case, $\det A = (\det B)^2$ and therefore, the Pfaffian is a determinant:

$$
\mathrm{Pf}\, C = \det B
\tag{2.10}
$$

Since, by construction, BCS type wave function $\Phi_{\mathrm{pairing}}$ is an antisymmetric sum over the perfect matchings [1] between particles, then Pfaffian is

---

[1]A perfect matching is a partition into pairs.

the quantity we need to compute. The pair function $\phi(r_{ij})$ is already a function that satisfies the antisymmetrization condition required for $h$. Then the pairing wave function can be written like:

$$\Phi_{\text{pairing}}(\mathbf{R}) = \text{Pf} \begin{pmatrix} 0 & \phi_{12} & \phi_{13} & \dots & \phi_{1N} \\ -\phi_{12} & 0 & \phi_{23} & \dots & \phi_{2N} \\ \vdots & \vdots & \ddots & \vdots & \vdots \\ -\phi_{1N} & -\phi_{2N} & \dots & \dots & 0 \end{pmatrix}$$

where the number of particles $N$ is assumed to be even. Notice that in the case of a *singlet* state, the matrix $C$ is bipartite, where the set $X$ corresponds to spin-up particles and $\overline{X}$ to spin-down particles. It follows that the Pfaffian can be written as a determinant and its calculation is straightforward. This is not true anymore if the pairing is of the $p$ type, for instance. Another important case of not-bipartite matrix concerns to spin-dependent Hamiltonians, this is the case of neutron matter in which we are interested in.

The Quantum Monte Carlo method to be used in these cases is the Auxiliary Field Diffusion Monte Carlo. The technique, originally developed by Schmidt and Fantoni [16], can be viewed as an extension of the method by Zhang *et. al.* [52], [53] for lattices in which the spin-isospin degrees of freedom of nucleons are sampled while the spatial degrees are handle with standard diffusion Monte Carlo. It has been successfully applied in the nuclear matter in the study of large nucleon system (up to $A \lesssim 100$) interacting via semirealistic [54] as well as full realistic
nuclear interactions [55] and in spin-polarized systems [56].

The study of superfluids in QMC implies the use of a correlated BCS state as a guiding function which is translated into introducing a correlated Pfaffian, namely:

$$\Psi(\mathbf{R}) = \prod_{i,j} f_J(\mathbf{r}_{ij}) \Phi_{\text{pairing}}(\mathbf{R}) \tag{2.11}$$

in which $\Phi_{\text{pairing}}(\mathbf{R})$ (the Pfaffian) corresponds to a projected BCS state with a fixed number of even particles, properly correlated with a Jastrow function $f_J(\mathbf{r}$.

In the following section we focus the attention on many-body theories in particular the Fermi Hyper-netted chain, to study BCS-superfluids in the strongly correlated regime.

## 2.2   FHNC method

Perturbation theory is one of the most common approaches to address many body problems. It uses the noninteracting states as a base to construct a solution in terms of a normalized parameter which modulates the strength of the interaction. The problem of long range interactions (electronic case for instance) can be properly cured by rearrangements or resummations. In particular the random-phase approximation is used to sum certain diagrams (ring diagrams) leading to produce a screening of the Coulomb long range potential. But any attempt to tackle hard core problems or very strongly repulsive potentials, like helium liquids, fails under any perturbative method. Still particular summations (ladder terms) can be performed under the Brueckner-Hartree-Fock theory to handle problems in nuclear matter at not very high densities.

Although the clear analysis that is possible to extract from a perturbative study, specially in limiting conditions, the feasibility of this method is very restricted.

On the other hand variational methods, can be easily adapted to cope with strongly correlated systems. When interactions are highly repulsive, the need of introducing dynamical correlations allows to overcome the difficulty. This approach starts from the construction of a many body wave function which describes the problem at the noninteracting level or weakly interacting. Next a proper correlation function if chosen to cure the strongly nature of the interactions. The most common choice is the Jastrow type, which forces a pair of particles to have the desired short range behavior. More sophisticated include for instance, triplet, backflow type (momentum depending), spin dependent and non central (tensorial) correlations. Dealing with such function improves cluster expansion and resummation methods. FHNC is the most powerful of such techniques, and it is the focus of our attention in this thesis.

A further improvement is given by the correlated basis function (CBF) perturbative theory, which is based upon a variational Jastrow correlation wave function and FHNC summations.
We will generalize in the following the FHNC theory to deal with Fermi systems in the superfluid phase.

## 2.2.1  FHNC for longitudinal spin dependent correlated Fermi gases

Before addressing the BCS problem, we will review the theory for the case of a pure Slater determinant as a model function, introducing longitudinal spin dependence in the Jastrow correlator, originally developed by Fantoni and Fabrocini [57], [58]. Since we are dealing with Fermions of spin 1/2, there are two possible spin configurations for the pair, either parallel or antiparallel, then the spin degeneracy $\nu = 2$, being the parallel case labeled by (p) and the antiparallel by (a). The two body correlation factor is given then by

$$f(i,j) = \sum_{k=1}^{\nu} f_{(k)}(r_{ij})\mathrm{P}_{\nu}^{(k)}(i,j), \qquad (2.12)$$

with $\mathrm{P}_{\nu}^{(k)}(i,j)$ the projection operator of the spin state of particles $i$ and $j$ on the state $(k)$. In the case $\nu = 2$ they are,

$$\mathrm{P}_{\nu=2}^{(p)}(i,j) = \frac{1}{2}(1 + \sigma_{iz}\sigma_{jz}), \qquad \mathrm{P}_{\nu=2}^{(a)}(i,j) = \frac{1}{2}(1 - \sigma_{iz}\sigma_{jz}).$$

The parallel and antiparallel component can be found by solving the Euler-Lagrange equations which will be stated.

Basically the calculation of the expectation value of the two body operators we are interested in, is done through the two body radial distribution function defined by

$$g^{(k)}(r_{12}) = \frac{N(N-1)}{\eta\rho^2} \int d\mathbf{x}_3...d\mathbf{x}_N \Phi^*(\mathbf{R})\mathrm{F}\mathrm{p}^{(m)}(1)\mathrm{p}^{(n)}(2)\mathrm{F}\Phi(\mathbf{R}) \qquad (2.13)$$

where $\eta$ is a normalization constant, $\mathrm{p}^{(m)}(i)$ is the projection operator for particle $i$ on state $m$ (defined $z$ spin component), and the integration is done over the position and spin coordinates of the N-2 particles different from 1 and 2. States $m$ and $n$ for particles 1 and 2 respectively, correspond to the pair state $k$. The many-body state $\Phi(\mathbf{R})$ describes the system at a noninteracting level or undergoing weak interactions. In this work a Fermi see in momentum space namely a Slater determinant in coordinates, was considered.

The main difference respect to the state independent correlated case, is the presence of the operators which in general introduce undesirable commutators. For the chosen Jastrow, due to the commutativity of the $z$ Pauli matrices, it is possible to group the correlators:

$$\mathrm{F}^2 = \prod_{i<j} f^2(i,j) = \prod_{i<j} \sum_{k=1}^{\nu} [f_{(k)}(r_{ij})]^2 \mathrm{P}_\nu^{(k)}(i,j) = 1 + \sum_{k=1}^{\nu} h_{(k)}(r_{ij}) \mathrm{P}_\nu^{(k)}(i,j).$$
(2.14)

having replaced Eq..(2.12) and defining $h_{(k)}(r_{ij}) = f_{(k)^2}(r_{ij}) - 1$. The function $h_{(k)}$ is used as a parameter of expansion since the property $\lim_{r_{ij}\to 0} h_{(k)}(r_{ij}) = 0$ holds.

The standard FHNC technique originally developed in [18], uses the fact that the denominator cancels against the unlinked and reducible (factorizable) parts of the numerator of $g_{(r_{12})}$, in that way its calculation is reduced to sum all the irreducible terms of the numerator; the so called *nodal* and *composite* diagrams. The presence of a state dependent Jastrow operator maintains the expansion linked, but in general the irreducibility does not hold. For the simplified version we chose, both of them still apply and no particular difficulties arise.
Essentially the convolutions used in the extended FHNC will link any two particles in $\nu$ different ways. A generic term in the cluster expansion is then of the form,

$$z(i,j) = \sum_{k=1}^{\nu} z^{(k)}(r_{ij}) \mathrm{P}_\nu^{(k)}(i,j) = \int d\mathbf{x}_m p(i,m) \rho(m,m) q(m,j) \qquad (2.15)$$

where the components are given by

$$z^{(p)}(r_{ij}) = \frac{\rho}{2} \int d\mathbf{r}_m [p^{(p)}(r_{im}) q^{(p)}(r_{mj}) + p^{(a)}(r_{im}) q^{(a)}(r_{mj})]$$

$$z^{(a)}(r_{ij}) = \frac{\rho}{2} \int d\mathbf{r}_m [p^{(p)}(r_{im}) q^{(a)}(r_{mj}) + p^{(a)}(r_{im}) q^{(p)}(r_{mj})].$$
(2.16)

Much care must be taken when there is a statistical correlation between particles $(\ell(k_F r) = \frac{1}{(2\pi)^3 \rho} \int_{k \leq k_F} d\mathbf{k} e^{i\mathbf{k}\cdot\mathbf{r}})$, because necessary the dynamical correlation (if existing) must be of type $h^{(p)}$, in which the spin of the particles

is the same.

The nodal equations are then given by,

$$
\begin{aligned}
N_{dd}(r_{12}) &= \{X_{dd}(r_{13}) + X_{de}(r_{13})|N_{dd}(r_{32}) + X_{dd}(r_{32})\} + \\
&\quad \{X_{dd}(r_{13})|N_{ed}(r_{32}) + X_{ed}(r_{32})\} \\
N_{de}(r_{12}) &= \{X_{dd}(r_{13}) + X_{de}(r_{13})|N_{de}(r_{32}) + X_{de}(r_{32})\} + \\
&\quad \{X_{dd}(r_{13})|N_{ee}(r_{32}) + X_{ee}(r_{32})\} \\
N_{ee}(r_{12}) &= \{X_{ed}(r_{13})|N_{ee}(r_{32}) + X_{ee}(r_{32})\} + \\
&\quad \{X_{ed}(r_{13}) + X_{ee}(r_{13}|N_{de}(r_{32}) + X_{de}(r_{32})\} \\
N_{cc}^{(p)}(r_{12}) &= \frac{\rho}{\nu} \int d\mathbf{r}_3 [X_{cc}^{(p)}(r_{13})(N_{cc}^{p}(r_{32}) + X_{cc}^{p}(r_{32})) - \ell(k_F r_{13})X_{cc}^{(p)}(r_{32})]
\end{aligned}
\tag{2.17}
$$

and the composite ones,

$$
\begin{aligned}
X_{dd}^{(k)}(r) &= F^{(k)}(r) - N_{dd}^{(k)}(r) - 1 \\
X_{de}^{(k)}(r) &= (F^{(k)}(r) - 1)N_{de}^{(k)}(r) \\
X_{ee}^{(k)}(r) &= F^{(k)}(r)[N_{ee}^{(k)}(r) - (\ell(k_F r) - N_{cc}^{(k)}(r))^2 \delta_{k,p} + N_{de}^{(k)2}(r)] - N_{ee}^{(k)} \\
X_{cc}^{(p)}(r) &= (F^{(p)}(r) - 1)(N_{cc}^{(p)} - \ell(k_F r)).
\end{aligned}
\tag{2.18}
$$

The subindexes $d$, dynamical and $e$, exchange (two statistical lines), refer to the kind of correlation reaching the external points (particles 1 and 2) while $cc$ means that both points are touched by only one statistical line. The function $F^{(k)}$ is defined by

$$
F^{(k)}(r) = f_{(k)}^2(r)e^{N_{dd}^{(k)}(r)}, \qquad k = a, p.
\tag{2.19}
$$

Those coupled equations constitute the FHNC/0 (elementary diagrams are neglected). Once they are solved, the expression for the radial distribution function in terms of nodal functions corresponds to,

$$
g^{(k)}(r_{12}) = F^{(k)}(r_{12})[(1 + N_{de}^{(k)}(r_{12}))^2 + N_{ee}^{(k)}(r_{12}) - (l(k_F r_{12}) - N_{cc}^{(k)}(r_{12}))^2 \delta_{k,1}].
\tag{2.20}
$$

## 2.3   FHNC/BCS

### 2.3.1   Correlated BCS ansatz and cluster expansion

In this section we extend the FHNC/BCS theory of I to Jastrow-type correlations which can distinguish between spin parallel and spin antiparallel pairs. It is well known that $\sigma_z$ dependent correlations do not improve significantly the variational upper bounds obtained with the simple Jastrow ansatz for Fermi systems in the normal phase, like for instance liquid $^3$He. However one expects that for superfluid systems, because of the pairing between $\mathbf{k} \uparrow$ and $-\mathbf{k} \downarrow$ states, the two-body correlation $f_p(r_{ij})$ between spin-parallel pairs be different from $f_a(r_{ij})$ correlating spin-antiparallel pairs. Such an extension of FHNC/BCS theory requires only minor modifications of the derivation given in I, since $\sigma_z$ dependent correlations commute among themselves. As a consequence differently from the case of full spin-dependent correlations (which do not commute each other) [47], one is still able to carry a full FHNC summations, the only limitation being a self consistent inclusion of bridge diagrams.

### 2.3.2   The correlated BCS ansatz

The correlated BCS state is defined by

$$|\text{CBCS}\rangle = \sum_N \sum_{\{m_N\}} \hat{F}_N |\Phi_{(m_N)}\rangle \langle \Phi_{(m_N)}|\text{BCS}\rangle, \qquad (2.21)$$

where the $|\text{BCS}\rangle$ state is given by

$$|\text{BCS}\rangle = \prod_{\mathbf{k}} [u_{\mathbf{k}} + v_{\mathbf{k}} a_{\mathbf{k}\uparrow}^\dagger a_{-\mathbf{k}\downarrow}^\dagger]|0\rangle, \qquad (2.22)$$

where $a_{\mathbf{k},\sigma}^\dagger$ ($a_{\mathbf{k},\sigma}$) is the creation (annihilation) operator of a Fermion in the single particle state having momentum $\mathbf{k}$ and $z$-spin component $\sigma$, namely

$$\langle r|a_{\mathbf{k},\sigma}^\dagger|0\rangle = \frac{1}{\sqrt{\Omega}} e^{i\mathbf{k}\cdot\mathbf{r}} \eta(\sigma) \equiv \varphi_{\mathbf{k},\sigma}(\mathbf{r}). \qquad (2.23)$$

The state $\Phi_{(m_N)}$ in Eq. (2.21) corresponds to a Slater determinant of $N$ single particle orbitals with labels $\{m_N\}$,

$$\langle r_1, \ldots, r_N|\hat{F}_N|\Phi_{(m_N)}\rangle = \prod_{i<j}^N F(ij) \frac{\hat{\mathcal{A}}\{\varphi_{m_1}(\mathbf{r}_1) \ldots \varphi_{m_N}(\mathbf{r}_N)\}}{\sqrt{N!}} \qquad (2.24)$$

where $r_i \equiv (\mathbf{r}_i, \eta_i)$ and $m_i \equiv (\mathbf{k}, \sigma)$ and $\mathrm{F}(ij)$ can be decomposed as:

$$\mathrm{F}(ij) = f_p(r_{ij})\mathrm{P}_p(ij) + f_a(r_{ij})\mathrm{P}_a(ij). \qquad (2.25)$$

The spin projection operators $\mathrm{P}_p(ij)$ and $\mathrm{P}_a(ij)$ are given by,

$$\mathrm{P}_p(ij) = \frac{1 + \sigma_z(i)\sigma_z(j)}{2}, \qquad \mathrm{P}_a(ij) = \frac{1 - \sigma_z(i)\sigma_z(j)}{2},$$

where $\sigma_z| \uparrow \rangle = 1$ and $\sigma_z| \downarrow \rangle = -1$. One can also write the $\sigma_z$-dependent correlation in the form,

$$\mathrm{F}(ij) = \frac{[f_p(r_{ij}) + f_a(r_{ij})]}{2} + \frac{[f_p(r_{ij}) - f_a(r_{ij})]}{2}\sigma_z(i)\sigma_z(j), \qquad (2.26)$$

the Jastrow case of I is recovered for $f_p(r_{ij}) = f_a(r_{ij}) = f(r_{ij})$.
In Eq. (2.21) the summation over $N$ is extended to any even number of particles, and for a given $N$ the summation over $\{m_N\}$ is done over all the possible orbital states, $m_N$ labeling a set of such $N$ orbital states. The state vector $|\mathrm{CBCS}\rangle$ is not an eigenstate of the particle-number operator $\hat{N}_{OP} = \sum_m a_m^\dagger a_m$. However, fluctuations around $\langle \hat{N}_{OP} \rangle / \Omega = \rho$, with $\rho$ being the density of the system, goes as $1/\Omega$ and therefore can be neglected in the thermodynamic limit of physical quantities, such as the energy per particle or the momentum distribution (see I).

### 2.3.3 Cluster expansion

Let us calculate the expectation value of a given two-body scalar (spin independent) operator $\hat{Y}$, whose representation in $R$ space is given by

$$\langle \mathbf{R}_N | \hat{Y} | \mathbf{R}_N \rangle = \sum_{j>i=1}^{N} Y(r_{ij}) = \frac{1}{2}\sum_{i \neq j} Y(r_{ij}) \qquad (2.27)$$

where $|\mathbf{R}_N\rangle = |\mathbf{r}_1 \ldots \mathbf{r}_N\rangle$. From Eq.. (2.21) and (2.24) we have

$$
\begin{aligned}
\langle \mathrm{CBCS}|\hat{Y}|\mathrm{CBCS}\rangle \;=\; & \frac{1}{2}\sum_{N}\frac{1}{(N-2)!}\sum_{\substack{n_1,\ldots,n_N \\ m_1,\ldots,m_N}}\int \mathrm{d}r_1 \ldots \mathrm{d}r_N \\
& [\varphi_{n_1}^*(\mathbf{r}_1) \ldots \varphi_{n_N}^*(\mathbf{r}_N)] \, Y(r_{12}) \prod_{j>i} \mathrm{F}^2(ij)[\varphi_{m_1}(\mathbf{r}_1) \ldots \varphi_{m_N}(\mathbf{r}_N)] \\
& \langle \mathrm{BCS}|a_{n_1}^\dagger \ldots a_{n_N}^\dagger|0\rangle\langle 0|a_{m_N} \ldots a_{m_1}|\mathrm{BCS}\rangle, \qquad (2.28)
\end{aligned}
$$

where the factor $\frac{1}{(N-2)!}\frac{1}{2}$ comes from the normalization factor $\frac{1}{N!}$ times $\frac{N(N-1)}{2}$ which is the number of pairs in $\hat{Y}$ for $N$-particles state. Integration $\int dr_i$ means both spatial integration $\int d\mathbf{r}_i$ and spin summation for particle $i$, namely

$$
\begin{aligned}
\langle \sigma_{n_i}(i)|\sigma_{m_i}(i)\rangle &= \left(s_{n_i}^{(1)}(i), s_{n_i}^{(2)}(i)\right) \begin{pmatrix} s_{m_i}^{(1)}(i) \\ s_{m_i}^{(2)}(i) \end{pmatrix} \\
&= \sum_{\alpha=1}^{2} s_{n_i}^{\alpha}(i) s_{m_i}^{\alpha}(i) \qquad\qquad (2.29)
\end{aligned}
$$

which gives 1 if both $\sigma_{n_i}$ and $\sigma_{m_i}$ are up-particle (1,0) states or down-particle (0,1) states and zero otherwise.

If the spin degeneracy $\nu$ is equal to 4, like for instance in nuclear matter, then the label $\alpha$ in Eq. (2.29) runs from 1 to 4 instead from 1 to 2.

Following the usual method of doing cluster expansion, let us expand the correlation term $\prod F^2(ij)$ in terms of cluster operators. Writing $F^2(ij)$ in the form,

$$
\begin{aligned}
\hat{F}^2(ij) &= f_p^2(r_{ij})\hat{P}_p(ij) + f_a^2(r_{ij})\hat{P}_a(ij) \\
&= 1 + h_p(r_{ij})\hat{P}_p(ij) + h_a(r_{ij})\hat{P}_a(ij) \\
&\equiv 1 + \hat{h}(ij), \qquad\qquad (2.30)
\end{aligned}
$$

we consider $\hat{h}(ij)$ as a "small" operator and we develop $\langle \mathbf{R}_N|\hat{Y}|\mathbf{R}_N\rangle$ as a power series of it. In order to do so we first expand $Y(r_{12})\prod \hat{F}^2(ij)$,

$$
Y(r_{12})\prod \hat{F}^2(ij) = \hat{X}_2(12) + \sum_{k>3}\hat{X}_3(1,2;k) + \dots \qquad (2.31)
$$

where

$$
\hat{X}_2(12) = Y(r_{12})\hat{F}^2(12) \qquad\qquad (2.32)
$$

is singled out in all the terms of the r.h.s. of Eq. (2.31). This is because 1 and 2 are the "interacting particles" (also denoted as "external indices"); in fact $Y(r_{12})$ may have strong repulsion at short distances and therefore need to be dressed by $F^2(12)$ in all the cluster terms since $Y(r_{12})F^2(12)$ is well behaved in the full range of $r_{12}$.

The three-body term in Eq. (2.31) is given by

$$
\hat{X}_3(1,2;k) = \hat{X}_2(1,2)\big(\hat{h}(1k) + \hat{h}(2k) + \hat{h}(1k)\hat{h}(2k)\big), \qquad (2.33)
$$

and the various expressions for $\hat{X}_p$ with $p > 3$ are obtained in a straightforward manner.

Let us now insert Eq. (2.31) into Eq. (2.28) with the result

$$\langle \text{CBCS} | \hat{Y} | \text{CBCS} \rangle = \frac{1}{2} \sum_p \frac{1}{(p-2)!} \int d\mathbf{r}_1 \ldots d\mathbf{r}_p \mathscr{L}_p(\mathbf{r}_1, \ldots, \mathbf{r}_p)$$

where

$$\mathscr{L}_p(\mathbf{r}_1, \ldots, \mathbf{r}_p) = \sum_{\substack{s_1, \ldots, s_p}} \sum_{\substack{n_1, \ldots, n_p \\ m_1, \ldots, m_p}} \varphi_{n_1}^*(\mathbf{r}_1) \ldots \varphi_{n_p}^*(\mathbf{r}_p) \, \hat{X}_p(12; 3, \ldots, p) \, \varphi_{m_1}(\mathbf{r}_1) \ldots \varphi_{m_p}(\mathbf{r}_p)$$

$$\langle \text{BCS} | a_{n_1}^\dagger \ldots a_{n_p}^\dagger a_{m_p} \ldots a_{m_1} | \text{BCS} \rangle, \tag{2.34}$$

where, differently from the Jastrow case of I, the cluster operator $\hat{X}_p(12; 3, \ldots, p)$ generates different functions depending on the spin states $\sigma_1, \ldots, \sigma_p$. The projector on the vacuum $|0\rangle\langle 0|$ of Eq. (2.28) is disappeared in Eq. (2.34). This is because in Eq. (2.28) any cluster term $\hat{X}_p$ involving $p$ particles appears in all the terms of summation over $N$, with $N \geq p$. Integration over the $N - p$ uncorrelated particles $p + 1, p + 2, \ldots, N$ gives 1 and implies $n_{p+1} = m_{p+1}, \ldots, n_N = m_N$. Such term has a factor $\frac{1}{(N-2)!}$ in Eq. (2.28), which after the summation over all the permutations of states $\varphi_{m_{p+1}}, \ldots, \varphi_{m_N}$ reduces to $\frac{1}{(p-2)!}$. Collecting up all such terms with $N \geq p$ one gets the overall projection operator

$$\hat{P}_p = |0\rangle\langle 0| + \sum_{m_{p+1}} a_{m_{p+1}}^\dagger |0\rangle\langle 0| a_{m_{p+1}} + \sum_{m_{p+1}, m_{p+2}} a_{m_{p+1}}^\dagger a_{m_{p+2}}^\dagger |0\rangle\langle 0| a_{m_{p+1}} a_{m_{p+2}} + \ldots$$

$$\tag{2.35}$$

which coincides with the identity operator. Therefore for any value of $p$, $\hat{P}_p = \mathbb{I}$.

The calculation of the r.h.s of Eq. (2.34) is performed by using the Wick's contraction algebra as in I, which leads to the following exchange functions

$$l_v(r_{ij}) = \frac{2}{(2\pi)^3 \rho_0} \int d\mathbf{k} \, v_{\mathbf{k}}^2 \, e^{i\mathbf{k}\cdot\mathbf{r}}, \tag{2.36}$$

for spin parallel pairs which are correlated with $f_p^2(r_{ij})$, and

$$l_u(r_{ij}) = \frac{2}{(2\pi)^3 \rho_0} \int d\mathbf{k} \, u_{\mathbf{k}} v_{\mathbf{k}} \, e^{i\mathbf{k}\cdot\mathbf{r}}, \tag{2.37}$$

for spin antiparallel pairs which are correlated with $f_a^2(r_{ij})$. As for the case of fluids in the normal phase, the exchange functions form disjoint loops. In the superfluid phase each exchange loop may have any number of $v$-exchanges, but only an even number of $u$-exchanges (there are no $u$-exchanges in the normal phase). For this reason it is convenient to collect both exchange correlations in a single complex operator

$$\hat{L}(r_{ij}) = -\frac{1}{2}l_v(r_{ij})\hat{P}_p(ij) + \frac{i}{2}l_u(r_{ij})\hat{P}_a(ij).$$ (2.38)

which reduces to the standard Fermi exchange function $-\frac{1}{2}l(r_{ij})$ for the normal phase, which can be obtained in the limit $v_{\mathbf{k}}^2 \to \Theta(k - k_F)$ and $u_{\mathbf{k}} \to 0$. The density of the uncorrelated BCS state $\rho_0$ is define in the following way:

$$\rho_0 = \frac{\nu}{(2\pi)^3} \int \mathrm{d}\mathbf{k}v^2(k)$$ (2.39)

and when the normal phase is recovered it coincides with the energy of the system, $\rho_0 = \rho$.

The $\sigma_z$-dependence of the correlations does not affect the linked cluster property of the expectation value of $\hat{Y}$,

$$\langle\hat{Y}\rangle = \frac{\langle\mathrm{CBCS}|\hat{Y}|\mathrm{CBCS}\rangle}{\langle\mathrm{CBCS}|\mathrm{CBCS}\rangle}.$$ (2.40)

As in the Jastrow case of I, the denominator $\langle\mathrm{CBCS}|\mathrm{CBCS}\rangle$ exactly cancels the unlinked portions present in the numerator, therefore only linked cluster diagrams containing the two interacting particles 1 and 2 are left, with the result,

$$\langle\hat{Y}\rangle = \frac{1}{2}\sum_p \frac{1}{(p-2)!} \int \mathrm{d}\mathbf{r}_1 \ldots \mathrm{d}\mathbf{r}_p \mathscr{L}_p^{(\mathrm{linked})}(\mathbf{r}_1, \ldots, \mathbf{r}_p),$$ (2.41)

where $\mathscr{L}_p^{(\mathrm{linked})}(\mathbf{r}_1, \ldots, \mathbf{r}_p)$ is given by a sum of linked cluster terms having $p$-particles,

$$\mathscr{L}_p^{(\mathrm{linked})}(\mathbf{r}_1, \ldots, \mathbf{r}_p) = \sum_\alpha \mathscr{L}_{p,\alpha}^{(\mathrm{linked})}(\mathbf{r}_1, \ldots, \mathbf{r}_p).$$ (2.42)

For instance $\mathscr{L}_2^{(\mathrm{linked})}(\mathbf{r}_1, \mathbf{r}_2)$ is made up of 3 cluster terms or equivalently of 3 cluster diagrams.

$$\mathscr{L}_2^{(\mathrm{linked})}(\mathbf{r}_1, \mathbf{r}_2) = Y(r_{12})\left\{\frac{1}{2}\big(f_p^2(r_{12})+f_a^2(r_{12})\big)-\frac{1}{2}h_p(r_{12})l_v^2(r_{12})+\frac{1}{2}h_a(r_{12})l_u^2(r_{12})\right\}$$ (2.43)

At the three-body level one has 33 cluster diagrams which can be easily constructed dressing the r.h.s of Eq. (2.33) with all the possible exchanges.
As for the Jastrow case of I, the cluster diagrams are not all irreducible and one has to use the renormalized version of FHNC theory RFHNC to sum them up [59]. The RFHNC cluster diagrams are irreducible, but each dot is "dressed" with a vertex correction which sums up the reducible portions attached to it.
The cluster terms $\mathscr{L}_{p,\alpha}^{(\text{linked})}$ are better represented by diagrams in which dots stand for particles and lines for correlations. The interacting particles 1 and 2 are represented by empty dots, and particles in the medium by full dots. Exchange correlations $l_v(r_{ij})$ and $l_u(r_{ij})$ are represented by oriented solid lines with labels $v$ and $u$ respectively, dynamical correlations $h_p(r_{ij})$ and $h_a(r_{ij})$ by dashed lines with labels $p$ and $a$ respectively.

The diagrammatical rules are very similar to those given in I for the Jastrow case. We report them here for clarity:

- Exchange correlations $l_v$ and $l_u$ form closed loops without common points.

- A given exchange loop with $p$ dots may have any number, $n_v \leqslant p$, of $l_v$ exchanges, whereas only an even number $n_u \leqslant p$ of $l_u$ exchanges is allowed.

- Each closed loop carries a factor $-2\nu(-1/\nu)^{n_v}(i/\nu)^{n_u}$ where $\nu = 2$ is the spin degeneracy.

- $v$-exchanged pairs can only be correlated with $h_p$ functions, whereas $u$-exchanged pairs can only be correlated with $h_a$. Not-exchanged pairs can be correlated with both $h_p$ and $h_a$ and therefore by the function $\frac{1}{2}(h_a + h_p)$.

- The interacting particles 1 and 2 are always dressed by $Y(r_{12})\hat{F}^2(12)$. The operator $\hat{F}^2(12)$ becomes $f_p^2(r_{12})$, $f_a^2(r_{12})$ or $\frac{1}{2}\big(f_p^2(r_{12}) + f_a^2(r_{12})\big)$ depending on the spin states of particles 1 and 2.
  The operator $\hat{F}^2(12)$ gives the correlation function $f_p^2(r_{12})$ if the 1-2 spin state is parallel, or $f_a^2(r_{12})$ if antiparallel. For the two-body cluster with no exchange, $\hat{F}^2(12)$ gives rises to $\frac{1}{2}\big(f_p^2(r_{12}) + f_a^2(r_{12})\big)$.

- Each dot (empty or full) carries a vertex correction. There are two types of vertex corrections

$$c_d = \rho_0 e^{U_d},$$
$$c = (1 + U_e)c_d, \tag{2.44}$$

  Dots which are reached by one or more exchange lines carry the vertex correction $c_d$ whereas the other ones are associated with $c$. Dots which are reach by exchange lines only carry the vertex correction $(c_d - 1)\rho_0$.

Fig. (2.1) displays an example of 4-body linked diagram corresponding to

$$\mathscr{L}_{4,\alpha}^{(\text{linked})} = -4\, Y(r_{12}) \frac{f_p^2(r_{12}) + f_a^2(r_{12})}{2} \frac{l_v(r_{23})h_p(r_{23})}{2} \frac{l_u(r_{34})h_a(r_{34})}{2} \frac{l_u(r_{24})}{2} \tag{2.45}$$

where the $v$-exchanged particles 2 and 3 are correlated with $h_p(r_{23})$ whereas the $u$-exchanged particles 3 and 4 are correlated with $h_a(r_{34})$. The interacting particles 1 and 2, which are not exchanged are correlated with $\frac{1}{2}(f_a^2 + f_p^2)$.
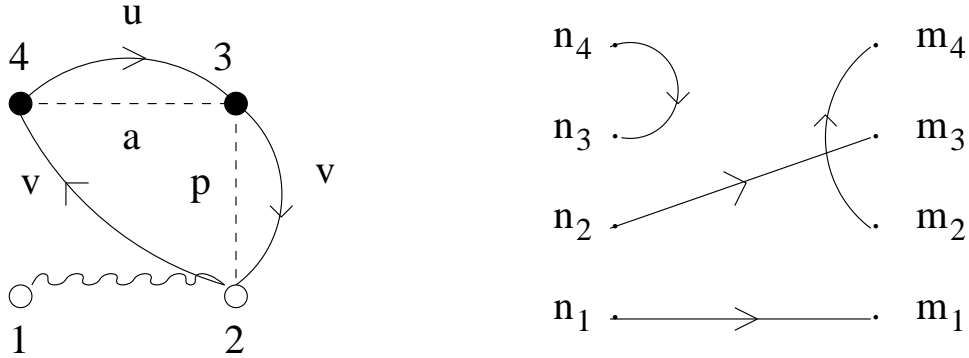


Figure 2.1: Graphical representation of $\mathscr{L}_{4,\alpha}$ of Eq. (2.45). The diagram on the right displays the corresponding set of Wick's contractions. The points in the left column correspond to the indices $n_\alpha$. Those in the right column correspond to the indices $m_\alpha$. An arrow connecting two points represents a contraction. The arrows along the columns correspond to contractions of the type $a^\dagger a^\dagger$ or $aa$, existing only in the superfluid phase.

The FHNC/BCS equations to compute the pair distribution function entering in the calculation of $\langle \hat{Y} \rangle$, through the equation

$$\langle \hat{Y} \rangle = \frac{1}{2} \langle \hat{N} \rangle \rho \int \mathrm{d}\mathbf{r}_{12} Y(\mathbf{r}_{12}) g(\mathbf{r}_{12}), \qquad (2.46)$$

where

$$\langle \hat{N} \rangle \rho = (c\rho_0)^2 \Omega, \qquad (2.47)$$

are given in Appendix A. Appendix B will present the FHNC/BCS equations to compute the expectation value of a spin-dependent two-body potential.

## 2.4 Energy expressions for the correlated BCS ansatz

In this section we derive the expressions to compute the energy expectation value of a superfluid Fermi system in the strongly interacting regime, described by a correlated BCS trial function having $\sigma_z$-dependent two-body correlations.

### 2.4.1 Potential energy

Let us first study the case of a scalar two-body potential given by

$$\hat{V} = \sum v_c(r_{ij}) \qquad (2.48)$$

like that used to describe the interaction between two atoms in dilute Fermi gas systems. From Eq. (2.46), it follows that

$$\frac{\langle \hat{V} \rangle}{\langle \hat{N} \rangle} = \frac{\rho}{2} \int \mathrm{d}\mathbf{r}_{12} \; v_c(r_{12}) \frac{1}{2} \big[ g^p(r_{12}) + g^a(r_{12}) \big], \qquad (2.49)$$

with $g^p(r_{12})$ and $g^a(r_{12})$ given by Eq. (A.19).
Notice that the density $\rho = c\rho_0$ does not necessarily coincide with $\rho_0$, which is fully determined by the BCS amplitude $v_\mathbf{k}^2$ and therefore is the density of the "uncorrelated" fluid. Neither $|\mathrm{BCS}\rangle$ nor $|\mathrm{CBCS}\rangle$ are eigenstates of $\hat{N}$. Therefore the correlation operator $\prod F(ij)$ modifies the expectation value of $\langle \hat{N} \rangle$ with respect to that obtained with the pure $|\mathrm{BCS}\rangle$ state.

Let us also consider the more complex case of a spin-dependent potential of the type

$$\hat{V} = \hat{V}_c + \hat{V}_\sigma = \sum [v_c(r_{ij}) + \boldsymbol{\sigma}_i \cdot \boldsymbol{\sigma}_j \, v_\sigma(r_{ij})], \qquad (2.50)$$

typical of semirealistic N-N interactions used to study the properties of the neutron matter which is formed in the interior of neutron stars (fully realistic interactions include tensor and spin-orbit components).

The expectation value of the scalar potential $\hat{V}_c$, leads to the same expression given in Eq. (2.49). On the contrary, the spin-dependent part $\hat{V}_\sigma$ requires the calculation of some extra FHNC quantities with respect to those given in Appendix A and given in Appendix B.

The spin operator $\boldsymbol{\sigma}_1 \cdot \boldsymbol{\sigma}_2$ has nonvanishing matrix elements between exchanged antiparallel spin states, namely

$$\langle \uparrow\downarrow \, |\boldsymbol{\sigma}_1 \cdot \boldsymbol{\sigma}_2| \, \downarrow\uparrow \rangle = 2. \qquad (2.51)$$

This implies that the correlation operator $\hat{F}(ij)$ with either $i$ or $j$ equal to the external points 1 or 2 may lead to a correlation function $\xi(r_{ij})$ different from $h_p(r_{ij})$ or $h_a(r_{ij})$ considered in Appendix A. To this aim let us distinguish between direct and exchange terms relatively to the interacting particles 1 and 2.

- <u>Direct terms</u>. Differently from the case of pure Jastrow correlation model, for which the spin operator $\boldsymbol{\sigma}_1 \cdot \boldsymbol{\sigma}_2$ has a vanishing trace, here the $\sigma_z$-dependence of $\hat{F}(ij)$ leads to a difference between spin-parallel and spin-antiparallel states, because $f_p(r_{ij}) \neq f_a(r_{ij})$. Since

$$\langle \uparrow\uparrow \, |\boldsymbol{\sigma}_1 \cdot \boldsymbol{\sigma}_2| \, \uparrow\uparrow \rangle = \langle \downarrow\downarrow \, |\boldsymbol{\sigma}_1 \cdot \boldsymbol{\sigma}_2| \, \downarrow\downarrow \rangle = \phantom{-}1, \qquad (2.52)$$

$$\langle \uparrow\downarrow \, |\boldsymbol{\sigma}_1 \cdot \boldsymbol{\sigma}_2| \, \uparrow\downarrow \rangle = \langle \downarrow\uparrow \, |\boldsymbol{\sigma}_1 \cdot \boldsymbol{\sigma}_2| \, \downarrow\uparrow \rangle = -1, \qquad (2.53)$$

the contribution of direct terms to the expectation value of $\hat{V}_\sigma$ is given by

$$\frac{\langle \hat{V}_\sigma \rangle_{\text{direct}}}{\langle \hat{N} \rangle} = \frac{\rho}{2} \int \text{d}\mathbf{r}_{12} \, v_\sigma(r_{12}) \frac{1}{2} \big[ g_p^{\text{dir}}(r_{12}) - g_a^{\text{dir}}(r_{12}) \big], \qquad (2.54)$$

which vanishes in the limiting case $f_p(r_{ij}) = f_a(r_{ij})$, and therefore $g_p(r_{12}) = g_a(r_{12})$, where

$$
\begin{aligned}
g_\alpha^{\text{dir}}(r_{12}) \;=\; & F^\alpha(r_{12}) \bigg\{ \Big[ 1 + \frac{c_d}{c} \big( N_{de}^\alpha(r_{12}) + E_{de}^\alpha(r_{12}) \big) \Big]^2 + \\
& + \Big( \frac{c_d}{c} \Big)^2 \Big[ N_{ee}^\alpha(r_{12}) + E_{ee}^\alpha(r_{12}) \Big] \bigg\}, \quad (\alpha = p, a), (2.55)
\end{aligned}
$$

where the quantities $F^\alpha(r_{12})$, $N_{nm}^\alpha(r_{12})$ and $E_{nm}^\alpha(r_{12})$ are given in Appendix A.

- Exchanged terms. We consider here the cluster terms in which particle 1 and/or 2 are exchanged either among themselves (1-2 exchange loops) or with other particles in the medium (1-2,3,... exchange loops). To this aim we distinguish the cluster terms A in which the spin states of particles 1 and 2 are not exchanged, from those, B, in which they are exchanged.

  In the cluster terms A the $\boldsymbol{\sigma}_1 \cdot \boldsymbol{\sigma}_2$ matrix elements are given in Eq. (2.52) (for the $v$-contractions) and Eq. (2.53) (for the $u$-contractions). They give the following contribution

$$
\begin{aligned}
\frac{\langle \hat{V}_\sigma \rangle_{\text{exch,A}}}{\langle \hat{N} \rangle} &= -\frac{\rho}{4} \int d\mathbf{r}_{12} \, v_\sigma(r_{12}) \left(\frac{c_d}{c}\right)^2 \Big\{ F^p(r_{12}) \text{Re}[N_{cc}^p(r_{12}) + L_{cc}^p(r_{12}) + E_{cc}^p(r_{12})]^2 \\
&\quad - F^a(r_{12}) \text{Re}[N_{cc}^a(r_{12}) + L_{cc}^a(r_{12}) + E_{cc}^a(r_{12})]^2 \Big\}
\end{aligned} \tag{2.56}
$$

Summing up the two contributions of Eq.. (2.54) and (2.56) we get

$$
\frac{\langle \hat{V}_\sigma \rangle_{\text{direct}} + \langle \hat{V}_\sigma \rangle_{\text{exch,A}}}{\langle \hat{N} \rangle} = \frac{\rho}{4} \int d\mathbf{r}_{12} \, v_\sigma(r_{12}) \big[ g_p(r_{12}) - g_a(r_{12}) \big]. \tag{2.57}
$$

Let us now consider the cluster terms B. These may result from both $v$- and $u$-contractions and require that the dynamical correlations linking 1 or 2 with any of the medium ones are of the form

$$
\xi(r_{ij}) = f_a(r_{ij}) f_p(r_{ij}) - 1, \tag{2.58}
$$

with $i$ and $j$ equal to 1 or 2. To compute the B terms one needs to solve another set of RFHNC integral equations which are given in Appendix B. Their contribution to the expectation value of $\hat{V}_\sigma$ is given by

$$
\begin{aligned}
\frac{\langle \hat{V}_\sigma \rangle_{\text{exch,B}}}{\langle \hat{N} \rangle} &= -\frac{\rho}{4} \left(\frac{c_\xi}{c}\right)^2 \int d\mathbf{r}_{12} \, 2 v_\sigma(r_{12}) f_a^2(r_{12}) e^{N_{\xi\xi}(r_{12}) + E_{\xi\xi}(r_{12})} \\
&\quad \Big\{ \big[ \text{Re}\big( N_{cc,\xi\xi}(r_{12}) - l_v(r_{12}) + E_{cc,\xi\xi}(r_{12}) \big) \big]^2 \\
&\quad + \big[ \text{Im}\big( N_{cc,\xi\xi}(r_{12}) + l_u(r_{12}) + E_{cc,\xi\xi}(r_{12}) \big) \big]^2 \Big\} \tag{2.59}
\end{aligned}
$$

The factor 2 multiplying $v_\sigma$ comes from Eq. (2.51). The plus sign in front of the Im part is due to the change of the sign in the Wick's contractions $a^\dagger a^\dagger$ and $aa$ in the B terms (see for instance diagrams of Fig. 2.2).
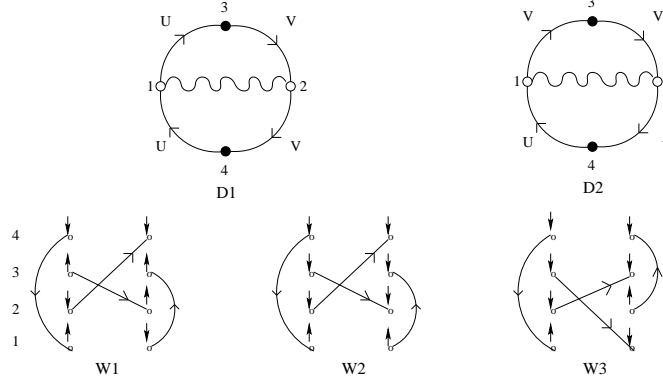


Figure 2.2: Examples of cluster diagrams contributing to the expectation value of $\langle \hat{V}_\sigma \rangle$, together with the graphical representation of Wick's contractions. W1 and W2 refers to the cluster diagram D1, whereas W3 to D2.

Diagrams W1 and W2 represent the contractions of the cluster diagram D1. In diagram W1 there is a spin exchange for particles 1 and 2 and it is included in the $[\mathrm{Im}(\ldots)]^2$ term of Eq. (2.59). Diagram W2 has no spin exchange and is included in Eq. (2.56). The global sign due to $a^\dagger a^\dagger$ and $aa$ contractions in W1 is the opposite of that of W2 and W3. Diagram W3, which refers to cluster diagram D2, has spin exchange for particle 1 and 2, like W1 and is included in the $[\mathrm{Re}(\ldots)]^2$ terms of Eq. (2.59).

## 2.4.2   Kinetic energy

Let us calculate the kinetic energy expression according to the Jackson-Feenberg identity (ref. [60]). Similarly to the expression given in Eq. (2.28),

one has

$$
\langle \text{CBCS}|\hat{T}|\text{CBCS}\rangle \;=\; -\frac{\hbar^2}{2m} \sum_N \frac{1}{(N-1)!} \sum_{\substack{n_1,\ldots,n_N \\ m_1,\ldots,m_N}} \int dr_1 \ldots dr_N
$$

$$
[\varphi_{n_1}^*(\mathbf{r}_1)\ldots\varphi_{n_N}^*(\mathbf{r}_N)]\mathrm{F}_N\,\nabla_1^2\,\{\mathrm{F}_N[\varphi_{m_1}(\mathbf{r}_1)\ldots\varphi_{m_N}(\mathbf{r}_N)]\}
$$

$$
\langle \text{BCS}|a_{n_1}^\dagger\ldots a_{n_N}^\dagger|0\rangle\langle 0|a_{m_N}\ldots a_{m_1}|\text{BCS}\rangle, \tag{2.60}
$$

where

$$
\mathrm{F}_N = \prod_{j>i=1}^{N} f(ij). \tag{2.61}
$$

After the application of the Jackson-Feenberg identity one gets the following result

$$
T_N = -\frac{\hbar^2}{2m}\int dr_1 \ldots dr_N [\varphi_{n_1}^*(\mathbf{r}_1)\ldots\varphi_{n_N}^*(\mathbf{r}_N)]\mathrm{F}_N\,\nabla_1^2
$$

$$
\{\mathrm{F}_N[\varphi_{m_1}(\mathbf{r}_1)\ldots\varphi_{m_N}(\mathbf{r}_N)]\}
$$

$$
= -\frac{\hbar^2}{2m}\int dr_1 \ldots dr_N \Big\{[\varphi_{n_1}^*(\mathbf{r}_1)\ldots\varphi_{n_N}^*(\mathbf{r}_N)]\mathrm{F}_N\,\nabla_1^2
$$

$$
\big[\mathrm{F}_N\big(\varphi_{m_1}(\mathbf{r}_1)\ldots\varphi_{m_N}(\mathbf{r}_N)\big)\big] - \boldsymbol{\nabla}_1\big[\big(\varphi_{n_1}^*(\mathbf{r}_1)\ldots\varphi_{n_N}^*(\mathbf{r}_N)\big)\mathrm{F}_N\big]
$$

$$
\boldsymbol{\nabla}_1\big[\mathrm{F}_N\big(\varphi_{m_1}(\mathbf{r}_1)\ldots\varphi_{m_N}(\mathbf{r}_N)\big)\big]\Big\}, \tag{2.62}
$$

which is most conveniently written in the following form:

$$
T_N = -\frac{\hbar^2}{2m}\int d\mathbf{r}_1 \ldots d\mathbf{r}_N [\varphi_{n_1}^*(\mathbf{r}_1)\ldots\varphi_{n_N}^*(\mathbf{r}_N)]\mathrm{F}_N^2\,\nabla_1^2[\varphi_{m_1}(\mathbf{r}_1)\ldots\varphi_{m_N}(\mathbf{r}_N)]
$$

$$
-\frac{\hbar^2}{4m}\int d\mathbf{r}_1 \ldots d\mathbf{r}_N [\varphi_{n_1}^*(\mathbf{r}_1)\ldots\varphi_{n_N}^*(\mathbf{r}_N)]\big[\mathrm{F}_N(\nabla_1^2\mathrm{F}_N) - (\boldsymbol{\nabla}_1\mathrm{F}_N)^2\big]
$$

$$
[\varphi_{m_1}(\mathbf{r}_1)\ldots\varphi_{m_N}(\mathbf{r}_N)]
$$

$$
+\frac{\hbar^2}{8m}\int d\mathbf{r}_1 \ldots d\mathbf{r}_N \nabla_{1\Phi}^2\Big\{[\varphi_{n_1}^*(\mathbf{r}_1)\ldots\varphi_{n_N}^*(\mathbf{r}_N)]\mathrm{F}_N^2
$$

$$
[\varphi_{m_1}(\mathbf{r}_1)\ldots\varphi_{m_N}(\mathbf{r}_N)]\Big\} \tag{2.63}
$$

where $\nabla_{1\Phi}^2$ acts on the single particle orbitals $\varphi_\alpha(\mathbf{r}_i)$ only. The main advantage of the Jackson-Feenberg form is that the three-body terms $\boldsymbol{\nabla}_{1i}\mathrm{F}(1i)\cdot\boldsymbol{\nabla}_{1j}\mathrm{F}(1j)$ cancel exactly. The remaining three-body terms are numerically

small and can safely be neglected.

The expectation value of the kinetic energy is given by

$$\frac{\langle T \rangle}{\langle N \rangle} = T_0 + T_2 + T_{2\Phi} + T_{3\Phi}, \tag{2.64}$$

where the uncorrelated term $T_0$ results from the fist of the three terms on the r.h.s of Eq. (2.63) and is given by

$$T_0 = 2 \sum_k \frac{\hbar^2 k^2}{2m} v_k^2 = \frac{1}{\pi^2 \rho} \frac{\hbar^2}{2m} \int dk \; k^4 v_k^2. \tag{2.65}$$

In the case of $v_k^2 = \Theta(k - k_F)$, $T_0$ reduces to the Fermi kinetic energy $\frac{3\hbar^2 k_F^2}{10m}$. The second term on the r.h.s of Eq. (2.63) gives rise to the "bosonic" kinetic energy $T_2$

$$T_2 = -\frac{\hbar^2}{4m} \rho \frac{1}{2} \sum_{\alpha=1}^{2} \int d\mathbf{r}_{12} \; g^\alpha(r_{12}) \nabla_1^2 \ln f^\alpha(r_{12}). \tag{2.66}$$

Finally, the third expression on the r.h.s of Eq. (2.63) produces a two-body and a three-body kinetic term $T_{2\Phi}$ and $T_{3\Phi}$. The resulting cluster diagrams are characterized by the fact that the external point 1 must be reached by a dynamical line, without counting those which may come from the vertex correction. To understand this property one should consider a cluster diagram, in whose irreducible portion of the exchange type in 1, there are no dynamical correlations either $h_p(r_{1i})$ or $h_a(r_{1i})$ reaching 1. In the corresponding cluster term the laplacian $\nabla_{1\Phi}^2$ can be substituted with $\nabla_1^2$, and, consequently its integral vanishes. This general rule drives the construction of the cluster terms contributing to $T_{2\Phi}$ and $T_{3\Phi}$.

Let us first consider those cluster diagrams having a two-body exchange loop $L_{cc}^2(r_{1i})$ passing through 1. They give rise to the following two-body kinetic energy term

$$T_{2\Phi}^{(A)} = -\frac{\hbar^2}{16m} \rho \left(\frac{c_d}{c}\right)^2 \int d\mathbf{r}_{12} \sum_{\alpha=1}^{2} \left[F^\alpha(r_{12}) - 1\right] \left[\nabla_{12}^2 L_{cc}^{\alpha \, 2}(r_{12})\right]. \tag{2.67}$$

The cluster diagrams having exchange loops with more than two exchange lines and passing through 1 produce a two-body term $T_{2\Phi}^{(B)}$ and the three-body one $T_{3\Phi}$. The two-body term is characterized by the laplacian acting

on $L_{cc}^\alpha(r_{12})$ and is given by [2]

$$
T_{2\Phi}^{(B)} = -\frac{\hbar^2}{8m}\frac{\rho}{c^2} \int d\mathbf{r}_{12} \, \mathrm{Re} \sum_{\alpha=1}^{2} \left\{ c_d^2 \big[F^\alpha(r_{12}) - 1\big]\big[N_{cc}^\alpha(r_{12}) + E_{cc}^\alpha(r_{12})\big] \right.
$$
$$
\left. + c_d^2 \big[N_{cc,hh}^\alpha(r_{12}) + E_{cc}^\alpha(r_{12})\big] + c_d(c_d - 1)N_{cc,hl}^\alpha(r_{12}) \right\} \nabla_{12}^2 L_{cc}^\alpha(r_{12}) \quad (2.68)
$$

$T_{2\Phi}$ in Eq. (2.64) is the sum of $T_{2\Phi}^{(A)}$ and $T_{2\Phi}^{(B)}$, namely

$$
T_{2\Phi} = T_{2\Phi}^{(A)} + T_{2\Phi}^{(B)}. \tag{2.69}
$$

The three-body term is characterized by the laplacian giving rise to $\big(\boldsymbol{\nabla}_1 L_{cc}^\alpha(r_{1i})\big)\cdot$ $\big(\boldsymbol{\nabla}_1 L_{cc}^\alpha(r_{1j})\big)$, and it is approximated by the following expression

$$
T_{3\Phi} \;=\; -\frac{\hbar^2}{8m}\frac{\rho^2}{c^3} \int d\mathbf{r}_{12} d\mathbf{r}_{13} \sum_{\substack{i,j,k \\ i',j',k'}} A_{ii}(1 - \delta_{ii',ll})A_{jk}A_{j'k'}
$$
$$
\frac{1}{2}\mathrm{Re}\Big\{ \big[\mathbf{X}_{ij}^p(r_{12})\mathbf{X}_{i'j'}^p(r_{13}) + \mathbf{X}_{ij}^a(r_{12})\mathbf{X}_{i'j'}^a(r_{13})\big]Y_{kk'}^p(r_{23})
$$
$$
+ \big[\mathbf{X}_{ij}^p(r_{12})\mathbf{X}_{i'j'}^a(r_{13}) + \mathbf{X}_{ij}^a(r_{12})\mathbf{X}_{i'j'}^p(r_{13})\big]Y_{kk'}^a(r_{23}) \Big\} \tag{2.70}
$$

where the matrix $A_{ij}$ is given by

$$
A_{ij} = \begin{pmatrix} c_d & c_d \\ c_d & c_d - 1 \end{pmatrix} \quad (ij = h, l), \tag{2.71}
$$

and

$$
\mathbf{X}_{hh}^\alpha(r) = \big[F^\alpha(r) - 1\big]\nabla^2 L_{cc}^\alpha(r),
$$
$$
\mathbf{X}_{hl}^\alpha(r) = \mathbf{X}_{lh}^\alpha(r) = 0,
$$
$$
\mathbf{X}_{ll}^\alpha(r) = \boldsymbol{\nabla} L_{cc}^\alpha(r), \tag{2.72}
$$

and

$$
Y_{hh}^\alpha(r) = \big[F^\alpha(r) - 1\big]\big[N_{cc}^\alpha(r) + L_{cc}^\alpha(r)\big] + N_{cc,hh}^\alpha(r),
$$
$$
Y_{hl}^\alpha(r) = Y_{lh}^\alpha(r) = N_{cc,hl}^\alpha(r),
$$
$$
Y_{ll}^\alpha(r) = N_{cc,ll}^\alpha + L_{cc}^\alpha(r). \tag{2.73}
$$

---

[2]Notice that the elementary diagrams of the $cc$-type have always dynamical lines reaching both 1 and 2

A full FHNC treatment of $T_{3\Phi}$ requires the solution of extra integral equations for the functions $\mathbf{X}_{ij}^{\alpha}(r_{13})$, for which the definitions given in Eq. (2.72) represent the lowest order approximation (See ref. ([60]). However, the term $T_{3\Phi}$ as given in Eq. (2.71 -2.73) is in general numerically very small, and the corrections coming from the full FHNC treatment of ref. ([60]) is negligible, and it is not reported here.

## 2.5    Euler equations

In this section we derive an Euler equation to compute the optimal correlation functions $f_p(r_{ij})$ and $f_a(r_{ij})$ as well as the BCS amplitude $v_{\mathbf{k}}^2$. This is formally obtained by performing a functional variation of the energy expectation value with respect to $f_p$, $f_a$ and $v_{\mathbf{k}}^2$, and equating them to zero. Instead of doing this, we approximate the energy expectation value with its two-body approximation $E_2$. Then, we set the functional variations $E_2$ with respect to $f_p$, $f_a$ and $v_{\mathbf{k}}^2$ equal to zero under the constraints that

$$f_p(r \geq d) = f_a(r \geq d) = 1 \tag{2.74}$$
$$f_p'(r \geq d) = f_a'(r \geq d) = 0, \tag{2.75}$$

where the healing distance $d$ is considered as a variational parameter. Such approximation has been widely used in a number of applications to nuclear matter and provides correlation functions with the correct short range behavior [47], [19]. The solutions of a "full" Euler equation improve this two-body approximation namely for the intermediate and long-range behavior of the correlation function. The derivation of a full Euler equation and the inclusion of long range correlation is a subject of future interest.

Let us calculate the energy expectation value at the second order of the cluster expansion. From the expresions given in the previous section we obtain the following results

$$
\begin{aligned}
\left.\frac{\langle \hat{V} \rangle}{\langle \hat{N} \rangle}\right|_2 = \ & \frac{\rho}{4} \int d\mathbf{r}_{12} \left\{ v_c(r_{12}) \left[ f_p^2(r_{12}) \left( 1 - \left( \frac{c_d}{c} \right)^2 l_v^2(r_{12}) \right) + f_a^2(r_{12}) \left( 1 + \left( \frac{c_d}{c} \right)^2 l_u^2(r_{12}) \right) \right] \right. \\
& + v_\sigma(r_{12}) \left[ f_p^2(r_{12}) \left( 1 - \left( \frac{c_d}{c} \right)^2 l_v^2(r_{12}) \right) - f_a^2(r_{12}) \left( 1 + \left( \frac{c_d}{c} \right)^2 l_u^2(r_{12}) \right) \right] \\
& \left. - v_\sigma \left( \frac{c_\xi}{c} \right)^2 2 f_a^2(r_{12}) \left( \frac{c_d}{c} \right)^2 \left[ l_v^2(r_{12}) + l_u^2(r_{12}) \right] \right\}
\end{aligned}
\tag{2.76}
$$

and

$$\frac{\langle \hat{T} \rangle}{\langle \hat{N} \rangle}\Bigg|_2 = \frac{\hbar^2}{2m}\frac{1}{\pi^2 \rho}\int \mathrm{d}k \; k^4 v^2(k) \tag{2.77}$$

$$-\frac{\hbar^2}{8m}\rho\int \mathrm{d}\mathbf{r}_{12}\left\{\left[f_p^2(r_{12})\nabla^2\ln f_p(r_{12})\right]\left[1-\left(\frac{c_d}{c}\right)^2 l_v^2(r_{12})\right]\right.$$

$$\left.+\left[f_a^2(r_{12})\nabla^2\ln f_a(r_{12})\right]\left[1+\left(\frac{c_d}{c}\right)^2 l_u^2(r_{12})\right]\right\}$$

$$+\frac{\hbar^2}{16m}\rho\left(\frac{c_d}{c}\right)^2\int \mathrm{d}\mathbf{r}_{12}\left\{-h_p(r_{12})\left[\nabla^2 l_v^2(r_{12})\right]+h_a(r_{12})\left[\nabla^2 l_u^2(r_{12})\right]\right\}$$

which can be more conveniently written as

$$\frac{\langle \hat{T} \rangle}{\langle \hat{N} \rangle}\Bigg|_2 = \frac{\hbar^2}{2m}\frac{1}{\pi^2 \rho}\int \mathrm{d}k \; k^4 v^2(k)$$

$$+\frac{\hbar^2}{4m}\rho\int \mathrm{d}\mathbf{r}_{12}\left\{f'^2_p(r_{12})\left[1-\left(\frac{c_d}{c}\right)^2 l_v^2(r_{12})\right]\right.$$

$$\left.+f'^2_a(r_{12})\left[1+\left(\frac{c_d}{c}\right)^2 l_u^2(r_{12})\right]\right\} \tag{2.78}$$

The vertex corrections $c_d$, $c_\xi$ and $c$ are functionals of the correlation functions $f_p$, $f_a$ and of the BCS amplitude $v^2(k)$. One can use the first order of the Power Series (PS) expansion to approximate them, as done in ref. [17]. The reason for such approximation is related to the fact that at any order of the PS expansion the normalization properties are reproduced correctly, which is not true for the expansion in the number of points. The expressions of the vertex corrections in such approximation are given by

$$c_d|_1 = 1+\frac{1}{2}\rho_0\int \mathrm{d}\mathbf{r}_{12}\left[h_p(r_{12})+h_a(r_{12})\right], \tag{2.79}$$

$$U_e|_1 = \frac{1}{2}\rho_0\int \mathrm{d}\mathbf{r}_{12}\left[-l_v^2(r_{12})h_p(r_{12})+l_u^2(r_{12})h_a(r_{12})\right]$$

$$+\frac{1}{4}\rho_0\int \mathrm{d}\mathbf{r}_2\mathrm{d}\mathbf{r}_3\left\{h_p(r_{23})l_v(r_{23})\left[l_v(r_{13})l_v(r_{12})-l_u(r_{13})l_u(r_{12})\right]\right.$$

$$\left.-h_a(r_{23})l_u(r_{23})\left[l_v(r_{13})l_u(r_{12})+l_v(r_{12})l_u(r_{13})\right]\right\} \tag{2.80}$$

$$c\,|_1 = c_d+U_e|_1 \tag{2.81}$$

$$c_\xi|_1 = 1+\rho_0\int \mathrm{d}\mathbf{r}_{12}\;\xi(r_{12}) \tag{2.82}$$

Notice that in the limit of $l_u(r_{ij}) \to 0$ and $f_p(r_{ij}) = f_a(r_{ij})$, the zeroth order approximation of the PS, we get $c_d|_0 = c_\xi|_0 = 1$, $U_e|_0 = 0$ and therefore $c = 1$. In first order, $c_d|_1 \neq c_\xi|_1 \neq 1$, but $c_d + U_e|_1$ is still equal to 1 as required by the normalization property. In the BCS ansatz, such property does not hold anylonger because of the non conservation of particles, but still the first order of PS expansion should be a reasonable approximation.

## 2.5.1   Energy expressions

In the following two tables, we summarize the expressions of the energy for the normal and superfluid phases, for both spin independent as well as longitudinal spin-dependent correlations. In table 2.5.1 we present the kinetic energy and table 2.5.1 the potential energy for the general case of spin dependent interactions.

| Kinetic Energy | State independent correlations | $\sigma_z$-dependent correlations |
|---|---|---|
| Normal Phase<br><br>$\frac{\langle T \rangle}{N} = T_F + T_{2A} + T_{2B}$ | $T_F = \frac{3\hbar^2}{10m} k_F^2$<br><br>$T_{2A} = -\rho \frac{\hbar^2}{4m} \int d\mathbf{r} g(r) \nabla^2 \ln f(r)$<br><br>$T_{2B} = \rho \frac{\hbar^2}{8m} \int d\mathbf{r}\, [F(r) - 1] \left[ 2N_{cc}(r)\nabla^2 \ell(k_F r) - \frac{\nabla^2 \ell^2(k_F r)}{\nu} \right]$ | $T_F = \frac{3\hbar^2}{10m} k_F^2$<br><br>$T_{2A} = -\frac{\rho}{\nu} \frac{\hbar^2}{4m} \sum_{\alpha=1}^{\nu} \int d\mathbf{r} g^{\alpha}(r)\nabla^2 \ln f^{(k)}(r)$<br><br>$T_{2B} = \frac{\rho}{\nu} \frac{\hbar^2}{8m} \int d\mathbf{r} \left[ F^{(p)}(r) - 1 \right] \left[ 2N_{cc}^{(p)}(r)\nabla^2 \ell(k_F r) - \nabla^2 \ell^2(k_F r) \right]$ |
| Superfluid Phase<br><br>$\frac{\langle T \rangle}{\langle N \rangle} = T_0 + T_2 + T_{2\Phi}^A + T_{2\Phi}^B$ | $T_0 = \frac{1}{\pi^2 \rho} \frac{\hbar^2}{2m} \int dk\ k^4 v_k^2$<br><br>$T_2 = -\rho \frac{\hbar^2}{4m} \int d\mathbf{r}\ g(r)\nabla^2 \ln f(r)$<br><br>$T_{2\Phi}^{(A)} = -\frac{\hbar^2}{4m} \rho \left(\frac{c_d}{c}\right)^2 \int d\mathbf{r}[F(r) - 1]\nabla^2 \frac{[l_v^2(r) - l_u^2(r)]}{\nu}$<br><br>$T_{2\Phi}^{(B)} = -\frac{\hbar^2}{8m} \frac{\rho}{c^2} 2\nu \int d\mathbf{r}\ \mathrm{Re}\ \nabla^2 \frac{-l_v(r) + i l_u(r)}{\nu} \cdot$<br><br>$\left\{ c_d^2 [F(r) - 1]N_{cc}(r) + c_d^2 N_{cc,hh}(r) + c_d(c_d - 1)N_{cc,hl}(r) \right\}$ | $T_0 = \frac{1}{\pi^2 \rho} \frac{\hbar^2}{2m} \int dk\ k^4 v_k^2$<br><br>$T_2 = -\frac{\hbar^2}{4m} \rho \frac{1}{2} \sum_{\alpha=1}^{2} \int d\mathbf{r}\ g^{\alpha}(r)\nabla^2 \ln f^{\alpha}(r)$<br><br>$T_{2\Phi}^{(A)} = -\frac{\hbar^2}{16m} \rho \left(\frac{c_d}{c}\right)^2 \int d\mathbf{r} \sum_{\alpha=1}^{\nu} [F^{\alpha}(r) - 1]\nabla^2 [l_v^2(r) - l_u^2(r)]$<br><br>$T_{2\Phi}^{(B)} = -\frac{\hbar^2}{8m} \frac{\rho}{c^2} \int d\mathbf{r}\ \mathrm{Re} \sum_{\alpha=1}^{2}$<br><br>$\left\{ c_d^2 [F^{\alpha}(r) - 1]N_{cc}^{\alpha}(r) + c_d^2 N_{cc,hh}^{\alpha}(r) + c_d(c_d - 1)N_{cc,hl}^{\alpha}(r) \right\} \nabla^2 L_{cc}^{\alpha}(r)$ |

Table 2.1: Kinetic Energy

| Potential energy | State independent correlations | $\sigma_z$-dependent correlations |
|---|---|---|
| Normal Phase | $\frac{\langle V \rangle}{N} = \frac{\rho}{2} \int d\mathbf{r}\{V_c(r)g_{dir}(r) + g_{exch}(r)\left[V_c(r) + 3V_\sigma(r)\right]\}$ <br><br> $g_{dir}(r) = F[1 + 2N_{de}(r) + N_{de}^2(r) + N_{ee}(r)]$ <br><br> $g_{exch}(r) = -F(r)\nu\left[N_{cc}(r) - \frac{\ell(k_F r)}{\nu}\right]$ | $\frac{\langle V \rangle}{N} = \frac{1}{\nu}\frac{\rho}{2} \int d\mathbf{r} \left\{V_c(r)\sum_{\alpha=1}^{\nu} g^\alpha(r) + V_\sigma(r)(g^p(r) - g^a(r))\right\}$ <br><br> $-2V_\sigma(r)n_a f_a^2(r)e^{N_{\xi\xi}(r)}\left[N_{\xi\xi cc}(r) - \ell(k_F r)\right]^2\}$ <br><br> $g_{dir}^\alpha(r) = F^\alpha(r)[1 + 2N_{de}^\alpha(r) + N_{de}^{\alpha\,2}(r) + N_{ee}^\alpha(r)]$ |
| Superfluid Phase | $\frac{\langle V \rangle}{N} = \frac{\rho}{2} \int d\mathbf{r} \left\{V_c(r)g(r) + 3V_\sigma(r)[g_{exch}^p(r) - g_{exch}^a(r)]\right\}$ <br><br> $g_{dir}(r) = F(r)\left\{1 + 2\frac{c_d}{c}N_{de}(r) + \left(\frac{c_d}{c}\right)^2[N_{de}^2(r) + N_{ee}(r)]\right\}$ <br> $g_{exch}^p(r) = \left(\frac{c_d}{c}\right)^2 F(r)\left\{-\frac{l_v^2(r)}{\nu} + 2l_v(r)\mathrm{Re}N_{cc}(r) - \nu(\mathrm{Re}N_{cc}(r))^2\right\}$ <br> $g_{exch}^a(r) = \left(\frac{c_d}{c}\right)^2 F(r)\left\{\frac{l_u^2(r)}{\nu} + 2l_u(r)\mathrm{Im}N_{cc}(r) - \nu(\mathrm{Im}N_{cc}(r))^2\right\}$ | $\frac{\langle V \rangle}{N} = \frac{1}{\nu}\frac{\rho}{2} \int d\mathbf{r} \left\{V_c(r)\sum_{\alpha=1}^{\nu} g^\alpha(r) + V_\sigma(r)(g^p(r) - g^a(r))\right\} - 2V_\sigma(r)\cdot$ <br> $\frac{c_\xi}{c}f_a^2(r)e^{N_{\xi\xi}(r)}\left[\mathrm{Re}[\nu N_{\xi\xi cc}(r) + L_{cc}^p(r)]^2 + \mathrm{Im}[\nu N_{\xi\xi cc}(r) + L_{cc}^a(r)]^2\right]\}$ <br><br> $g_{dir}^\alpha(r) = F^\alpha(r)\left\{1 + 2\frac{c_d}{c}N_{de}^\alpha(r) + \left(\frac{c_d}{c}\right)^2[N_{de}^{\alpha\,2}(r) + N_{ee}^\alpha(r)]\right\}$ <br><br> $g_{exch}^\alpha(r) = \left(\frac{c_d}{c}\right)^2 F^\alpha(r)\mathrm{Re}\left[N_{cc}^\alpha(r) + L_{cc}^\alpha(r)\right]$ |

Table 2.2: Potential Energy for spin dependent interactions.

# Chapter 3

# Equation of state for neutron matter and dilute Fermi gases

In this section we report the results obtained for two cases: a) dilute Fermi atoms with large and negative scattering length, b) Neutron matter. We have used the FHNC theory in the normal and superfluid phase (FHNC/BCS) for the situations of Jastrow state independent and longitudinal spin-dependent correlations.

## 3.1 Dilute Fermi gases with large scattering length

We will consider a non-polarized Fermi gas with attractive interactions which will lead to pairing effects supporting a superfluid state. The density $\rho$ of the non interacting gas determines the Fermi momentum $k_F = \sqrt[3]{6\pi^2\rho/\nu}$ and the total energy, corresponding to:

$$E_{FG} = \frac{3}{5}\frac{\hbar^2 k_F^2}{2m} \tag{3.1}$$

where $\nu$ is the spin degeneracy and $m$ is the mass of the fermionic atom. We are interested in dilute systems at very low temperatures, therefore the basic consequences of the interactions are governed by two body colliding process. In the dilute regime, the range of the interaction $R_0$ is much smaller than the interparticle distance $r_0 = \sqrt[3]{\frac{9\pi}{2\nu}}\frac{1}{k_F}$. The interactions between atoms

can be strong but they only occur when the atoms are close to each other. The relevant scattering processes involve states with zero angular momentum $\ell = 0$, namely $s$-wave states. If no other internal degrees of freedom are considered then two interacting atoms must have different spin states, due to the Pauli exclusion principle. At this level the collision process can be described by the Schrödinger equation written in relative coordinates system:

$$\left[-\frac{\hbar^2}{2\mu}\nabla^2 + V(r)\right]\varphi(r) = E\varphi(r), \tag{3.2}$$

where $\mu$ is the reduced mass ($\mu = m/2$ for identical atoms). The solution for $E > 0$ consists in a superposition of the incoming plane wave in the $z$ direction and a scattered wave,

$$\varphi(\mathbf{r}) = e^{ikz} + \varphi_{sc}(\mathbf{r}). \tag{3.3}$$

At large distances the scattered wave is an outgoing spherical wave, $\varphi_{sc}(\mathbf{r}) = f(\theta)\frac{e^{ikr}}{r}$ where the $f(\theta)$ is the scattering amplitude and the dependency $1/r$ ensures the conservation of energy. At low energies, the scattering amplitude approaches a constant value $-a$, and the wave function becomes

$$\varphi(\mathbf{r}) = 1 - \frac{a}{r}, \tag{3.4}$$

$a$ is the known $s$-wave *scattering length*, which gives the intercept of the asymptotic wave function Eq. 3.4.

Different model potentials can be employed to describe the low energy process, as long as they reproduce the available scattering length data. Then the details of the potential $V(r)$ are not important at this point. At the many body level it is convenient to replace the microscopic potential by an effective one; a very well-known example is the zero range ($R_0 = 0$) pseudo potential, $V_{eff}(\mathbf{r}) = g\delta(r)\partial/\partial r$ where the strength of the interaction is related to $a$, through $g = 2\pi\hbar^2 a/\mu$.

Instead we will consider an interaction of the Lennard-Jones type, namely

$$V(r) = 4\epsilon\left[\left(\frac{\sigma}{r}\right)^{12} - \left(\frac{\sigma}{r}\right)^6\right] \tag{3.5}$$

The range of the interaction is chosen to be smaller than the interparticle distance, while the depth of the potential is found in order to satisfy the

value of the experimental scattering length. We will consider as a particular example a fermionic lithium gas. Following O'Hara *et. al.* [4] which we refer as case $Li$, the zero-energy scattering length is $a_s = -10^4 a_0$ ($a_0$ the Bohr radius), while the density corresponds to $\rho_{Li} = 0.93 \times 10^{13}$ cm$^{-3}$. In the experiment the gas is load in an optical trap and evaporatively cooled, later an external magnetic field induces strongly interactions through the Feshbach mechanism. The gas is released from the trap while maintaining the field, and the expansion is imaged with a charge-coupled device camera. The output reveals an anisotropic expansion which is interpreted as consequence of the strong interactions and a possible signature of superfluidity.

In the mentioned work, the dimensionless parameter $\zeta_{Li} = k_F |a_s| = 7.4$, which we adopt as a reference. By solving Eq. 3.2 at $E = 0$, we found that the parameters that determine the Lennard-Jones potential to fit the condition reported [4] are:

$$r_0 = 1.3 \times 10^3 \text{ Å} \quad \text{(unit of length)} \qquad E_{FG} = 7.9 \ \mu K \text{ (unit of energy)}$$
$$\sigma = 0.09 \ r_0$$
$$\epsilon = 610.10 \ E_{FG}$$

In Fig. 3.1 a sketch of the potential and the reduced radial solution $u(r)$ whose intercept with the $r$ axis corresponds to the $s$ scattering length are presented. The large value of the scattering length ($a_s = -42.84 \ \sigma$) is not visible in the figure [1].

## 3.1.1 Normal phase

Having set the parameters of the Lennard-Jones potential, the next step in order to apply a FHNC calculation is to find the correlation function induced by such potential. We will consider a two body Jastrow correlator $f(r)$, coming from the solution of the Euler-Lagrange equation obtained by

---

[1] The wave function can be written like $\varphi(\mathbf{r}) = Y_{\ell,m}(\theta, \phi) R_{k\ell}(r)$, where the radial part is usually expressed as $R_{k\ell}(r) \equiv u_{k\ell}(r)/r$. Then the equation to be solved in terms of the reduced radial wave function $u_{kl}(r)$ is:

$$\left[ -\frac{\hbar^2}{2\mu} \frac{d^2}{dr^2} + \frac{\ell(\ell+1)\hbar^2}{2\mu r^2} + V(r) \right] u_{kl}(r) = E u_{kl}(r). \tag{3.6}$$
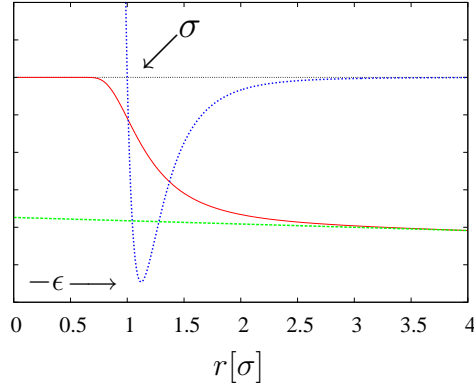
In the present case $\ell = 0$

Figure 3.1: Lennard-Jones potential (blue line) and solution of the reduced radial wave function $u(r)$ (red line) at energy $E = 0$. The intercept of the asymptotic behavior of $u(r)$ with the $r$ axis (not visible in the plot) corresponds to the scattering length

performing a variation of the energy expression at second order in the cluster expansion . The resulting equation is given by,

$$\Upsilon''(r) = \left\{ \frac{\phi''(r)}{\phi(r)} + \frac{m}{\hbar^2}(V(r) - \lambda) \right\} \Upsilon(r) \qquad (3.7)$$

$$\text{where} \quad \Upsilon(r) \equiv \phi(r)f(r) \qquad (3.8)$$

$$\text{and} \quad \phi^2(r) \equiv r^2\left[1 - \frac{\ell^2(k_F r)}{\nu}\right]. \qquad (3.9)$$

$\ell(k_F r)$ is the Slater function and $\lambda$ is a Lagrange multiplier introduced to force the Jastrow function to be short ranged. The distance at which $f(r)$ becomes 1.0 is called the *healing distance*, $d$. The boundary conditions satisfied by $f(r)$ are then,

$$f(d) = 1, \qquad\qquad f'(d) = 0. \qquad (3.10)$$

In Fig. 3.2 we show the value of the FHNC energy versus the healing distance. For the region out of the range showed in the figure ($d > 0.17\ r_0$), the larger the healing distances the worse the normalization condition becomes, while the energy decreases monotonically down to reach a situation of no
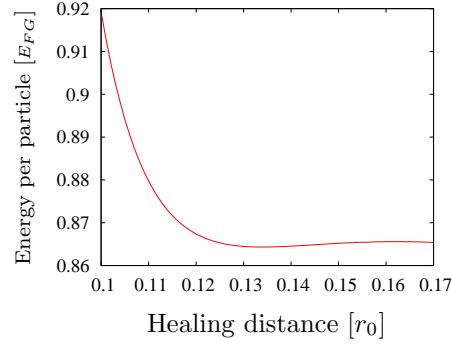
Figure 3.2: Variational energy versus healing distance for a dilute Fermi gas with the Lennard-Jones potential.

convergence [2] at $d > 0.9 \ r_0$ . This fact is an effect of the large contributions from the elementary diagrams, which are neglected. The plateau reached by the energy is a sign of the good convergence of the method. The optimum healing distance is found at $d = 0.134 \ r_0$, corresponding to an energy, $E_{normal} = 0.864 \ E_{FG}$.

The optimal Jastrow correlator $f(r)$ and the pair distribution function $g(r)$ are shown in Fig. 3.3. The effect of the repulsive part of the Lennard-Jones potential is manifested as a hard core in these quantities, forcing any pair of particles to avoid approaching within a distance $r \sim 0.05 \ r_0$. The effects of the dynamical correlations are appreciable in a small range while the intermediate and long range are dominated by the statistical correlations exhibiting a behavior of noninteracting particles at such distances. The pair distribution function for free particles $g(r) = 1 - \frac{1}{2}\ell^2(k_F r)$ is shown in green coinciding with the pair distribution of our problem at distances larger than the healing distance.

Next we have varied the density of the system while keeping the value

---

[2]The following normalization condition (in the normal state) has to be fulfilled;

$$S(k = 0) = 1 + \rho \int \mathrm{d}\mathbf{r}_{12}\big(g(r_{12}) - 1\big) = 0, \tag{3.11}$$

implying no long range pathologies for the correlations functions.
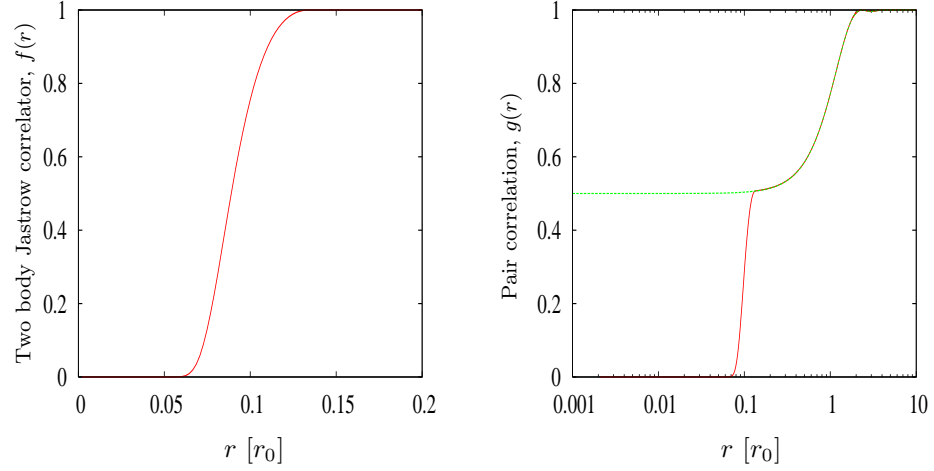
Figure 3.3: Left: Jastrow correlation function. Right:Pair distribution function for a dilute Fermi gas. Both correspond to the case $\rho_{Li}$. The marked difference in the spatial extension of the statistical ($\sim 1/k_F$) and the dynamical correlations ($\sim d$) is noticeable in the shape of $g(r)$. The free particle pair distribution is also shown in green. The behavior of $g(r)$ in the dilute problem differs form the free particle only at distances smaller than the healing distance.

of the scattering length fixed ($a_s = -10^4 a_0$). We have calculated the energy of the normal phase for the following cases: $k_F|a_s| = 1, 3, 5, 9, 12, 14$. The energy as a function of the density, is presented in Fig. 3.4, referred to the density $\rho_{Li}$.
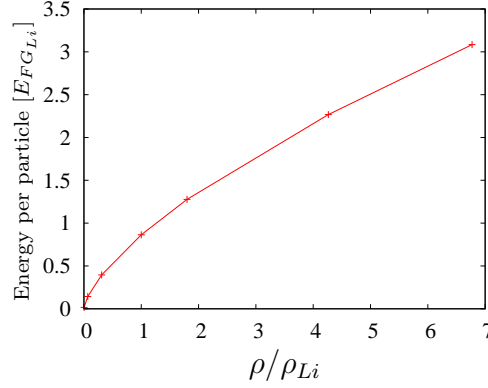


Figure 3.4: Energy of the normal phase for a dilute Fermi gas with the Lennard-Jones potential at various densities. The energies are given in terms of $E_{FG_{Li}} = 7.9 \ \mu K$ and the densities in terms of $\rho_{Li} = 0.93 \times 10^{13} \ \text{cm}^{-3}$.

The inclusion of $\sigma_z$-dependence in the correlations introduces a small difference between the parallel and antiparallel components of the Jastrow, as we show in Fig. 3.5. On the contrary the parallel component of the pair distribution function is dominated by the Slater function which only acts for particles having the same spin, while the antiparallel is short ranged (See right of Fig. 3.5). The state dependent choice reduces weakly the energy of the normal phase, being this effect more notorious at larger densities as it is presented in Table 3.1.

## 3.1.2 Superfluid phase

In the superfluid phase the Euler-Lagrange equation is identical to Eq. 3.7 with the following definitions:

$$\Upsilon(r) \ \equiv \ \phi(r)f(r) \tag{3.12}$$

$$\phi^2(r) \ \equiv \ r^2\left[1 - \left(\frac{c_d}{c}\right)^2\left(\frac{l_v^2(r) - l_u^2(r)}{\nu}\right)\right] \tag{3.13}$$
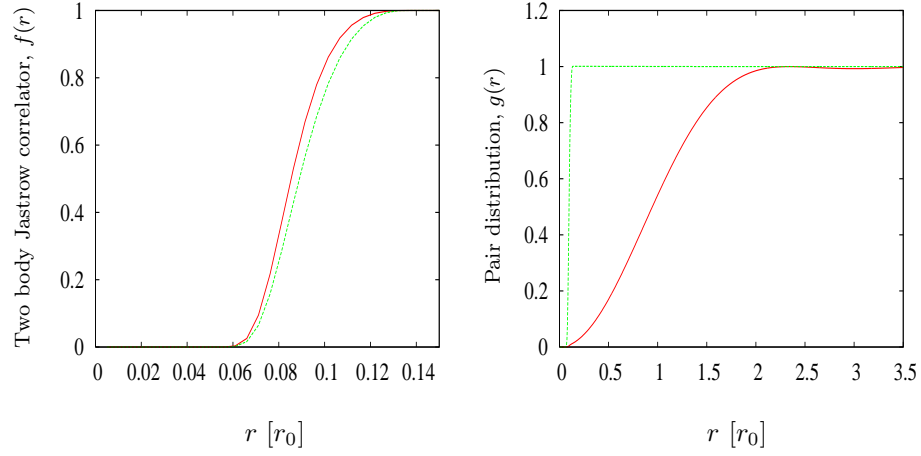
Figure 3.5: Left: Parallel (red line) and antiparallel (green line) components of the Jastrow correlation function. Right: Parallel (red line) and antiparallel (green line) components of the pair distribution function. Both situations correspond to the reference case for $Li^7$ ultracold atoms interacting via a Lennard-Jones potential.

| $k_F a_s$ | $\rho/\rho_{Li}$ | $E[E_{FG_{Li}}]$ | $E^{\sigma_z}[E_{FG_{Li}}]$ |
|---|---|---|---|
| 1 | 0.0024 | 0.0179 | 0.0179 |
| 3 | 0.0666 | 0.1556 | 0.1556 |
| 5 | 0.3085 | 0.4155 | 0.4155 |
| 7.4 | 1.0000 | 0.8643 | 0.8642 |
| 9 | 1.7990 | 1.2309 | 1.2307 |
| 12 | 4.2643 | 2.0187 | 2.0179 |
| 14 | 6.7716 | 2.5813 | 2.5795 |

Table 3.1: Energy of the ground state for ultracold $Li^7$ atoms at various densities in the normal phase (the scattering length is $a_s = -10^4 a_0$, in all the cases). The third column corresponds to the energies of the state independent choice and the forth column labeled with $\sigma_z$ to the case of Jastrow correlations depending on the longitudinal spin.

where the two statistical functions $l_v(r)$ and $l_u(r)$ are defined in analogy to Eq. 2.38, in paper 1 [20] as:

$$l_v(r) = \frac{\nu}{(2\pi)^3 \rho_0} \int d\mathbf{k}\, v_{\mathbf{k}}^2\, e^{i\mathbf{k}\cdot\mathbf{r}} \qquad (3.14)$$

$$l_u(r) = \frac{\nu}{(2\pi)^3 \rho_0} \int d\mathbf{k}\, u_{\mathbf{k}} v_{\mathbf{k}}\, e^{i\mathbf{k}\cdot\mathbf{r}}. \qquad (3.15)$$

The Jastrow function is then found under the constrains of Eq. 3.10. We have considered a variational form for the uncorrelated amplitudes $u(k)$ and $v(k)$ of the uncorrelated BCS state. The new variational parameter defining them is called $\beta$. For large values of this variable one obtains the Fermi distribution of the normal phase, as it is explained in detail in the next section. At this point it is pertinent to mention, that due to the strength of the Lennard-Jones potential, for any choice of the amplitudes $u(k)$ and $v(k)$ and therefore of the statistical correlations $l_v(r)$ and $l_u(r)$, the resulting Jastrow is not very different from the normal case. The calculation of the energy for the parameters of the potential $\sigma = 0.09\, r_0$ and $\epsilon = 610.10\, E_{FG_{Li}}$ does not support the existence of a superfluid phase at any of the trial densities, as it is displayed in Fig 3.6. The different points of any colored branch represent a particular choice of the parameter $\beta$ determining the BCS state. For high values namely $\beta \to \infty$, the energy approaches to the normal value, but it is always above the normal line. We conclude that the range of the potential is important (in this theory) to lead the system into a superfluid transition.

We have enlarged the range of potential maintaining the dilute condition and the scattering length measured by O'Hara *et. al.* [4]. We have performed calculations for:

| | |
|---|---|
| $\sigma = 0.2\, r_0$ | $\epsilon = 120.23\, E_{FG_{Li}}$ |
| $\sigma = 0.3\, r_0$ | $\epsilon = E_{FG_{Li}}$ |

Theses choices allow a window of densities (O'Hara *et. al.* contained in) for which the BCS state is energetically preferred. The gain in energy is scarcely visible, but the behavior of the branches at the densities where the superfluid is favored is clearly different. In Fig. 3.7 the EOS for $\sigma = 0.2\, r_0$ is presented, the minimum density at which the BCS is energetically preferred is estimated in $\rho = 0.8464\rho_{Li}$ corresponding to $k_F a_s = 7$ and while the maximum value of the density is $\rho = 4.2643\rho_{Li}$ corresponding to $k_F a_s = 12$.
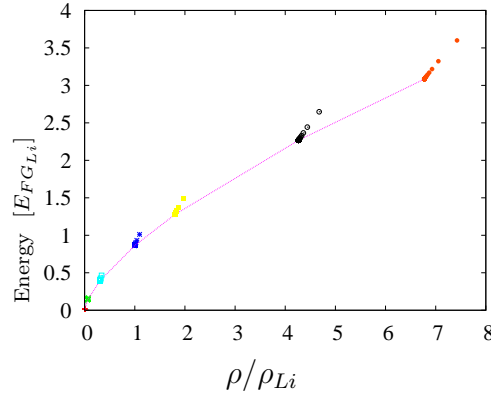
Figure 3.6: Equation of state for a Lennard-Jones potential with $\sigma = 0.09\ r_0$ and $\epsilon = 610.10\ E_{FG_{Li}}$. The full line represents the energy of the normal phase. Every colored branch of points has been calculated using as a correlated BCS as a trial wave function, where the coefficients $u(k)$ and $v(k)$ depend on the parameter $\beta$. At large values of $\beta$ the energy tends to the normal one. For this potential the superfluid phase is not favored at any density.

The inclusion of $\sigma_z$-dependent correlations slightly reduces the energy of the superfluid phase, as it is shown in Fig. 3.8. We show a zoom in of the output coming for $k_F a_s = 10$ Fig 3.9. The range of densities for which the superfluid phase is preferred is not modified by the presence of longitudinal spin dependent correlations, although more precise calculations are needed.

Considering longer ranged potentials induce the particles into a condensation regime which is not the case we are interested in. Therefore, we restrict the possible parameters of the Lennard-Jones potential to describe a dilute Fermi gas with large scattering length ($a_s = -10^4 a_0$) undergoing superfluidity to $\sigma \in (0.2, 0.4)$. The proportionality constant [3] closest to the value in the unitary limit was obtained when $\sigma = 0.3$, being estimated in $\xi = 0.46$, which is not far to the MC estimates even if we are not strictly working in the unitary regime.

---

[3]In the unitary limit $|k_F a_s| \to \infty$, Monte Carlo calculations [3] establish that the constant $\xi$ in $E = \xi \frac{3}{5} \frac{\hbar^2 k_F^2}{2m}$ is $\xi = 0.44$.
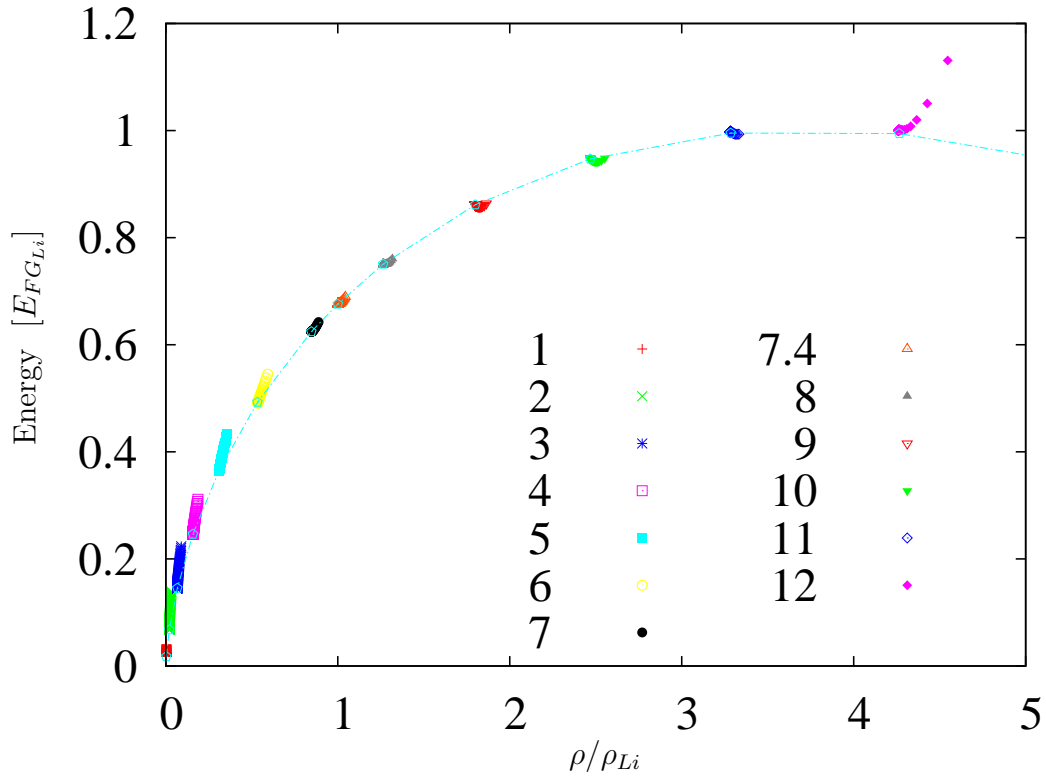
Figure 3.7: Equation of state for a Lennard-Jones potential with $\sigma = 0.2 \; r_0$ and $\epsilon = 120.23 \; E_{FG_{Li}}$. For a range of densities higher than $\rho = 0.8464\rho_{Li}$ the superfluid phase is energetically favored.
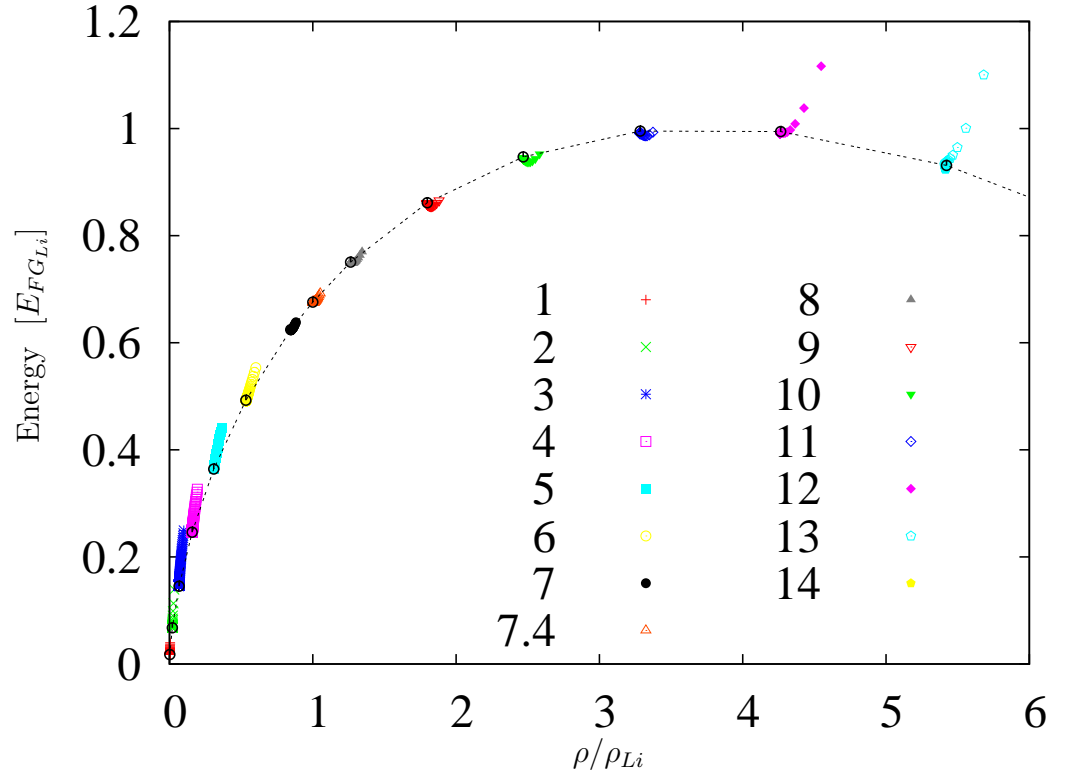
Figure 3.8: Equation of state for a Lennard-Jones potential with $\sigma = 0.2\ r_0$ and $\epsilon = 120.23\ E_{FG_{Li}}$. A BCS state with longitudinal spin dependent Jastrow is considered. This dependence does not bring any new features in the EOS.
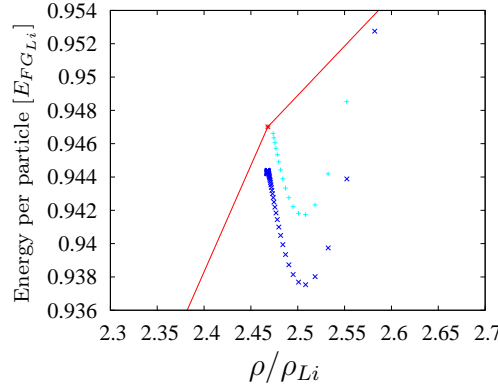
Figure 3.9: Detail of the equation of state for a Lennard-Jones potential with $\sigma = 0.2 \ r_0$ and $\epsilon = 120.23 \ E_{FG_{Li}}$. The full red line corresponds to the normal FHNC energy, the light blue points reprensent the energy obtained for differente BCS trials correlated with a simple Jastrow and the dark blue points to a BCS choice having a longitudinal spin dependent Jastrow.

## 3.2   Neutron matter

We present in this section the results of FHNC/BCS calculations of pure neutron matter with Jastrow-type correlation functions with and without longitudinal spin-dependence. We use a spin-dependent semi-realistic NN two body interactions which fits the low energy NN scattering data up to $\sim 60$ MeV. The chosen interaction is the S3 potential proposed by Afnan and Tang [61], which reproduce the binding energy of the deuteron and $\alpha$ particle. It is of the form

$$
\begin{aligned}
V_{ij}(r) \ = \ & V_S^e(r) \ \mathrm{P}_0(ij)\Pi_1(i,j) + V_T^e(r) \ \mathrm{P}_1(ij)\Pi_0(ij) + \\
& V_S^o(r) \ \mathrm{P}_0(ij)\Pi_0(i,j) + V_T^o(r) \ \mathrm{P}_1(ij)\Pi_1(i,j),
\end{aligned} \tag{3.16}
$$

where the superscripts $e$ and $o$ indicates the spatial parity of the corresponding pair wave function and the subscript $S$ and $T$ labels the singlet or triplet spin state. The spin-isospin projector operators are given by,

$$
\begin{aligned}
\mathrm{P}_0(i,j) = \frac{1 - \boldsymbol{\sigma}_i \cdot \boldsymbol{\sigma}_j}{4}, \qquad \mathrm{P}_1(i,j) = \frac{3 + \boldsymbol{\sigma}_i \cdot \boldsymbol{\sigma}_j}{4}, \\
\Pi_0(i,j) = \frac{1 - \boldsymbol{\tau}_i \cdot \boldsymbol{\tau}_j}{4}, \qquad \Pi_1(i,j) = \frac{3 + \boldsymbol{\tau}_i \cdot \boldsymbol{\tau}_j}{4}.
\end{aligned} \tag{3.17}
$$

For pure neutron matter $\boldsymbol{\tau}_i \cdot \boldsymbol{\tau}_j = 1$, and Eq. 3.16 becomes,

$$V_{ij}(r) = V_c(r) + V_\sigma(r)\boldsymbol{\sigma}_i \cdot \boldsymbol{\sigma}_j \tag{3.18}$$

where,

$$V_c(r) = \frac{V_S^e(r) + 3V_T^o(r)}{4} \tag{3.19}$$

$$V_\sigma(r) = \frac{-V_S^e(r) + V_S^o(r)}{4}. \tag{3.20}$$

The S3 potential is given by:

$$V_S^o(r) = V_T^o(r) \equiv V_{odd}(r) = 1000.0e^{-3.0r} \tag{3.21}$$

$$V_S^e(r) = V_{odd}(r) - 166.0e^{-0.80r^2} - 23.0e^{-0.4r^2}. \tag{3.22}$$

The calculation of the scattering length for the two body system in the singlet spin configuration at zero energy gives $a_{NN} = -16.3$ fm, whose absolute value is large compared with the range of the potential around ($R_0 \sim 2$ fm). The experimental value of $a_{NN}$ is estimated in $-18.5 \pm 0.3$ fm from the $^2\mathrm{H}(\pi^-, \gamma n)n$ reaction [13] and $-18.7 \pm 0.3$ fm from the $^2\mathrm{H}(n, nn)p$ reaction [62]. The good agreement in not surprising because the Afnan-Tang potential reproduces the low energy NN data. We present in Fig. 3.10 the singlet part of the Afnan-Tang interaction, together with the radial reduced part of the wave function solution of Eq. 3.2 and its asymptotic limit at large distances.

In what follows, we want to compare the FHNC results obtained for pure neutron matter (PNM) with the Afnan-Tang interaction for the normal phase with and without longitudinal spin dependence in the Jastrow factor and for the superfluid phase in the same situation.

### 3.2.1    Normal phase

We first consider the correlations induced by the strong interactions to be independent on the spin states of the particles, namely we take simple Jastrow ansatz. The optimal Jastrow correlation is found in the standard way, by solving the second order Euler equation under the boundary condition given in Eq. 3.10. Then, we solve the FHNC equations to find the pair correlation which is used to compute the energy per particle. The energy is minimized to get the optimal value of the healing distance $d$. In Fig. 3.11 we show a typical example of $f(r)$ and $g(r)$ at $\rho = 0.030$ fm$^{-3}$.
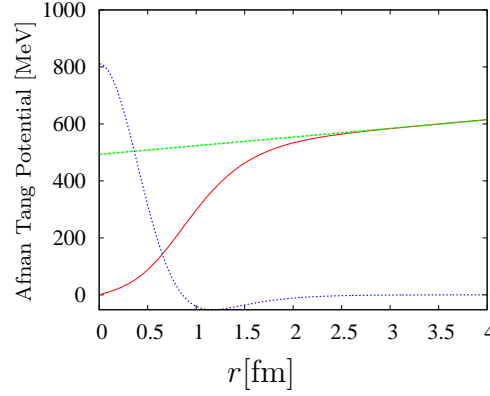
Figure 3.10: Singlet part of the Afnan-Tang potential (blue line) and solution of the reduced radial wave function at energy $E = 0$ (red line) with its asymptotic behavior at large $r$ (green line). The intercept of the green line with the $r$ axis, give the value of the scattering length, not visible in the figure. The units of $u(r)$ are not displayed.
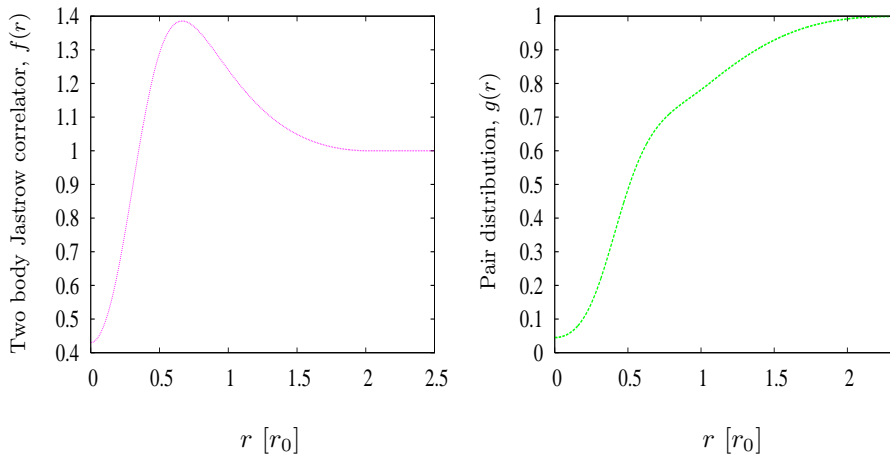


Figure 3.11: Left: Jastrow correlation function for PNM. Right: Pair distribution function. Both figures were obtained at $\rho = 0.030$ fm$^{-3}$ and the optimal healing distance corresponds to $d = 1.07\ r_0$.

| $\rho$ [fm$^{-3}$] | $d/r_0$ | $E_2$ [MeV] | $E_{FHNC}$[MeV] | $E_{FG}[MeV]$ |
|---|---|---|---|---|
| 0.0020 | 0.82 | 1.30 | 1.36 | 1.89 |
| 0.0080 | 0.98 | 3.04 | 3.14 | 4.76 |
| 0.0140 | 1.04 | 4.32 | 4.38 | 6.92 |
| 0.0200 | 1.07 | 5.45 | 5.41 | 8.77 |
| 0.0260 | 1.08 | 6.49 | 6.34 | 10.45 |
| 0.0320 | 1.05 | 7.49 | 7.21 | 12.00 |

Table 3.2: Energy of the ground state for PNM at various densities in the normal phase. The Jastrow-correlation is state independent.
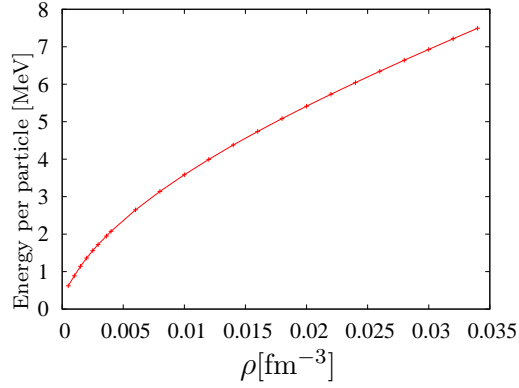


Figure 3.12: FHNC energy per particle of the normal phase of pure neutron matter with state independent correlations.

Notice that g(r) reaches the value of 1 at a distance much larger than the healing distance. This is a consequence of the presence of the statistical correlations. On the other side, $g(r)$ differs considerably from the free gas pair correlation function $g_{FG}(r)$, as can be appreciated in the figure.

The only variational parameter in this case is the healing distance $d$ which we report in Table 3.2 for different densities. (The energy at second order is also reported). In Fig. 3.12 is possible to see the energy per particle as a function of the density.

The inclusion of a longitudinal spin dependent Jastrow correlator, changes

the Euler Lagrange equation as follows:

$$\Upsilon_p''(r) = \left\{\frac{\phi_p''(r)}{\phi_p(r)} + \frac{m}{\hbar^2}\big(V_c(r) + V_\sigma(r) - \lambda_p\big)\right\}\Upsilon_p(r) \tag{3.23}$$

$$\Upsilon_a''(r) = \left\{\frac{\phi_a''(r)}{\phi_a(r)} + \frac{m}{\hbar^2}\Big(V_c(r) - V_\sigma(r)\big[1 + 2n_a\ell^2(k_F r)\big] - \lambda_a\Big)\right\}\Upsilon_a(r)$$

$$\text{where} \quad \Upsilon_p(r) \equiv \phi_p(r)f_p(r) \tag{3.24}$$

$$\Upsilon_a(r) \equiv \phi_a(r)f_a(r)$$

$$\text{and} \quad \phi_p^2(r) \equiv r^2\big[1 - \ell^2(k_F r)\big] \tag{3.25}$$

$$\phi_a(r) \equiv r. \tag{3.26}$$

The results shown in the following have been obtained by keeping the vertex correction $n_a = 1$ (see Appendix) in the solution of the Euler-Lagrange equation given in Eq. 3.23. One can see from Table 3.3 that its FHNC value is always close to 1. We have also assumed the same healing distance for both $f_p(r)$ and $f_a(r)$. In Fig. 3.13 (left) the parallel and antiparallel correlation functions are shown at $\rho = 0.030$ fm$^{-3}$. The shape of the antiparallel component shows a peak at $r = 0.72\, r_0$ which is manifested as well in the corresponding pair distribution function. In the same figure on the right, the two components of $g(r)$ are displayed.

The FHNC calculation of the energy is performed using the FHNC equations given in Table 2.5.1 and 2.5.1, for the case of $\sigma_z$-dependent Jastrow. We have introduced an extra variational parameter $\gamma$ as a quenching parameter of the $\sigma_z$ dependence, namely:

$$f(12) = f_{central}(r) + \gamma f_{\sigma_z}(r)\sigma_{1z}\sigma_{2z}. \tag{3.27}$$

When $\gamma = 0$, the correlation between particles 1 and 2 is purely central while for $\gamma = 1$, the spin-dependent part of the Jastrow is fully set. The parallel and antiparallel components can be written in terms of the central and $\sigma_z$ components as follows,

$$f_{central}(r) = \frac{f_p(r) + f_a(r)}{2}$$

$$f_{\sigma_z}(r) = \frac{f_p(r) - f_a(r)}{2} \tag{3.28}$$

The results are reported in Fig. 3.14 and Table 3.3. We find that $\gamma = 1$ is always is good variational choice for all the cases. One can see that the $\sigma_z$-dependence have little effect on the EOS of the normal phases of pure neutron
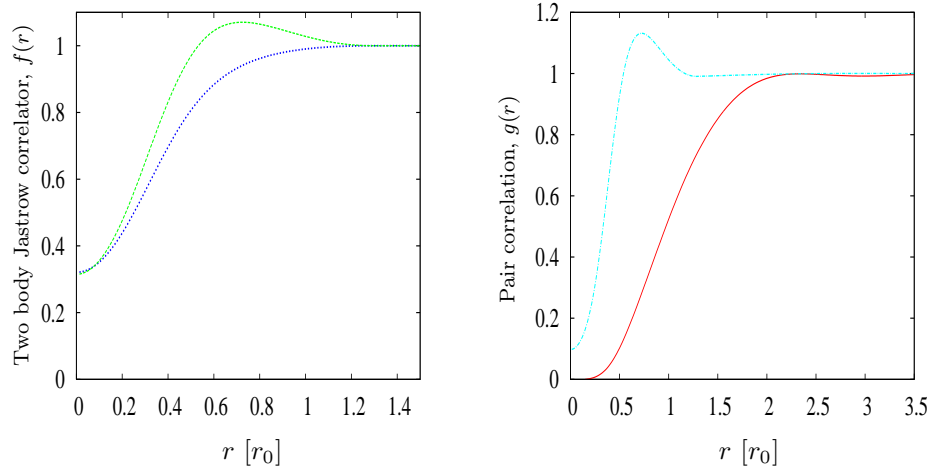
Figure 3.13: Left: Parallel (red line) and antiparallel (light blue line) components of the Jastrow function for PNM. Right: Parallel (red line) and antiparallel (light blue line) components of the pair distribution function. Both figures were obtained at $\rho = 0.030$ fm$^{-3}$ and the optimal healing distance corresponds to $d = 1.29\ r_0$.

matter. A comparison of the EOS for scalar Jastrow and and $\sigma_z$-dependent Jastrow is displayed in Fig. 3.15.

## 3.2.2   Superfluid phase

We present an application of the FHNC/BCS theory proposed in I to the case of PNM, for spin-independent Jastrow correlations. Notice that in I there was no derivation of the expression to compute the energy per particle. This is the first calculation of the EOS for a superfluid system with FHNC/BCS theory. The first ingredient needed to apply FHNC/BCS theory, consist of finding the Jastrow function as well as the probability factors $u(k)$ and $v(k)$ entering in the definition of the uncorrelated BCS state. Lacking of a full Euler-Lagrange set of equations for $f$ and the uncorrelated BCS amplitudes, we proceed with an intermediate approach. We choose a trial probability distribution of the form:

$$v^2(k) = \frac{1}{1 + e^{(k^2 - k_{0_F}^2)\beta}}, \tag{3.29}$$

| $\rho$ [fm$^{-3}$] | $d/r_0$ | $\gamma$ | $E_2$ [MeV] | $E_{FHNC}$[MeV] | $n_a$ |
|---|---|---|---|---|---|
| 0.0020 | 1.00 | 1.0 | 1.16 | 1.29 | 0.97 |
| 0.0080 | 1.14 | 1.0 | 2.75 | 3.02 | 0.98 |
| 0.0140 | 1.20 | 1.0 | 3.98 | 4.25 | 0.98 |
| 0.0200 | 1.24 | 1.0 | 5.08 | 5.29 | 0.99 |
| 0.0260 | 1.27 | 1.0 | 6.12 | 6.23 | 0.99 |
| 0.0320 | 1.30 | 1.0 | 7.10 | 7.11 | 0.99 |

Table 3.3: Energy of the ground state for PNM at various densities for the normal phase. The correlation function is a longitudinal spin-dependent Jastrow whose strength is modulated by $\gamma$. The vertex correction $n_a$ is also reported.
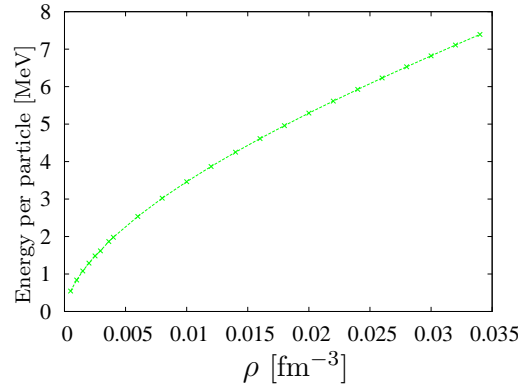


Figure 3.14: Energy of the normal phase for pure neutron matter when the correlations are longitudinal spin dependent.
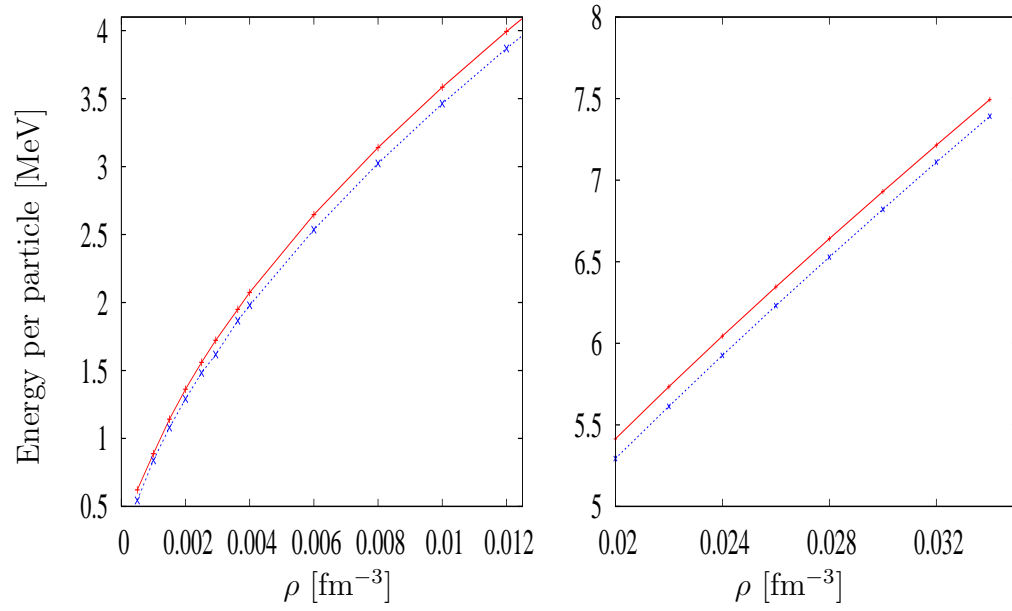
Figure 3.15: Energy of the normal phase for pure neutron matter. The red line corresponds to a pure simple Jastrow correlation, while the blue line to a longitudinal spin-dependent Jastrow.

this quantity determines the uncorrelated density $\rho_0$ (see Eq. 2.39) of the system. Notice that in the limiting case of $\beta \to \infty$, the Fermi distribution function $v^2(k)|_{\beta \to \infty} = \Theta(k - k_{0_F})$ (and consequently $u^2(k)|_{\beta \to \infty} = 0$), is recovered. Therefore the corresponding exchange correlation functions $l_v(r) \to \ell(k_F r)$, $l_u(r) \to 0$, and the FHNC for the normal phase is fully recovered (see Appendix). Let us call $\rho_{0_F}$ the density at which this situation holds ($\beta \to \infty$). Notice that for $\beta$ finite, $\rho_0 \neq \rho_{0_F}$.

The Euler-Lagrange equation to find the dynamical correlation is given then by:

$$\Upsilon''(r) \;=\; \left\{ \frac{\phi''(r)}{\phi(r)} + \frac{m}{\hbar^2}\left[ V_c(r) - \frac{3V_\sigma\left(\frac{c_d}{c}\right)^2\left(\frac{l_v^2+l_u^2}{\nu}\right)}{1-\left(\frac{c_d}{c}\right)^2\left(\frac{l_v^2-l_u^2}{\nu}\right)} - \lambda \right] \right\}\Upsilon(r) \quad (3.30)$$

where $\Upsilon(r)$ and $\phi(r)$ are defined in Eq. 3.12 and Eq. 3.13 respectively and the solutions of $f(r)$ satisfy the boundary conditions Eq. 3.10. We have approximated the vertex corrections $c$ and $c_d$ to 1. We show in Fig. 3.16 (left) an example of the Jastrow function for a density $\rho = 0.0020$ fm$^{-3}$. The FHNC/BCS allows to find the corresponding pair distribution function, displayed on the right.
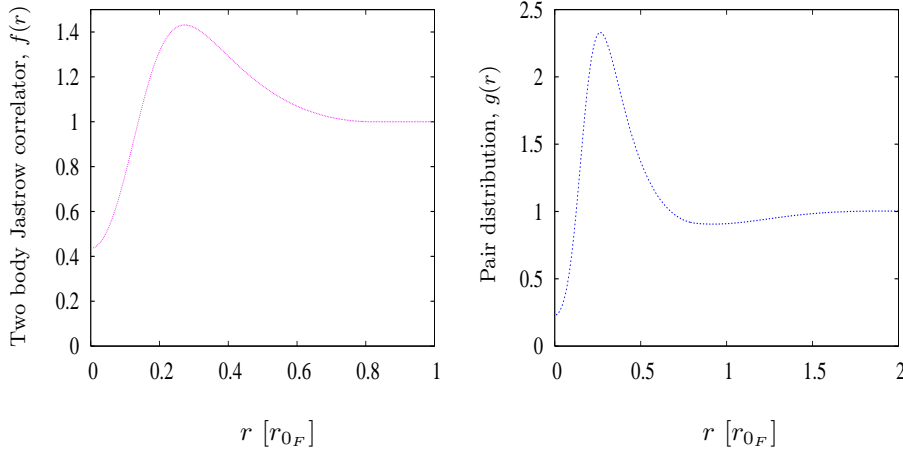


Figure 3.16: Left: Jastrow correlation function for PNM in the superfluid state. Right: Corresponding pair distribution function. Both figures were obtained at $\rho = 0.0020$ fm$^{-3}$, $\beta = 15$ and the healing distance is the same than the normal phase namely, $d_{0_F} = 0.82 \, r_{0_F}$. The value of $r_{0_F}$ refers to the uncorrelated interparticle distance obtained in the limit of $\beta \to \infty$.

Three variational parameters have been defined so far, the healing distance $d$, $\beta$ and $k_{0_F}$. The search of their optimal values is much more difficult than in standard variational calculations, because the density $\rho = c\rho_0$ of the system depends on the variational parameters. That is because $|BCS\rangle$ does not conserve the number of particles and therefore $\rho_0$ is defined as an average of the number operator. Moreover the correlations do change such an average. For this reason the energy expectation values to be compared must refer to trial functions providing the same density $\rho$.

To achieve this we have proceeded in the following way. The parameter $k_{0_F}$ fixes the density $\rho_{0_F}$ of the underlying normal phase system, which is recovered in the limit $\beta \to \infty$. We have found that the healing distance parameter has an optimal value which is always very close to that of the normal phase at $\rho_{0_F}$ (denoted here as $d_{0_F}$), therefore we kept such value. The parameter $\beta$ is the one which gives the largest effect in the density $\rho_0$ and consequently in $\rho = c\rho_0$. We varied the $\beta$ parameter, for $k_{0_F}$ and $d_{0_F}$ fixed, from $\beta \sim \infty$ to $\beta \sim 1$. Fig. 3.18 displays the results obtained in such a way for the case of spin-independent Jastrow.

The EOS of the BCS phase is obtained by the envelope of the various branches. Such envelop crosses the EOS of the normal phase in two points which delimit the region when the BCS phase is energetically favorable with respect to the normal one. In Fig. 3.18, it is shown that the density at which the superfluid phase becomes unfavorable occurs at $\rho = 0.02$ fm$^{-3}$.

A similar procedure has been used to the case of $\sigma_z$-dependent correlations. An example of the parallel and antiparallel components for the Jastrow and the pair correlation function is shown in Fig. 3.17 at $\rho = 0.012$ fm$^{-3}$. The equation of state is presented in Fig. 3.19. The energy per particle is significantly lower than in the case of spin-independent correlations. The effect of the $\sigma_z$-dependency is much larger than in the normal phase. Moreover the limiting value of the superfluid density is enlarged to $\rho = 0.027$ fm$^{-3}$. Table 3.4 report the results displayed in Fig. 3.19.

In Table 3.4 some values of the energy for the optimal parameter $\beta$ are shown, together with the value of the energy at second order of the cluster expansion in the number of points (considering $c = 1$ and $c_d = 1$).

Notice that for large values of $\beta$ the FHNC energy tends to the value found in the normal phase at a density given by $\rho_{0_F}$.
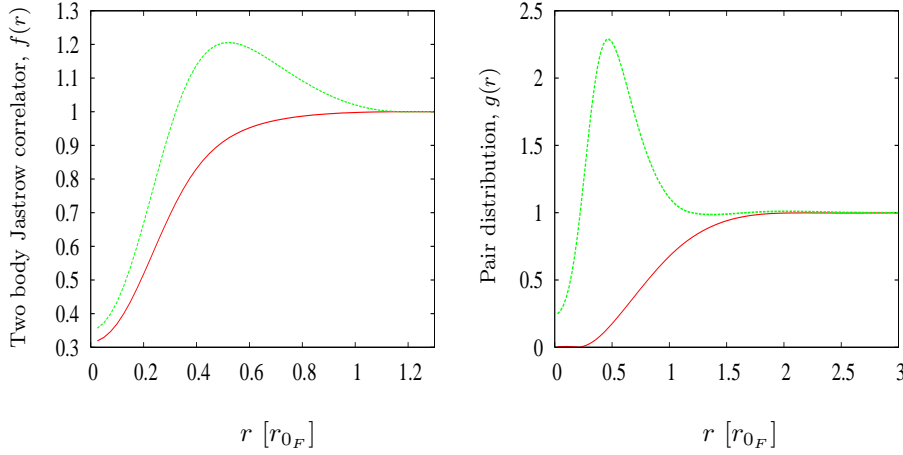
Figure 3.17: The parallel (red line) and antiparallel (green line) components of the Jastrow correlation function (left) and the pair correlation (right) for PNM in the superfluid state. Both figures were obtained at $\rho = 0.012$ fm$^{-3}$, $\beta = 6.5$ and the healing distance is the same than the normal phase namely, $d_{0_F} = 1.18 \ r_{0_F}$.

| $\rho_{0_F}$ [fm$^{-3}$] | $d/r_{0_F}$ | $\beta$ | $c$ | $c_d$ | $E_{FHNC}$[MeV] | $E_2$ [MeV] |
|---|---|---|---|---|---|---|
| 0.0020 | 0.82 | 15.0 | 1.13 | 1.18 | 1.12 | 1.09 |
| 0.0060 | 0.94 | 8.0 | 1.09 | 1.13 | 2.52 | 2.68 |
| 0.012 | 1.03 | 10.5 | 1.02 | 1.06 | 3.89 | 3.97 |
| 0.0020 | 1.00 | 15.0 | 1.28 | 1.23 | 0.69 | 0.45 |
| 0.0060 | 1.11 | 10.0 | 1.15 | 1.15 | 1.89 | 1.88 |
| 0.012 | 1.18 | 6.5 | 1.09 | 1.07 | 3.65 | 3.83 |

Table 3.4: Energy of the ground state for PNM for the superfluid phase. A state independent Jastrow is consider in the first three rows while a longitudinal spin dependent Jastrow corresponds to the last three rows. $\beta$, healing distance and the vertex corrections $c$ and $c_d$ are also reported. The energy of the FNHC/BCS calculation is close to the second order approximation.
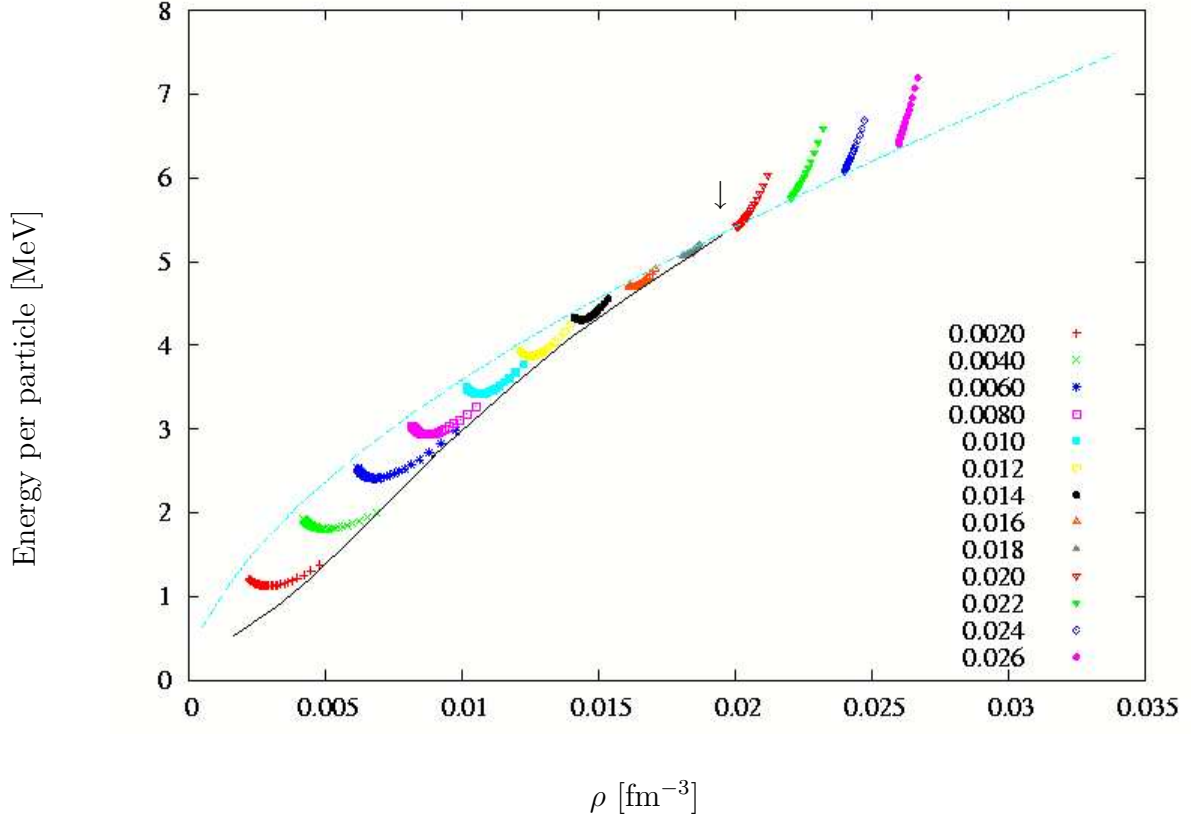
Figure 3.18: Energy of the superfluid phase for pure neutron matter. It corresponds to a choice of pure simple Jastrow correlation. The arrow points to the density at which the BCS state is unfavorable $\rho = 0.02$ fm$^{-3}$. The dashed blue line delineate the normal phase while the black lower full line the BCS phase. The branches are labeled by the corresponding $\rho_{0_F}$.
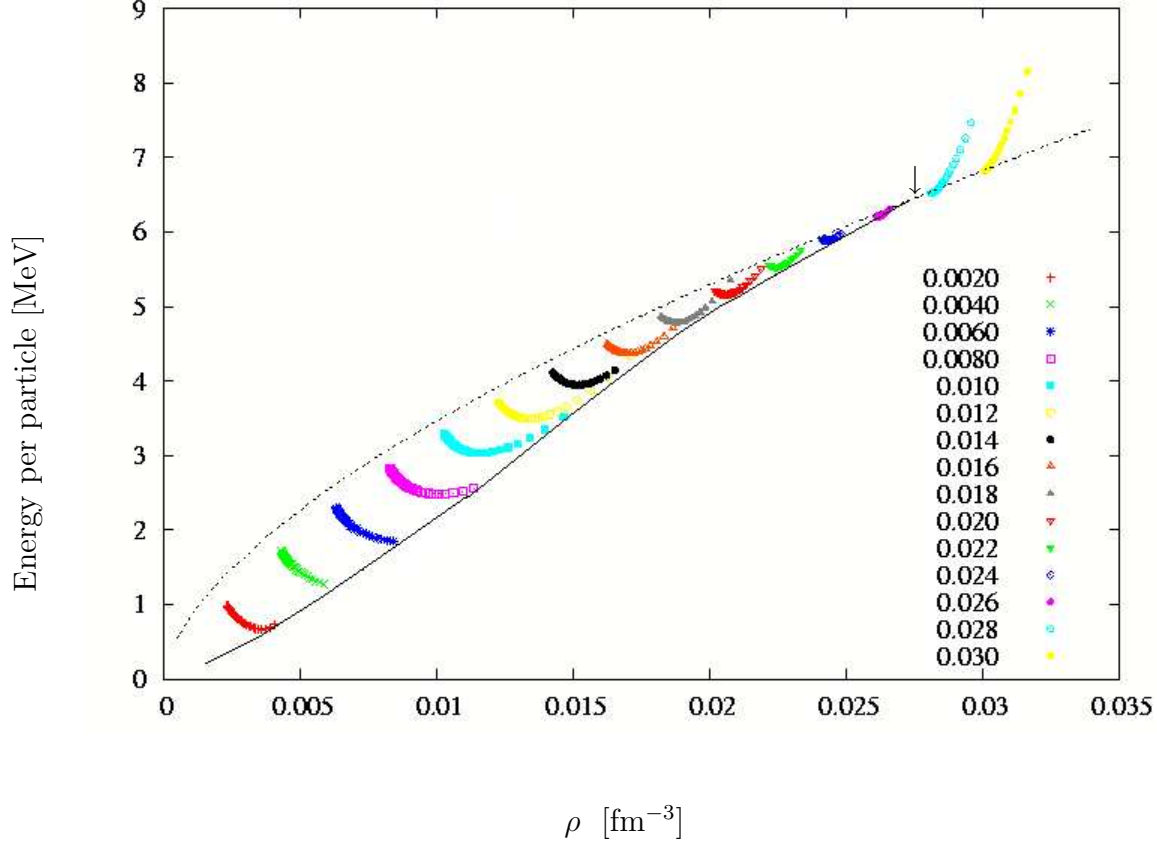
Figure 3.19: Energy of the superfluid phase for pure neutron matter. A longitudinal spin-dependent Jastrow is considered. The arrow points to the density at which superfluid is unfavorable, $\rho = 0.027\,\text{fm}^{-3}$. The normal phase is indicated with the upper dashed line. The envelope (lower dashed line) defines the superfluid phase. The labels refer to the corresponding density, $\rho_{0_F}$.

# Chapter 4

# Calculation of the gap and excitation energy

The gap measurements provide a tool for investigating the nature of the paired particles responsible for the frictionless currents at low temperatures. In the BCS theory (weak coupling regime, small scattering length) the Gap is proportional to the critical temperature, $\Delta(T = 0) = 1.76 k_B T_c$, in good agreement with the experiments. In general the existence of a gap energy is a signature of the superfluid state and this feature is valid even far from the weak coupling side; in the BEC regime and even through the crossover. Recently the possibility of changing the effective interactions with the tunable Feshbach resonances has been exploited to study the dependence of the gap with the coupling strength, temperature and Fermi energy from the BCS regime to the BEC one. Experiments on $Li^7$ using evaporative cooling have evidenced the appearance of a gap in the radio-frequency excitation spectra [63]. In this chapter we develop a formalism to calculate the gap energy when strongly correlations are present. We present an application of the theory for the case of neutron matter at low density.

## 4.1  The gap in the FHNC/BCS theory

We calculate in this section the gap energy and the excitation energy spectrum of a Fermi system in the superfluid phase. We follow the procedure used in [64], [65] to compute the excitation energy for a strongly correlated Fermi fluid in the normal phase. In this case one has a particle-hole excitation,
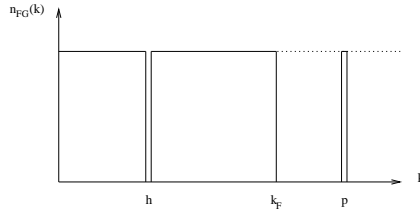
namely
$$|\Psi_{ph}\rangle = a_p^\dagger a_h |\mathrm{SL}\rangle = (a_p^\dagger a_h) a_{k_1}^\dagger \ldots a_{k_N}^\dagger |0\rangle. \tag{4.1}$$

Note that $p \equiv (\mathbf{p}, \sigma)$ where $\sigma$ is the spin projection ($\uparrow$ or $\downarrow$).
One can view $|\Psi_{ph}\rangle$ as a new Slater determinant of the form

$$|\Psi_{ph}\rangle = a_{k_1}^\dagger \ldots a_p^\dagger \ldots a_{k_N}^\dagger |0\rangle, \tag{4.2}$$

where $a_p^\dagger$ is in the same position of $a_h^\dagger$ in Eq. (4.1). Therefore the set of orbitals of $|\Psi_{ph}\rangle$ is $\{k_1, k_2, \ldots, p, \ldots, k_N\}$ with $h$ missing, namely



$$\begin{cases} n_{\mathrm{FG}} = 1 & \text{for } k \leq k_F \text{ except for } k = h \text{ where it is zero} \\ n_{\mathrm{FG}} = 1 & \text{for } k = p \end{cases}$$

One can do the summations independently on all the set of orbitals. The process of cancellation of the denominator in the cluster expansion for the excitation energy has been derived in [64], [65]. One removes a small fraction $x$ of particles from a thin spherical shell at $\mathbf{q}'$ and put them in a thin spherical shell at $\mathbf{q}$. The widths $\mathrm{d}_{q'}$ and $\mathrm{d}_q$ are related in the following way

$$x = \frac{1}{\pi^2 \rho} q'^2 \mathrm{d}_{q'} = \frac{1}{\pi^2 \rho} q^2 \mathrm{d}_q$$

$$\mathrm{d}_q = \frac{q'^2}{q^2} \mathrm{d}_{q'} \tag{4.3}$$

$$\tag{4.4}$$

in general the width is given by,

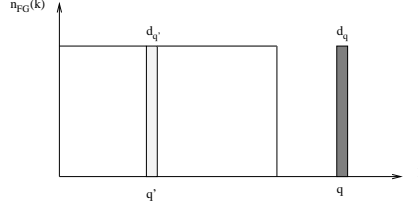$$\mathrm{d}_\alpha = \frac{x \pi^2 \rho}{\alpha^2}. \tag{4.5}$$

Figure 4.1: Pictorial representation of the creation of a particle-hole excitation in the normal phase.

The cluster terms in the FHNC equations remain the same in the not exchanged particles, whereas the exchange functions $\ell_{GS}(k_F r)$

$$\ell_{GS}(k_F r) \rightarrow l(r, p, h, x) = \ell_{GS}(k_F r) + x \left[ \frac{\sin(pr)}{pr} - \frac{\sin(hr)}{hr} \right] \tag{4.6}$$

The factor $x$ should be of order $\frac{1}{\Omega}$ but, in reality is treated numerically as a smallness parameter. For an operator $O$, for instance the Hamiltonian, the energy to create such excitation is given by,

$$
\begin{aligned}
\langle O \rangle_{ph} - \langle O \rangle_0 &= \text{linear terms of } \langle O(x) \rangle \text{ in } x \\
&= \left. \frac{\partial}{\partial x} O(x) \right|_{x=0}. \tag{4.7}
\end{aligned}
$$

In order to use a similar procedure for the gap energy, we have first to understand the structure of the excitation $|\Psi_{qq'}\rangle$. Let us define

$$
\begin{aligned}
|\Psi_{qq'}\rangle &= \frac{a_q^\dagger a_{q'}}{v_{q'} u_q} |\text{BCS}\rangle \\
&= \frac{(a_q^\dagger a_{q'})}{v_{q'} u_q} \prod (u_k + v_k a_{\mathbf{k}\uparrow}^\dagger a_{-\mathbf{k}\downarrow}^\dagger) |0\rangle \tag{4.8}
\end{aligned}
$$

where $v_{q'} u_q$ acts as a normalization factor. In fact one can view $|\Psi_{qq'}\rangle$ as follows

$$|\Psi_{qq'}\rangle = a_q^\dagger a_{q'}^\dagger \prod_{k \neq q, q'} (u_k + v_k a_{\mathbf{k}\uparrow}^\dagger a_{-\mathbf{k}\downarrow}^\dagger) |0\rangle \tag{4.9}$$

which implies that both the pairs $q\bar{q}$ and $q'\bar{q}'$ are missing in any term of the series Eq.(4.9) whereas the orbitals $q$ and $\bar{q}'$ ($\frac{1}{\Omega}e^{i\mathbf{q}\cdot\mathbf{r}}\uparrow$ and $\frac{1}{\Omega}e^{-i\mathbf{q}'\cdot\mathbf{r}}\downarrow$) are present in any term with strength 1.

Normalization of $|\Psi_{qq'}\rangle$ given in Eq.(4.9) is 1,

$$\langle\Psi_{qq'}|\Psi_{qq'}\rangle = \prod_{k\neq q,q'}(u_k^2 + v_k^2) = 1 \tag{4.10}$$

because $u_k^2 + v_k^2 = 1$ for all k. It follows that the contraction rules on $|\Psi_{qq'}\rangle$ are very similar to those of the correlated $|BCS\rangle$ state (see [20]), namely

$$
\begin{aligned}
\underline{a_\alpha^\dagger a_{\alpha'}} &= \langle\Psi_{qq'}|a_\alpha^\dagger a_{\alpha'}|\Psi_{qq'}\rangle \\
&= \begin{cases} \delta_{\alpha\alpha'}v_\alpha^2 & \text{if } \alpha \neq q, q' \\ \delta_{\alpha\alpha} & \text{if } \alpha = q, q' \end{cases}
\end{aligned} \tag{4.11}
$$

and

$$\underline{a_\alpha^\dagger a_{\alpha'}^\dagger} = \underline{a_\alpha a_{\alpha'}} = \begin{cases} t_\alpha\delta_{\alpha\bar{\alpha}'}u_\alpha v_\alpha & \text{if } \alpha \neq q, q' \\ 0 & \text{if } \alpha = q, q' \end{cases} \tag{4.12}$$

We can now proceed in deriving the FHNC equations for $|\Psi_{qq'}\rangle$ which are structurally the same of FHNC/BCS. As in the case of $|SL_{ph}\rangle$ we have to modify the exchange functions, only

$$
\begin{aligned}
l_v(r) &\rightarrow l_v(r, q, q', \epsilon) = \\
&\quad l_v(r) + \epsilon\left[(1 - 2v_q^2)\frac{\sin(qr)}{qr} + (1 - 2v_{q'}^2)\frac{\sin(q'r)}{q'r}\right] \tag{4.13}
\end{aligned}
$$

$$
\begin{aligned}
l_u(r) &\rightarrow l_u(r, q, q', \epsilon) = \\
&\quad l_u(r) - \epsilon\left[2u_q v_q\frac{\sin(qr)}{qr} + 2u_{q'}v_{q'}\frac{\sin(q'r)}{q'r}\right] \tag{4.14}
\end{aligned}
$$

The factors $(1 - 2v_q^2)$ comes from adding an orbital with strength 1 and subtracting a pair with strength $v_q^2$, and similarly for $(1 - 2v_{q'}^2)$. Analogous arguments hold for the factors $2u_q v_q$ and $2u_{q'}v_{q'}$ in Eq.(4.14).

In contrast with the normal phase, we have here also a modification for the $\rho_0$ factor form the unchanged particles. Here

$$\rho_0 \rightarrow \rho_0[1 + 2\epsilon(1 - v_q^2 - v_{q'}^2)]. \tag{4.15}$$

Notice that the normal phase case is fully recovered. If $v_q^2 = 0$ and $v_{q'}^2 = 1$ (normal phase) and correspondingly $u_q^2 = 1$ and $u_{q'}^2 = 0$, there are no changes

in $\rho_0$ and $l_u(r)$ (which is zero in this case), and $l_v(r)$ is modified as $l$ in Eq.(4.6).

Let us now consider the case of excitation of the Fermi surface $|\mathbf{q}| = |\mathbf{q}'| = k_F$, with $v_{k_F}^2 = u_{k_F}^2 = 1/2$, for which the excitation energy is $2\Delta$ (twice the gap) where $\Delta$ is the gap energy. In this case $l_v(r)$ and $\rho_0$ are not modified and one is left with the modification of $l_u(r)$

$$l_u(r, k_F, k_F, \epsilon) = l_u(r) - 2\epsilon \frac{\sin(k_F r)}{k_F r}. \tag{4.16}$$

The set of Nodal and Composite diagrams in the FHNC are solved in the usual way, once one have performed the new replacements in the exchange functions. The calculation of the gap energy $q = q' = k_F$ and the excitation energy $E(q)$, $q' = k_F$ are reached in the limit of $\epsilon \to 0$.

To compute $2\Delta$ the procedure consist of the following steps:

1. The solution of the FHNC/BCS for $\epsilon = 0$, gives the ground state energy $E_0$.

2. Solving the FHNC/BCS equations with the modifications in the statistical correlation Eq. 4.16, at $\epsilon = 0.1$ gives the energy $E(\epsilon)$. Then the calculation of the gap is given by:

$$\frac{E(0.1) - E_0}{0.1} = 2\Delta_1$$

3. The value of $\epsilon$ is decreased and step 2 is repeated up to reaching convergence.

To calculate the excitation energy $E(q)$:

1. The gap $\Delta$ is computed as it was described before.

2. By introducing the modified statistical correlations Eq. (4.13) and (4.14) and the modified uncorrelated density (4.15) in the FHNC/BCS at $|\mathbf{q}'| = k_F$, one calculates in the same way as for $\Delta$. After reducing $\epsilon$ up to convergence one gets the excitation energy $E_q$ from:

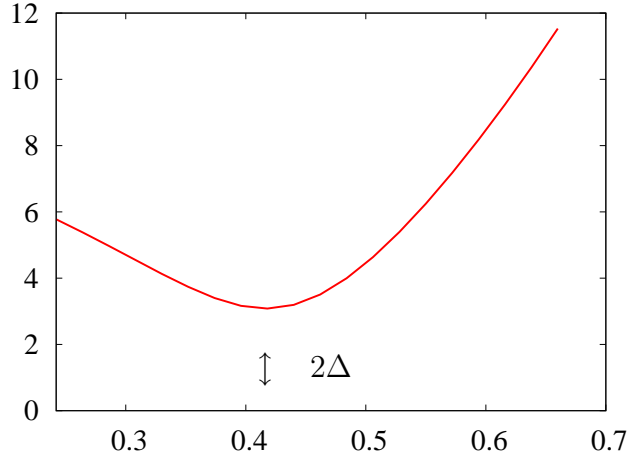$$\begin{aligned} E &= \Delta + E(q) \\ E(q) &= E - \Delta \end{aligned}$$

Figure 4.2: $E(q)$ for pure neutron matter with Afnan Tang potential at $\rho = 0.003$ fm$^-$3.

One may want to put $E(q)$ in the typical form of $\sqrt{\varepsilon^2(q) + \Delta^2}$. The energy $\varepsilon(q)$ is given by

$$
\begin{aligned}
\sqrt{\varepsilon^2(q) + \Delta^2} &= E_q - \Delta \\
\varepsilon^2(q) + \Delta^2 &= E_q^2 + \Delta^2 - 2E_q\Delta \\
\varepsilon(q) &= \sqrt{E_q(E_q - 2\Delta)}
\end{aligned}
$$

We have computed the gap for the Afnan-Tang potential S3 in pure neutron matter at a typical superfluid density $\rho_{0_F} = 0.03$ fm$^{-3}$. We have used the statistical correlation functions $l_v(r)$ and $l_u(r)$ obtained from solution of the Euler-Lagrange equation at second order calculation for the simple Jastrow ansatz [17]. In Fig. 4.2 we present the energy versus the momentum of the excitation. The minimum of this quantity gives twice the gap of the systems. The value we obtain $\Delta = 1.54$ MeV at $q = 0.42$ fm$^{-1}$, is in agreement with calculations performed at second order [17], reporting 1.61 MeV.

## 4.1.1   Neutron matter

In this section we present the calculation of the Gap performed by considering the variational choice for the BCS amplitudes that we used in the previous
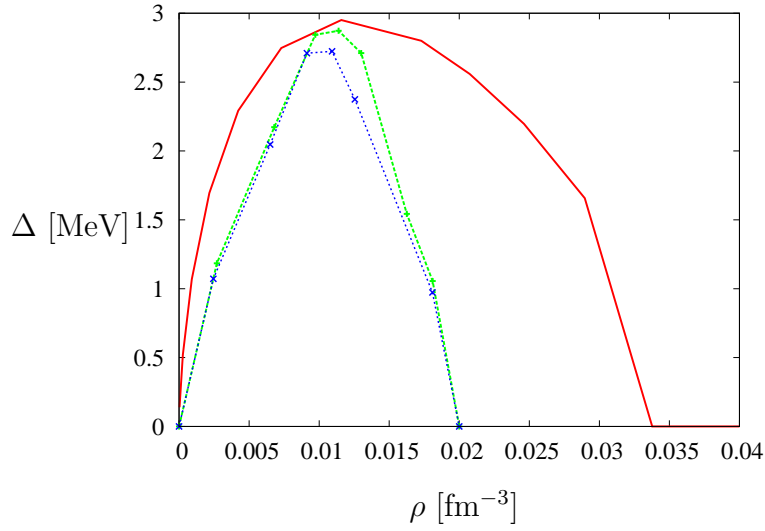
Figure 4.3: Gap versus density in pure neutron matter with Afnan Tang potential. The red line is obtained for $v_4'$ and the green for Afnan-Tang by performing second order calculations [17], [66]. The BCS amplitudes in their calculations come from the solution of a BCS gap equation. The blue line shows the results of this work by performing the theory previously described and by using a variational ansatz for the amplitudes $u(k)$ and $v(k)$. A simple Jastrow correlation was considered.

chapter (See Eq. 3.29). In Fig 4.3 we show the behaviour of the gap as a function of the density using the FHNC theory. We compare the result with the those obtained in [17] for $v_4'$ potential and for Afnan-Tang [66].

# Chapter 5

# Conclusions and perspectives

This thesis addresses the pairing problem in low density Fermi systems, interacting through a force with large and negative scattering length, and therefore are in the strongly correlated regime. Two systems have been studied in detail: i) ultracold dilute Fermi gases and ii) pure neutron matter. In both cases the scattering length has large values compared to the range of the interactions and the interparticle distance.

In order to handle the strong correlations arising amongst the particles we developed a correlated variational theory based upon FHNC theory and we performed calculations in both normal and superfluid phases. The main results reported in this thesis are the following:

1. The FHNC/BCS theory has been generalized to deal with Jastrow correlations depending on the longitudinal spin component. The expressions for the energy per particle, the pair distribution function, the one- and two- body momentum distributions for central and spin dependent potentials have been derived.

2. The equation of state for dilute Fermi gas interacting via Lennard-Jones potential around the value $k_F a_s = -7.4$ of the $^6Li$ [4], has been calculated (the range of values considered is $k_F a_s \equiv [-1; -14]$) for both normal and superfluid phases.

3. The equation of state of pure neutron matter interacting via a central spin dependent potential fitting low energy NN scattering data, has been calculated for both normal and superfluid phases. The range

of densities considered is $\rho \equiv [0.002 - 0.03]$ fm$^{-3}$ corresponding to $k_F a_s \equiv [-6.4; -15.7]$.

4. A formal theory for the calculation of the excitation energy and the gap has been developed in the FHNC formalism, for the case of simple Jastrow correlations, in full analogy to the calculation of the particle-hole excitation energy in the normal phase.

5. The energy gap has been calculated for both dilute Fermi gas and PNM with and without $\sigma_z$-dependence of the Jastrow correlations.

The results obtained deserve the following comments:

- The $\sigma_z$-dependence of the Jastrow correlation, namely the inclusion of a degree of freedom to distinguish parallel from antiparallel spin pairs, has little effect in normal phase, but leads to a significant lowering of the energy in the BCS phase.

- The equation of states are characterized by a region at low densities for which the superfluid phase is energetically favorable. The maximum density at which the BCS configuration is preferred has been estimated in neutron matter to be $\rho_M = 0.020$ fm$^{-3}$ when the simple Jastrow ansatz is considered. The introduction of $\sigma_z$-dependence, increases the value of this critical density, up to $\rho_M = 0.027$ fm$^{-3}$.

- The gap has been previously calculated either with low order many-body theory (CBF, Brueckner, etc.) or with QMC estimating the odd-even effect. This is the first calculation of a many body theory at all cluster orders and in the thermodynamic limit. Comparison show reasonable agreement with QMC the with low-order cluster theories.


The field of fermionic pairing is extremely rich in perspectives. In particular we think that studies of the role played by long range of correlations is particularly needed; the FHNC theory offers the possibility of performing quantitative studies on that. Moreover FHNC theory can be used to evaluate finite size effects in QMC calculations, along the lines of Periodic Box-FHNC [67].

Finally let us cite the most appealing scenarios to be treated by a correlated variational theory as a preliminary study to more sophisticated tools like Monte Carlo methods:

- Fermi-Fermi and Fermi-Bose mixtures: An increasing activity in this field is expected to understand the interplay between different mixtures of different atomic species. The superfluid behavior of Fermi-Fermi mixtures of different atomic masses and Fermi-Bose mixtures in optical latices [68] are important topics for future research.

- p-wave superfluidity: The recent production and detection of molecules of $^{40}$K by using a p-wave Feshbach resonance, and the measurement of its life time and binding energy, envisioned the realization of a p-wave superfluid in ultracold gases. Investigations by Cheng *et al.* [69], Iskin *et al.* [70], and Gurarie *et al.* [71], have been pioneers in predicting a rich phase diagram as a function of the interaction strength.

- BCS/BEC crossover can be studied in greater detail with FHNC theory than with QMC methods.

# Appendix A

# FHNC/BCS equations for longitudinal spin-dependent Jastrow

In this appendix we derive the set of FHNC/BCS equations which have to be solved to sum up the linked cluster diagrams $\mathscr{L}_{p,\alpha}^{(\text{linked})}$ contributing to $\langle \hat{Y} \rangle$ in Eq. (2.41).

The basic operations of FHNC theory are (i) The nodal (or convolution) integration, which is used to sum up nodal diagrams and (ii) the construction of composite diagrammatical structures out of nodal ones. They are performed in a circular and iterative way up the inclusion of all the terms of the nodal and composite series. The only diagrammatical structure left by the solution of the FHNC integral equations are the elementary or bridge diagrams which nobody knows how to include in a closed form like the nodal or composite ones. They can be accounted for, with progressive approximations.

Let us first consider the nodal operation schematically displayed in Fig. A.1

Due to the presence of $\sigma_z$-dependent correlations, the various two-body FHNC quantities, like $X_{\alpha\beta}$, $X_{\alpha'\beta'}$ and $N_{\alpha\beta'}$ of Fig. A.1, have two components in correspondence to the spin-parallel or spin antiparallel configuration of their external pairs. The nodal diagram $N_{\alpha\beta'}(r_{ij})$ is formally given by

$$N_{\alpha\beta'}(r_{ij}) = \left( X_{\alpha\beta} \ c_{\beta\alpha'} \big| X_{\alpha'\beta'} \right) \tag{A.1}$$
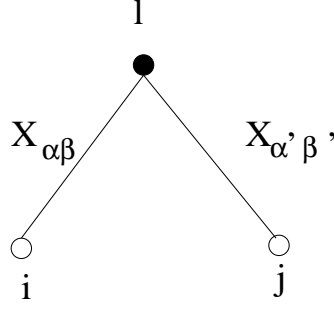
Figure A.1: Generic FHNC nodal diagram $N_{\alpha\beta'}(r_{ij})$, where $l$ is the node, and $X_{\alpha\beta}$, $X_{\alpha'\beta'}$ are the two substructures, where the subindices $\alpha\beta$ and $\alpha'\beta'$ denote the topological nature of their external points. Integration is done on the variable $\mathbf{r}_l$ represented by the node $l$.

which means

$$N_{\alpha\beta'}^p(r_{ij}) = \frac{1}{2} \int d\mathbf{r}_l \ [X_{\alpha\beta}^p(r_{il})X_{\alpha'\beta'}^p(r_{lj}) + X_{\alpha\beta}^a(r_{il})X_{\alpha'\beta'}^a(r_{lj})]c_{\beta\alpha'}$$

$$N_{\alpha\beta'}^a(r_{ij}) = \frac{1}{2} \int d\mathbf{r}_l \ [X_{\alpha\beta}^p(r_{il})X_{\alpha'\beta'}^a(r_{lj}) + X_{\alpha\beta}^a(r_{il})X_{\alpha'\beta'}^p(r_{lj})]c_{\beta\alpha'} \qquad (A.2)$$

where the two terms on the r.h.s of both equations correspond to a spin up or spin down particle $l$. The subindices $\alpha\beta\ldots$ may be $d$, $e$ or $c$ which stand for direct, exchange or cyclic type of external points. The vertex correction $c_{\beta\alpha'}$, can be either $c_d$ or $c$ given in Eq. (2.44) depending whether $\beta\alpha'$ include an exchange line ($de, ed, cc$) or not ($dd$). There may be nodes with $\beta\alpha' = cc$, which are not reached by dynamical corelations; in these cases the vertex correction must be $c_d - 1$ instead of $c_d$ (see Eq. (A.10)).

Given the two component structures of the FHNC quantities and the nodal operation of Eq. (A.1) and Eq. (A.2), the FHNC/BCS equations have the same structure given in I for the pure Jastrow case,

$$N_{dd}(r_{ij}) = \left(X_{dd}\ c\ \middle|X_{dd} + N_{dd}\right) + \left(X_{de}\ c_d\middle|X_{dd} + N_{dd}\right) +$$
$$\left(X_{dd}\ c_d\middle|X_{ed} + N_{ed}\right)$$
$$N_{de}(r_{ij}) = \left(X_{dd}\ c\ \middle|X_{de} + N_{de}\right) + \left(X_{de}\ c_d\middle|X_{de} + N_{de}\right) +$$
$$\left(X_{dd}\ c_d\middle|X_{ee} + N_{ee}\right)$$
$$N_{ee}(r_{ij}) = \left(X_{ed}\ c\ \middle|X_{de} + N_{de}\right) + \left(X_{ee}\ c_d\middle|X_{de} + N_{de}\right) +$$
$$\left(X_{ed}\ c_d\middle|X_{ee} + N_{ee}\right) \tag{A.3}$$

The above six coupled integral equation sum up all the nodal diagrams built up with the substructures (composite diagrams) $X_{dd}, X_{de}, X_{ee}$ appearing on their r.h.s.

Other six coupled integral equations sum up the nodal diagrams of the cyclic type. Let us denote with $N_{cc,hh}$ the cyclic nodal type diagrams having both external points reached by dynamical lines represented either $h_p$ or $h_a$; with $N_{cc,hl} = N_{cc,lh}$ those having one external point reached by an exchange line $l_v$ or $l_u$ only and the other one is reached by a dynamical line, and with $N_{cc,ll}$ those having both external points reached by $l$ lines only. The integral equations are given by

$$N_{cc,hh}(r_{12}) = \left(X_{cc}\ c_d\middle|X_{cc} + N_{cc,lh} + N_{cc,hh}\right) \tag{A.4}$$
$$N_{cc,hl}(r_{12}) = \left(X_{cc}\ c_d\middle|L_{cc} + N_{cc,hl} + N_{cc,ll}\right) \tag{A.5}$$
$$N_{cc,ll}(r_{12}) = \left(L_{cc}\ (c_d - 1)\middle|L_{cc} + N_{cc,ll}\right) + \left(L_{cc}\ c_d\middle|N_{cc,hl}(r_{32})\right) \tag{A.6}$$

with

$$L_{cc}^p(r_{ij}) = -l_v(r_{ij})$$
$$L_{cc}^a(r_{ij}) = il_u(r_{ij}) \tag{A.7}$$

Notice that in the first convolution on the r.h.s of Eq. (A.6) the vertex correction is $(c_d - 1)$, whereas for all the other convolutions in Eq.. (A.4)-(A.6) the vertex correction is $c_d$. The integral equations Eq.. (A.4)-(A.6) can be decoupled and written in the following form

$$N_{cc,hh}(r_{12}) = \left(X_{cc}\middle|c_d X_{cc}\right) + \left(X_{cc}\middle|c_d L_{cc}\middle|X_{cc}\right) + \left(N_{cc,hh}\middle|P_{cc}\right) \tag{A.8}$$
$$N_{cc,lh}(r_{12}) = \left(L_{cc}\middle|c_d X_{cc}\right) + \left(N_{cc,lh}\middle|P_{cc}\right) \tag{A.9}$$
$$N_{cc,ll}(r_{12}) = \left(L_{cc}\middle|(c_d - 1)L_{cc}\right) + \left(L_{cc}\middle|c_d X_{cc}\middle|L_{cc}\right) + \left(N_{cc,ll}\middle|P_{cc}\right) \tag{A.10}$$

where

$$P_{cc}(r_{ij}) = (c_d - 1)L_{cc}(r_{ij}) + c_d X_{cc}(r_{ij}) + \big(X_{cc}(r_{il})\big|c_d L_{cc}(r_{lj})\big). \qquad (A.11)$$

The sum of all the cyclic nodal functions $N_{cc,\alpha\beta}$ gives

$$N_{cc}(r_{12}) = N_{cc,hh}(r_{12}) + N_{cc,hl}(r_{12}) + N_{cc,lh}(r_{12}) + N_{cc,ll}(r_{12}) \qquad (A.12)$$

It is possible to write a single integral equation for the two components of $N_{cc}(r_{12})$, namely

$$N_{cc}(r_{ij}) = \big(X_{cc}(r_{il}) + L_{cc}(r_{il}) + N_{cc}(r_{il})\big|P_{cc}(r_{lj})\big) + \big(X_{cc}(r_{il})\big|L_{cc}(r_{lj})\big) \quad (A.13)$$

which is useful to solve and Eq. (A.12).

Let us now construct the composite functions $X_{\alpha\beta}$,

$$X_{dd}^{\alpha}(r_{ij}) = F^{\alpha}(r_{ij}) - N_{dd}^{\alpha}(r_{ij}) - 1$$
$$X_{de}^{\alpha}(r_{ij}) = F^{\alpha}(r_{ij})\{N_{de}^{\alpha}(r_{ij}) + E_{de}^{\alpha}(r_{ij})\} - N_{de}^{\alpha}(r_{ij})$$
$$X_{ee}^{\alpha}(r_{ij}) = F^{\alpha}(r_{ij})\{N_{ee}^{\alpha}(r_{ij}) + E_{ee}^{\alpha}(r_{ij}) + [N_{de}^{\alpha}(r_{ij}) + E_{de}^{\alpha}(r_{ij})]^2$$
$$-\mathrm{Re}[N_{cc}^{\alpha}(r_{ij}) + L_{cc}^{\alpha}(r_{ij}) + E_{cc}^{\alpha}(r_{ij})]^2\} - N_{ee}^{\alpha}(r_{ij})$$
$$X_{cc}^{\alpha}(r_{ij}) = F^{\alpha}(r_{ij})\{N_{cc}^{\alpha}(r_{ij}) + L_{cc}^{\alpha}(r_{ij}) + E_{cc}^{\alpha}(r_{ij})\} - N_{cc}^{\alpha}(r_{ij}) - L_{cc}^{\alpha}(r_{ij}) \quad (A.14)$$

with $\alpha \equiv a, p$ and where $E_{xy}^{\alpha}$ represents the sum of all the $\alpha$-component of elementary diagrams of class $xy$, and $F^{\alpha}(r_{ij})$ is given by

$$F^{\alpha}(r_{ij}) = f_{\alpha}^2(r_{ij})e^{N_{dd}^{\alpha}(r_{ij})+E_{dd}^{\alpha}(r_{ij})}. \qquad (A.15)$$

The expressions of the one-body FHNC quantities $U_d$ and $U_e$ entering the vertex corrections $c_d$ and $c$ are given by:

$$U_d = E_d + \frac{\rho_0}{2}\sum_{\alpha}\int \mathrm{d}\mathbf{r}_{ij}\Big\{c\big\{X_{dd}^{\alpha}(r_{ij}) - E_{dd}^{\alpha}(r_{ij}) - S_{dd}^{\alpha}(r_{ij})T_{dd}^{\alpha}(r_{ij})\big\} +$$

$$c_d\big\{X_{de}^{\alpha}(r_{ij}) - E_{de}^{\alpha}(r_{ij}) - S_{dd}^{\alpha}(r_{ij})T_{de}^{\alpha}(r_{ij}) - S_{de}^{\alpha}(r_{ij})T_{dd}^{\alpha}(r_{ij})\big\}\Big\},$$

$$U_e = E_e + \frac{\rho_0}{2}\sum_{\alpha}\int \mathrm{d}\mathbf{r}_{ij}\Big\{ c\big\{X_{ed}^{\alpha}(r_{ij}) - E_{ed}^{\alpha}(r_{ij}) - S_{de}^{\alpha}(r_{ij})T_{dd}^{\alpha}(r_{ij}) - S_{dd}^{\alpha}(r_{ij})T_{de}^{\alpha}(r_{ij})\big\} +$$

$$c_d\big\{X_{ee}^{\alpha}(r_{ij}) - E_{ee}^{\alpha}(r_{ij}) - S_{dd}^{\alpha}(r_{ij})T_{ee}^{\alpha}(r_{ij}) - S_{ee}^{\alpha}(r_{ij})T_{dd}^{\alpha}(r_{ij}) - 2S_{de}^{\alpha}(r_{ij})T_{de}^{\alpha}(r_{ij})\big\} +$$

$$\big\{c_d \,\mathrm{Re}\big[N_{cc}^{\alpha}(r_{ij})\big(S_{cc}^{\alpha}(r_{ij}) + L_{cc}^{\alpha}(r_{ij})\big)\big] +$$

$$\mathrm{Re}\big[L_{cc}^{\alpha}(r_{ij})\big(N_{cc,lh}^{\alpha}(r_{ij}) + N_{cc,ll}^{\alpha}(r_{ij}) + L_{cc}^{\alpha}(r_{ij})\big)\big]\big\}\Big\}, \qquad (A.16)$$

where

$$S_{xy}^\alpha(r_{ij}) = N_{xy}^\alpha(r_{ij}) + X_{xy}^\alpha(r_{ij}) \tag{A.17}$$

$$T_{xy}^\alpha(r_{ij}) = \frac{1}{2} N_{xy}^\alpha(r_{ij}) + E_{xy}^\alpha(r_{ij}) \tag{A.18}$$

and $E_x$ stands for the sum of all one-body vertex corrected elementary diagrams of the $x$ type.

The above FHNC/BCS set of coupled integral equation is not linear and therefore has to be solved with an iterative procedure. Let us consider the approximation of neglecting all the elementary diagrams $E$. One can use the following numerical procedure

1. Set the nodal functions $N_{xy}^\alpha$ equal to zero.

2. Use Eq.. (A.3)-(A.10) and (A.16) for a new approximation of the nodal vector functions and for $U_d$ and $U_e$.

3. Check the differences between the new and old nodal vector functions. If it is too large go back to point 2. Otherwise compute the spin parallel and spin antiparallel pair distribution functions

$$
\begin{aligned}
g_\alpha(r_{12}) = {} & 1 + N_{dd}^\alpha(r_{12}) + X_{dd}^\alpha(r_{12}) + 2\frac{c_d}{c}\Big[N_{de}^\alpha(r_{12}) + X_{de}^\alpha(r_{12})\Big] \\
& + \Big(\frac{c_d}{c}\Big)^2 \Big[N_{ee}^\alpha(r_{12}) + X_{ee}^\alpha(r_{12})\Big]. \tag{A.19}
\end{aligned}
$$

The pair distribution function $g(r_{ij})$ appearing on the r.h.s of Eq. (2.46) is given by

$$g(r_{12}) = \frac{1}{2}\Big[g_p(r_{12}) + g_a(r_{12})\Big] \tag{A.20}$$

The lowest order approximation of the pair distribution function is given by

$$
\begin{aligned}
g_p(r_{12}) &= f_p^2(r_{12})\Big[1 - \frac{1}{2}l_v^2(r_{12})\Big] \\
g_a(r_{12}) &= f_a^2(r_{12})\Big[1 + \frac{1}{2}l_u^2(r_{12})\Big] \tag{A.21}
\end{aligned}
$$

# Appendix B

# Calculation of the exchange terms in the potential energy

In this appendix we derive the set of FHNC/BCS integral equations underlying the calculation of the nodal functions $N_{\xi\xi}(r_{12})$ and $N_{cc,\xi\xi}(r_{12})$ appearing on the r.h.s of Eq. (2.59), which gives the contribution of B-terms to the expectation value of $\hat{V}_\sigma$.

The cluster diagrams associated with these nodal functions are characterized by the property of having the dynamical correlations with indices equal to either 1 or 2 or both of the type $\xi(r_{ij})$ given in Eq. (2.56). The derivation of the integral equations follows the standard methods of FHNC theory. They result to be

$$
\begin{aligned}
N_{\xi\xi}(r_{12}) &= \big[ X_{\xi d}(r_{13}) \; c + X_{\xi e}(r_{13}) \; c_d \big| X_{d\xi}(r_{32}) + N_{d\xi}(r_{32}) \big] + \\
&\quad \big[ X_{\xi d}(r_{13}) \; c_d \big| X_{e\xi}(r_{32}) + N_{e\xi}(r_{32}) \big],
\end{aligned}
\tag{B.1}
$$

where the convolution $[\ldots|\ldots]$ means:

$$
N_{\alpha\beta'}(r_{12}) = \big[ X_{\alpha\beta}(r_{13}) \; c_{\beta\alpha'} \big| X_{\alpha'\beta'}(r_{32}) \big] = \rho_0 \; c_{\beta\alpha'} \int d\mathbf{r}_3 \; X_{\alpha\beta}(r_{13}) X_{\alpha'\beta'}(r_{32}),
\tag{B.2}
$$

which differs from the convolution defined in Eq.. (A.1) and (A.2), because is dealing with one-component FHNC quantities. The spin state of an interacting particle is in a mixed state, namely is up in the ket and down in the bra or viceversa.

The FHNC quantities appearing on the r.h.s of Eq. (B.1) are given by

$$
\begin{aligned}
N_{\xi d}(r_{12}) &= \big[X_{\xi d}(r_{13})\ c\big|X_{dd}(r_{32}) + N_{dd}(r_{32})\big] + \big[X_{\xi e}(r_{13})\ c_d\big|X_{dd}(r_{32}) + N_{dd}(r_{32})\big] + \\
&\quad \big[X_{\xi d}(r_{13})\ c_d\big|X_{ed}(r_{32}) + N_{ed}(r_{32})\big] \hspace{3cm} (B.3)\\
N_{\xi e}(r_{12}) &= \big[X_{\xi d}(r_{13})\ c\big|X_{de}(r_{32}) + N_{de}(r_{32})\big] + \big[X_{\xi e}(r_{13})\ c_d\big|X_{de}(r_{32}) + N_{de}(r_{32})\big] + \\
&\quad \big[X_{\xi d}(r_{13})\ c_d\big|X_{ee}(r_{32}) + N_{ee}(r_{32})\big] \hspace{3cm} (B.4)
\end{aligned}
$$

where

$$
X_{\xi d}(r_{12}) = F_\xi(r_{12}) - N_{\xi d}(r_{12}) - 1, \hspace{2cm} (B.5)
$$
$$
X_{\xi e}(r_{12}) = \big[F_\xi(r_{12}) - 1\big] N_{\xi e}(r_{12}), \hspace{2cm} (B.6)
$$

and

$$
F_\xi(r_{12}) = \big[1 + \xi(r_{12})\big] e^{N_{\xi d}(r_{12}) + E_{\xi d}(r_{12})}. \hspace{1.5cm} (B.7)
$$

To calculate the cyclic nodal function $N_{cc,\xi\xi}(r_{12})$ it is convenient, as in appendix A, to distinguish between $N^{\xi\xi}_{cc,\xi\xi}(r_{12})$, $N^{\xi h}_{cc,\xi\xi}(r_{12})$, $N^{\xi l}_{cc,\xi\xi}(r_{12})$ and $N^{ll}_{cc,\xi\xi}(r_{12})$, which are characterized by having $\xi$-correlations at both ends (superscripts $\xi\xi$), $\xi$ correlation at one end and $h$-correlation (either $h_p$ or $h_a$) at the other, a $\xi$-correlation at one end and a single $l$-correlation (either $l_v$ or $l_u$) at the other and $l$-correlations at both ends. The function $N^{ll}_{cc,\xi\xi}(r_{12})$ coincides with $N_{cc,ll}(r_{12})$ given in appendix A. The FHNC integral equations are given by

$$
\begin{aligned}
N^{\xi\xi}_{cc,\xi\xi}(r_{12}) &= \big[X_{\xi c}(r_{13})\ c_d\big|X_{c\xi}(r_{32}) + N^{h\xi}_{cc,\xi\xi}(r_{32}) + N^{l\xi}_{cc,\xi\xi}(r_{32})\big], \\[2mm]
N^{\xi l}_{cc,\xi\xi}(r_{12}) &= \Big[X_{\xi c}(r_{13})\ c_d\Big|\frac{1}{2}\sum_\alpha \big(L^\alpha_{cc}(r_{32}) + N^\alpha_{cc,hl}(r_{32}) + N^\alpha_{cc,ll}(r_{32})\big)\Big], \\[2mm]
N^{h\xi}_{cc,\xi\xi}(r_{12}) &= \Big[\frac{1}{2}\sum_\alpha X^\alpha_{cc}(r_{13})\ c_d\Big|X_{c\xi}(r_{32}) + N^{h\xi}_{cc,\xi\xi}(r_{32}) + N^{l\xi}_{cc,\xi\xi}(r_{32})\Big], \\[2mm]
N_{cc,\xi\xi}(r_{12}) &= N^{\xi l}_{cc,\xi\xi}(r_{12}) + N^{\xi h}_{cc,\xi\xi}(r_{12}) + N_{cc,lh}(r_{12}) + N_{cc,ll}(r_{12}), \hspace{0.8cm} (B.8)
\end{aligned}
$$

where

$$
X_{c\xi}(r_{12}) = \big[F_\xi(r_{12}) - 1\big]\Big[N_{cc,\xi\xi}(r_{12}) + \frac{1}{2}\sum_\alpha L^\alpha_{cc}(r_{12})\Big]. \hspace{1cm} (B.9)
$$

Notice that, in the limit of the normal phase trial function, namely when $v_{\mathbf{k}}^2 = \theta(k - k_F)$ and consequently $l_u(r) = 0$, the above equation are equivalent to those given in ref. [57]. The vertex correction $c_\xi$ is given by

$$
c_\xi = e^{U_\xi}, \hspace{3cm} (B.10)
$$

where

$$U_\xi = E_\xi + \rho_0 \int d\mathbf{r}_{12} \Big\{ c\big[X_{\xi d}(r_{12}) - E_{\xi d}(r_{12}) - S_{\xi d}(r_{12})T_{\xi d}(r_{12})\big] +$$

$$c_d\big[X_{\xi e}(r_{12}) - E_{\xi e}(r_{12}) - S_{\xi d}(r_{12})T_{\xi e}(r_{12}) - S_{\xi e}(r_{12})T_{\xi d}(r_{12})\big] \Big\} \quad \text{(B.11)}$$

with $S_{xy}(r_{12})$ and $T_{xy}(r_{12})$ as obtained in Eq. (A.17) and (A.18)

# Bibliography

[1] Leggett, A. *Modern Trends in the Theory of Condensed Matter*. Springer-Verlag, Berlin, (1980).

[2] Bertsch, G. F. http://www.phys.washington.edu/∼mbx/george.html, (1998).

[3] Carlson, J., Chang, S.-Y., Pandharipande, V. R., and Schmidt, K. E. *Phys. Rev. Lett.* **91**(5), 050401 (2003).

[4] O'Hara, K. M., Hemmer, S., Gehm, M., Granade, S., and Thomas, J. *Science* **298**, 2179 (2002).

[5] Randeria, M. *Bose Einstein Condensation*, volume 1. Cambridge, (1995).

[6] Engelbrecht, J. R., Randeria, M., and Sá de Melo, C. A. R. *Phys. Rev. B* **55**(22), 15153–15156 (1997).

[7] Stenger, J., Inouye, S., Andrews, M. R., Miesner, H.-J., Stamper-Kurn, D. M., and Ketterle, W. *Phys. Rev. Lett.* **82**(12), 2422–2425 (1999).

[8] Roberts, J. L., Claussen, N. R., Cornish, S. L., Donley, E. A., Cornell, E. A., and Wieman, C. E. *Phys. Rev. Lett.* **86**, 4211 (2001).

[9] Cowell, S., Heiselberg, H., Mazets, I. E., Morales, J., Pandharipande, V. R., and Pethick, C. J. *Phys. Rev. Lett.* **88**(21), 210403 (2002).

[10] Giorgini, S., Boronat, J., and Casulleras, J. *Phys. Rev. A* **60**, 5129 (1999).

[11] Fantoni, S., Nguyen, T. M., Shenoy, S. R., and Sarsa, A. *Phys. Rev. A* **66**, 033604 (2002).

[12] Pethick, C. and Ravenhall, D. *Ann. Rev. Nucl. Part. Science* **45**, 429 (1995).

[13] Howell, C. R., Chen, Q., Carman, T. S., Hussein, A., Gibbs, W. R., Gibson, B. F., Mertens, G., Moore, C. F., Morris, C., Obst, A., Pasyuk, E., Roper, C. D., Salinas, F., Slaus, I., Sterbenz, S., Tornow, W., Walter, R. L., Whiteley, C. R., and Whitton, M. *Phys. Lett. B* **444**, 252 (1998).

[14] Huhn, V., Wätzold, L., Weber, C., Siepe, A., von Witsch, W., Witała, H., and Glöckle, W. *Phys. Rev. C* **63**, 014003 (2000).

[15] Schmidt, K. and Kalos, M. *Monte Carlo Methods I, Statistical Physics.* Number 125. Springer-Verlag, Berlin, (2001).

[16] Schmidt, K. and Fantoni, S. *Phys. Lett. B* **446**, 99 (1999).

[17] Fabrocini, A., Fantoni, S., Illarionov, A. Y., and Schmidt, K. E. *Phys. Rev. Lett.* **95**, 192501 (2005).

[18] Fantoni, S. and Rosati, S. *Nuovo Cim.* **25**, 593 (1975).

[19] Fantoni, S. and Fabrocini, A. *Microscopic Quantum Many-Body theories and their Applications.* Springer-Verlag, Berlin, (1998).

[20] Fantoni, S. *Nucl. Phys. A* **363**, 381 (1981).

[21] Wang, X. Q., Fantoni, S., Tosatti, E., Yu, L., and Viviani, M. *Phys. Rev. B* **41**, 11479 (1990).

[22] Wang, X. Q. G., Fantoni, S., Tosatti, E., and Yu, L. *Phys. Rev. B* **46**, 8894 (1992).

[23] Wang, X. Q. G., Fantoni, S., Tosatti, E., and Yu, L. *Phys. Rev. B* **49**, 10027 (1994).

[24] M. H. Anderson, J. R. Ensher, M. R. M. C. E. W. and Cornell, E. A. *Science* **269**, 198 (1995).

[25] Davis, K. B., Mewes, M. O., Andrews, M. R., van Druten, N. J., Durfee, D. S., Kurn, D. M., and Ketterle, W. *Phys. Rev. Lett.* **75**, 3969 (1995).

[26] Bradley, C. C., Sackett, C. A., Tollett, J. J., and Hulet, R. G. *Phys. Rev. Lett.* **75**, 1687 (1995).

[27] Cataliotti, F. S., Burger, S., Fort, C., Maddaloni, P., Minardi, F., Trombettoni, A., Smerzi, A., and Inguscio, M. *Science* **293**, 843 (2001).

[28] Albiez, M., Gati, R., Folling, J., Hunsmann, S., Cristiani, M., and Oberthaler, M. K. *Phys. Rev. Lett.* **95**(1), 010402 (2005).

[29] Abo-Shaeer, J. R., Raman, C., Vogels, J. M., and Ketterle, W. *Science* **292**, 476 (2001).

[30] Andrews, M. R., Townsend, C. G., Miesner, H.-J., Durfee, D. S., Kurn, D. M., and Ketterle, W. *Science* **275**, 637 (1997).

[31] Hagley, E. W., Deng, L., Kozuma, M., Wen, J., Helmerson, K., Rolston, S. L., and Phillips, W. D. *Science* **283**, 1706 (1999).

[32] DeMarco, B. and Jin, D. S. *Science* **285**, 1703 (1999).

[33] Truscott, A. K., Strecker, K. E., McAlexander, W., Partridge, G. B., and Hulet, R. G. *Science* **291**, 2570 (2001).

[34] S. Giorgini, L. P. and Stringari, S. arXiv:0706.3360 [cond-mat.other].

[35] Feshbach, H. *Ann. Phys.* **19**, 287 (1962).

[36] Inouye, S., Andrews, M. R., Stenger, J., Miesner, H.-J., Stamper-Kurn, D. M., and Ketterle, W. *Nature* **392**, 151 (1998).

[37] Courteille, P., Freeland, R. S., Heinzen, D. J., van Abeelen, F. A., and Verhaar, B. J. *Phys. Rev. Lett.* **81**, 69 (1998).

[38] Cornish, S. L., Claussen, N. R., Roberts, J. L., Cornell, E. A., and Wieman, C. E. *Phys. Rev. Lett.* **85**, 1795 (2000).

[39] Loftus, T., Regal, C. A., Ticknor, C., Bohn, J. L., and Jin, D. S. *Phys. Rev. Lett.* **88**, 173201 (2002).

[40] Dieckmann, K., Stan, C. A., Gupta, S., Hadzibabic, Z., Schunck, C. H., and Ketterle, W. *Phys. Rev. Lett.* **89**, 203201 (2002).

[41] Q. Chen, J. Stajic, S. T. and Levin, K. arXiv:cond-mat/0404274v3 [cond-mat.supr-con], (2005).

[42] Nozieréres, P. and Schmitt-Rink, S. *J. Low Temp. Phys* **59**, 195 (1985).

[43] Sá de Melo, C. A. R., Randeria, M., and Engelbrecht, J. R. *Phys. Rev. Lett.* **71**, 3202 (1993).

[44] Migdal, A. B. *Nucl. Phys* **13**, 655 (1959).

[45] http://www.astroscu.unam.mx.

[46] Reid, R. V. J. *Ann. of Phys.* **50**, 411 (1968).

[47] Pandharipande, V. R. and Wiringa, R. B. *Rev. Mod. Phys.* **51**, 821 (1979).

[48] Chen, J. M. C., Clark, J. W., Krotscheck, E., and Smith, R. A. *Nucl. Phys. A* **451**, 509 (1986).

[49] Hammond, B. L., Lester, W. A., and Jr., P. J. R. *Monte Carlos Methods Ab Initio Quantum Chemistry*, volume 1. World Scientific, (1994).

[50] Schmidt, K. E. and Kalos, M. H. *Monte Carlo Methods in Statistical Mechanics.* Springer-Verlag, (1984).

[51] Knuth., D. E. *Elec. J. Comb.* (3) (1996).

[52] Zhang, S., Carlson, J., and Gubernatis, J. E. *Phys. Rev. Lett.* **74**, 3652 (1995).

[53] Zhang, S., Carlson, J., and Gubernatis, J. E. *Phys. Rev. B* **55**, 7464 (1997).

[54] S. Fantoni, A. S. and Schimidt, K. E. *Prog. Part. Nucl. Phys* **44**, 63 (2000).

[55] Sarsa, A., Fantoni, S., Schmidt, K. E., and Pederiva, F. arXiv:nucl-th/0303035v1, (2003).

[56] Fantoni, S., Sarsa, A., and Schmidt, K. E. *Phys. Rev. Lett.* **87**, 181101 (2001).

[57] Rosati, S. and Fantoni, S. *Correlations in infinite systems. Lecture Notes in Physics: The many-body problem Jastrow correlations versus Brueckner theory*, volume 138. Springer-Verlag, (1980).

[58] Fabrocini, A. and Fantoni, S. *Phys. Lett. B* **507** (1981).

[59] Fantoni, S. and Rosati, S. *Nucl. Phys. A* **328**, 478 (1979).

[60] Fantoni, S. and Rosati, S. *Phys. Lett. B* **84**, 23 (1979).

[61] Afnan, I. R. and Tang, Y. C. *Phys. Rev.* **175**(4), 1337 (1968).

[62] González Trotter, D. E., Salinas, F., Chen, Q., Crowell, A. S., Glöckle, W., Howell, C. R., Roper, C. D., Schmidt, D., Šlaus, I., Tang, H., Tornow, W., Walter, R. L., Witała, H., and Zhou, Z. *Phys. Rev. Lett.* **83**, 3788 (1999).

[63] Chin, C., Bartenstein, M., Altmeyer, A., Riedl, S., Jochim, S., Denschlag, J. H., and Grimm, R. *Science* **305**, 1128 (2004).

[64] Friedman, B. and Pandharipande, V. *Phys. Lett. B.* **100**, 205 (1981).

[65] Fantoni, S., Pandharipande, V. R., and Schmidt, K. E. *Phys. Rev. Lett* **48**, 878 (1982).

[66] Fantoni, S. and Illarionov, A. Y. Private communication, (2007).

[67] Fantoni, S. and Schmidt, K. E. *Nucl. Phys. A* **690**, 456 (2001).

[68] Günter, K., Stöferle, T., Moritz, H., Köhl, M., and Esslinger, T. *Phys. Rev. Lett.* **96**(18), 180402 (2006).

[69] Cheng, C.-H. and Yip, S.-K. *Phys. Rev. Lett.* **95**(7), 070404 (2005).

[70] Iskin, M. and Sá de Melo, C. A. R. *Phys. Rev. Lett.* **97**(10), 100404 (2006).

[71] Gurarie, V. and Radzihovsky, L. *Ann. Phys.* **322**, 2 (2007).